UNIVERSITY OF WASHINGTON
DEPARTMENT OF MECHANICAL ENGINEERING

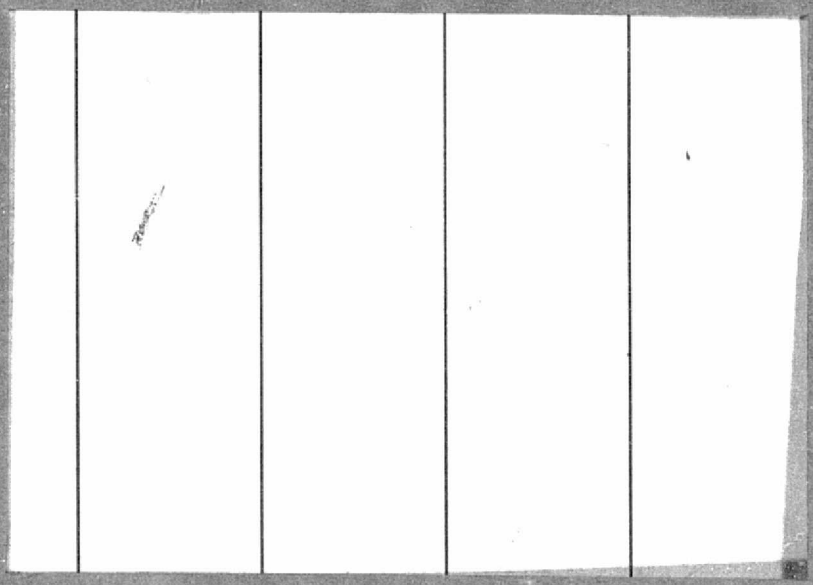

Sound and Vibration Research Laboratory

SEATTLE, WASHINGTON 98195

Final Report on

NASA Grant No. ~~NGR-002-144~~
NGR-48-002-144

A STUDY OF SOUND GENERATION IN SUBSONIC ROTORS

Report No. ME 73-11

Volume 1 of 2

J. D. Chalupnik, Associate Professor

L. T. Clark, Research Assistant Professor

University of Washington

Department of Mechanical Engineering

Seattle, Washington 98195

Abstract

A model for the prediction of wake related sound generation by a single airfoil is presented. The basis of the model is an assumption that the net force fluctuation on an airfoil may be expressed in terms of the net momentum fluctuation in the near wake of the airfoil. This near wake model results in the forcing function for sound generation being the spectra of the two point velocity correlations in the turbulent region near the airfoil trailing edge.

The spectra of the two point velocity correlations were measured for the longitudinal and transverse components of turbulence in the wake of a 91.4 cm (36 inch) chord NACA series 63-009 airfoil. The airfoil was installed in the 7 by 10 tunnel at the NASA Ames Research Center. The test velocity was 45.7 m/sec (150 ft/sec) and incidence angles were set at 0° and 6°. Two x-probe hot wire sensors were used in the measurements. Cross power spectra of the signals from these sensors provided the data required for the two point velocity correlations. Some preliminary experiments were conducted using a 25.4 cm (10 inch) chord airfoil similar to the larger one in a free jet facility at the University of Washington.

A scaling procedure was developed using the turbulent boundary layer thickness as the primary measure. The model was then used to predict the radiated sound from a 5.1 cm chord airfoil for which acoustical data were available. Agreement between the predicted and measured sound radiation spectra was good both in level and spectral shape.

The single airfoil result was extended to a rotor geometry and comparisons studied for various aerodynamic parameters.

The motion of the source was found to influence the spectrum of radiated sound very little. This was due to the relatively broad band spectrum of the source. Sample computations were made for large subsonic rotors and the noise levels due to the wake mechanism alone was found to be significant. This was due in part to the concentration of the acoustic energy in the frequency range 2000 to 9000 Hz which is the range of highest subjective response by the human ear.

Table of Contents

List of Figures

List of Plates

Acknowledgement

This program was funded by NASA Grant No. NGR 48-002-144. The program was coordinated by Mr. B. K. Hodder and Mr. D. L. Hickey of the Ames Research Center. Their cooperation in this program is appreciated.

Mr. Hodder also set up the experiment in the Ames 7 by 10 wind tunnel and worked with the authors in obtaining the experimental data. The authors wish to thank him for his very able efforts and also to thank Mr. A. Rufiange for his assistance during the actual testing.

The authors express their gratitude to Dr. M. E. Childs, Dr. H. C. Merchant, and Dr. R. B. Osborn of the Mechanical Engineering Department and Dr. G. C. Oates of the Department of Aeronautics and Astronautics for helpful conversations throughout the program and for reading the manuscript.

1.0 Introduction

The noise radiated from helicopter rotors and other aircraft fans consists of a combination of pure tones and broad band effects. The pure tones typically occur at frequencies which are the blade passage of the rotor and its higher harmonics. When the Mach number of operation approaches unity other pure tones associated with the rotational frequency appear. These are the "multiple pure tones" or Buzz Saw components" which one hears when the current super jet takes off. The blade passage frequency pure tone mechanism appears to be due to the steady state pressure distribution on the individual blades and the interactions between the rotor and stator rows. Recently, there has been evidence to suggest that the interaction of inflow turbulence with the rotor blading will give rise to this pure tone as well.

Broad band noise is usually associated with the interaction of the blading with turbulence in the flow, either with inflow turbulence or wake turbulence of the airfoils themselves. Possible mechanisms of this type include boundary layer turbulence, random static pressure fluctuations related to the wake shedding at the trailing edge of the blade, radiation from the stresses in the wake turbulence itself; and force fluctuations caused by the interaction of the airfoil with inflow turbulence. All these mechanisms are present and there are probably more that are yet undefined. The one which dominates the others depends upon the flow being considered and the geometry of the body in the flow. There is ample evidence to suggest that the dominant mechanism is dependent upon both the Reynolds and Mach

numbers of the flow.

The present study is an attempt to relate noise generation by a single airfoil operating in a smooth turbulence free flow field to the properties of the turbulence in the wake of the airfoil. Then, once the mechanism is identified, to extend the model to a rotor to provide a design tool. What is hoped from this approach is that a model for the prediction of the spectrum of broad band noise generation in the design phase of a turbomachine may be developed.

Extension of the results from the single airfoil to a rotating array of airfoils was made analytically using an existing multipole analysis. By using the single airfoil results as a source of information on the statistical properties of the fluctuating forces, the effect of rotation of an array of blades could be determined.

It is expected that for large rotors such as may be expected to be used in large STOL and helicopter aircraft, the blades and hence their wakes will be large enough that wake related noise will be an important feature in the noise considerations of these designs. Because the wake is related to aerodynamic design and certain possibilities exist for its modification (for example, boundary layer suction to reduce the size of the turbulence correlation volumes) it is important to understand the detailed mechanism so that flow control can be directed most efficiently. In current designs, the small size and high speed of operation make the frequency of wake related noise too high to be of practical interest (except for some tip vortex shedding on large helicopter rotors). This also

tends to degrade the usefulness of typical model rigs for studying this mechanism; they are too small in size. However, when Mach numbers are reduced to decrease the tone noise and blading size is increased to accomodate the aerodynamic loading, then the wake noise will be in a frequency range of very critical subjective importance.

The most important wake parameters in terms of noise generation appear to be the actual size of the wake and the velocity of operation. Normally one sees the sound power expressed as proportional to velocity to the 5.5 or 6th power. The effect of wake correlation volume is as important as velocity since the acoustic power scales with the geometric size (correlation volume times physical volume) scale to the sixth power. As a result, one might experience a sixth power variation of acoustic power with geometric scale. Unfortunately it isn't that simple and there appear to be few shortcuts to the rather pragmatic procedure of comparing designs one by one using the most complete model available. It is only in this way that all the effects of a given change can be properly accounted for. General dependencies can of course be stated but when the actual practical designs are put down it will be a complex interrelationship of parameters which will determine the correct choice. For an example, a designer might feel that by reducing the velocity of operation he can reduce the sound generation; but, when he designs the fan he finds he must increase the chord to maintain the same aerodynamic loading. When he tests the machine he finds it to be as noisy but with the sound shifted to another part of the spectrum. In order to design for noise one must

have a clear understanding of the implications of design changes.

In this study an attempt is made to relate sound generation to wake properties so that the effects of such things as geomctric scaling can be assessed. Experimental measurements of the cross power spectra of two point velocity correlations were made since these were found to provide the forcing function information needed by the model. The results were extended to a multibladed rotor so that design considerations could be made using a model more closely approximating the actual rotor. An effort has been made to simplify the final results to a point where they may be used by the designer who may not be a specialist in the details of aerodynamic noise theories and methods.

2.0 Review of the Literature

This review will be restricted to the literature which applies most directly to the problem of sound generation by bodies immersed in smooth turbulence free flows. This means the concern will be with those investigations which have attempted to relate sound generation to either the static pressure fluctuations on the surfaces of the body or to the turbulence which is generated by the airfoil as the flow passes over it. Published efforts dealing with airfoils are somewhat limited and for the most part recent since motivation for this research has been public concern with aircraft noise. Some earlier work has relevance. This is the study of Aeolian tones generated by flows over cylinders. The very first works were concerned with musical instruments and later with loadings on telegraph lines and other cables. This early literature will be referred to only in the context of its relevance to the problem of aerodynamic noise and how it relates to aerodynamic performance parameters.

Modern studies of aerodynamic sound generation are based on solutions of the non-homogeneous wave equation developed by M. J. Lighthill (1,2,3). It is his work which has provided the basis for the large volume of analysis in the field of aerodynamic sound generation. By combining the equations of conservation of linear momentum with that of conservation of mass, Lighthill was able to write a non-homogeneous wave equation which would govern the radiation of aerodynamic sound from a region of turbulent motion. Justification of the approach is best expressed in Lighthill's own description. It is important

to understand this reasoning to best judge its scope of applicability. To quote Lighthill:

> Considering a fluctuating fluid flow occupying a limited part of a very large volume of fluid of which the remainder is at rest. Then the equations governing the fluctuations of density in the real fluid will be compared with those which would be appropriate to a uniform acoustic medium at rest, which coincided with the real fluid outside the region of flow. The difference between the two sets of equations will be considered as if it were the effect of a fluctuating external force field, known if the flow is known, acting on the said uniform acoustic medium at rest, hence radiating sound in it according to the ordinary laws of acoustics.

In this way all the forcing effects are lumped into a forcing function from which the resulting sound radiation may be predicted. The consequence of the method is that one must be able to specify the unsteady aerodynamics of the source region.

To show the way the model is constructed, consider the equation of conservation of linear momentum and use the summation convention where repeated indices imply summation:

$$\frac{\partial(\rho u_i)}{\partial t} + \frac{\partial}{\partial x_j}(\rho u_i u_j) = -\frac{\partial}{\partial x_j}(p\delta_{ij}) + \frac{\partial}{\partial x_j}\tau_{ij}$$

and the equation of conservation of mass:

$$\frac{\partial \rho}{\partial t} + \frac{\partial}{\partial x_j}(\rho u_i) = 0$$

Taking the partial derivative of continuity with respect to time and the partial derivative of linear momentum with respect to the space variable then subtracting the two equations, one can express the result as a wave equation of the form

$$\frac{\partial^2 \rho}{\partial t^2} - a_0^2 \nabla^2 \rho = \frac{\partial^2}{\partial x_i \partial x_j}(T_{ij})$$

where T_{ij} is the "Lighthill tensor" and is defined as

$$T_{ij} = \rho u_i u_j - \sigma_{ij} - a_o^2 \rho \delta_{ij} .$$

In these expressions; ρ = density, a_o = speed of sound in the fluid at rest, σ_{ij} = stress tensor, u_i = velocity in direction x_i (i = 1,2,3). It is this wave equation which forms the basis for the many theories recently developed for sound generation by aerodynamic flows.

The general Kirchhoff solution can be used to solve the non-homogeneous wave equation (Sobolev, reference 4). This original theory by Lighthill did not include the effect of solid bodies contained in the region of fluid motion. This was done by N. Curle (5). Curle wrote the Kirchhoff solution for the case of aerodynamic flows as

$$\rho(\vec{x},t) - \rho_o = \frac{1}{4\pi a_o^2} \int_V \frac{\partial^2}{\partial y_i \partial y_j} T_{ij}\left(\vec{y}, t - \frac{r}{a_o}\right) \frac{dV(\vec{y})}{r}$$

$$+ \frac{1}{4\pi} \int_S \left(\frac{1}{r} \frac{\partial \rho}{\partial n} + \frac{1}{r^2} \frac{\partial r}{\partial n} \rho + \frac{1}{a_o r} \frac{\partial r}{\partial n} \frac{\partial \rho}{\partial t} \right) dS(\vec{y})$$

where $r = |\vec{x} - \vec{y}|$.

The integrands of both terms are taken at the retarded time. This simply means in the present case that the sound observed in the far field was generated at the source location at an earlier time and the relevant source strength is that which occurred at the earlier time. The first integral is over the volume of the turbulent region and the second is over the surface of the active region.

In studying the solution for the case of immersed solid

bodies, Curle was able through several manipulations to cast the solution in a particularly revealing form. He was able to show an equivalent solution as

$$\rho(\vec{x},t)-\rho_o = \frac{1}{4\pi a_o^2}\frac{\partial^2}{\partial x_i \partial x_j}\int_V \frac{T_{ij}\left(\vec{y},t-\frac{r}{a_o}\right)}{r}\,dv(\vec{y})$$

$$-\frac{1}{4\pi a_o^2}\frac{\partial}{\partial x_i}\int_S \frac{P_i\left(\vec{y},t-\frac{r}{a_o}\right)}{r}\,dS(\vec{y})$$

Here again the solution is the sum of a volume and a surface integral. The sound produced is due to a volume distribution of quadrapoles represented by the fluctuating stresses and a surface distribution of dipoles represented by the pressure on the surface of the body. P_i is exactly the force per unit area exerted by the solid boundaries on the fluid in the x_i direction. This second integral is the additional effect of the solid boundary to the original solution written by Lighthill. The solution presented by Lighthill was for no boundaries and is exactly the first integral of Curle's result.

Using dimensional analysis, Curle developed a relationship between sound power and aerodynamic parameters. The total acoustic power output was shown to take the form

$$E \propto \rho_o \bar{U}^6 a_o^{-3} L^2$$

where $\bar{U}$ is a typical velocity and L is a characteristic length.

Another approach to the solution of the wave equation with immersed bodies was presented by P. E. Doak using the method of Green's functions (6). Once the appropriate Green's function is known for a space, the solution can be written immediately.

Actually, the Green's function approach has not been used much because free space problems have proven difficult enough. In work on tone noise generation the method has been used. Doak wrote expressions for the radiated sound intensity in terms of the covariances of the first time derivative of the surface pressure. It was these forms which provided the starting point for I. J. Sharland's (7) prediction of noise generation by small flat plates immersed in jet flow and the extension to broad band sound generation by fans. For a flat surface with dimensions small with respect to the wavelength of the radiated sound, the total radiated sound energy could be written:

$$E = \frac{1}{12\pi\rho_o a_o^3} \int_S \int_S \overline{\frac{\partial p}{\partial t}(x_1, x_2, t') \frac{\partial p}{\partial t}(x_1', x_2', t')}\, dx_1 dx_2 dx_1' dx_2'$$

where t' is the retarded time, the surface S is in the x_1, x_2 (or x_1',x_2') plane, p is the pressure difference fluctuation at (x_1,x_2) and the overbar denotes a time average. The integration is taken over only one side of the plate. Since the wavelength is larger than the plate dimension, x_1' and x_2' can be taken as equal to x_1 and x_2. To express the integral, a proportionality factor S_c can be used which has the units of area and is called the correlation area. The integral may then be written as

$$\overline{\left[\frac{\partial p}{\partial t}(x_1, x_2, t')\right]^2} S_c\left(x_1, x_2, \frac{\partial p}{\partial t}\right) = \int_S \overline{\frac{\partial p}{\partial t}(x_1, x_2, t') \frac{\partial p}{\partial t}(x_1', x_2', t')}\, dx_1' dx_2'$$

and the total radiated acoustic energy as

$$E = \frac{1}{12\pi\rho_o a_o^3} \int_S \overline{\left[\frac{\partial p}{\partial t}(x_1, x_2, t)\right]^2} S_c\left(x_1, x_2, \frac{\partial p}{\partial t}\right) dx_1 dx_2$$

Sharland now related the pressure to a fluctuating lift force per unit area. He wrote the pressure derivative as

$$\frac{\partial p}{\partial t}(x_1, x_2, t') = \frac{1}{2}\rho_0 \bar{U}^2(x_1, x_2) \frac{\partial C_L}{\partial t}(x_1, x_2, t')$$

where $\bar{U}$ is the local mean velocity parallel to the plate and C_L is described as a lift coefficient.

Sharland used some boundary layer assumptions to express the vortex shedding noise and derived the expression for overall sound power:

$$E = \frac{\rho_0}{a_0^3} 10^{-7} \int_{\text{Span}} C \bar{U}^6 dx_2$$

He compared this prediction with some measurements of overall sound pressure for one inch chord flat plates located in the potential core of a one inch diameter round jet. His radiation pattern suggested a dipole as did the power law of the sound power with velocity. A dipole yields a dependence upon velocity to the sixth power. A plot of the radiated sound as a function of velocity taken from Sharland's paper is shown in Figure 1. It may be seen that the agreement is quite good. This is extraordinary in view of the simplicity of both the model and the experimental measurements. The agreement does provide encouragement that the general approach is valid and further work along this path would be worthwhile.

The efforts of Sharland were the first to attempt the problem of wake related sound generation from airfoils, but there were some some attempts using circular cylinders. The most complete approach using modern theories was made by O. M. Phillips on vortex sound generation from small cylinders (8).

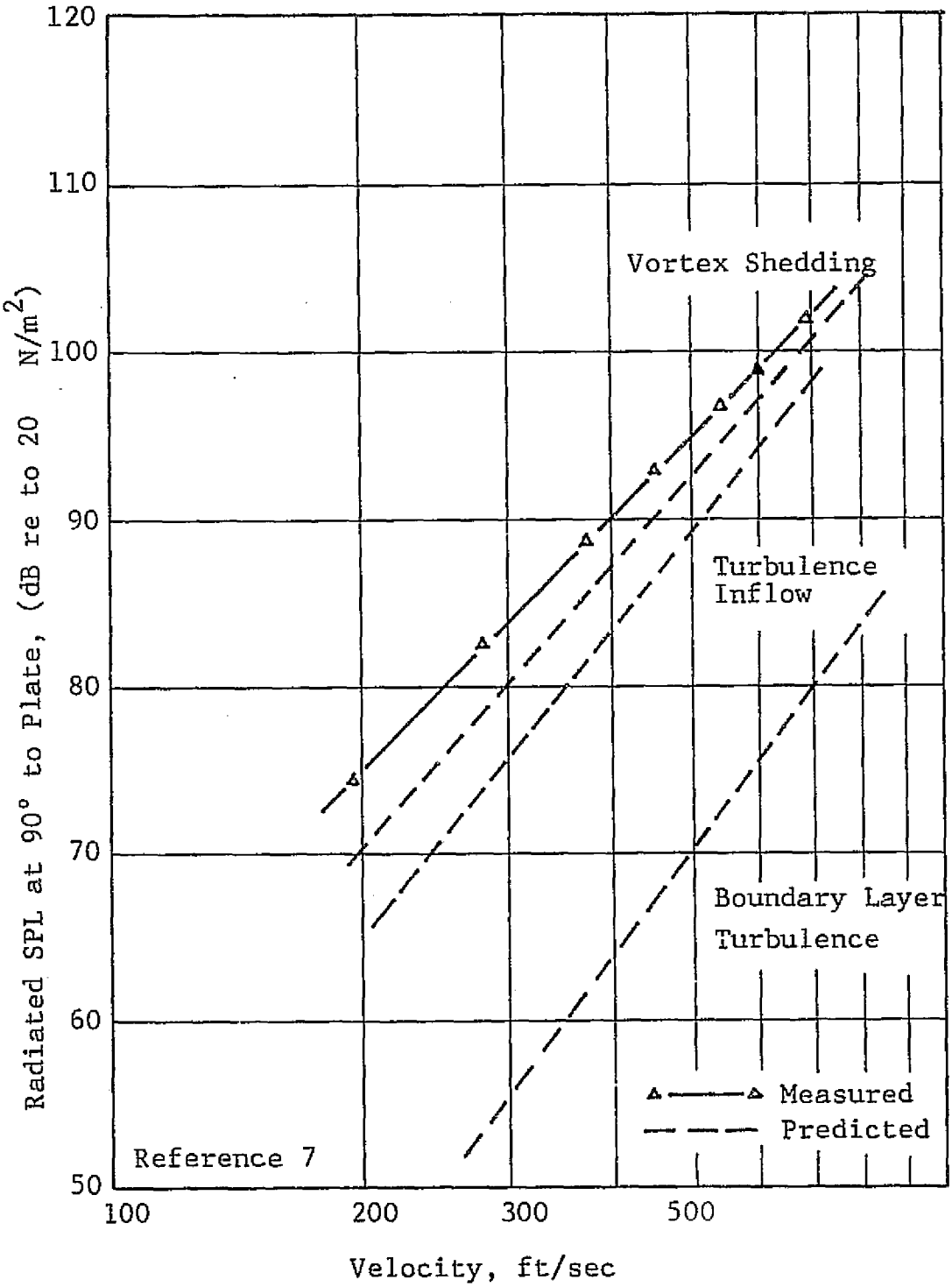

Figure 1 Sound Radiated from a One Inch Flat Plate Immersed in a Smooth Flow

Fluctuations in lift and drag were computed for Reynolds numbers from 40 to 160 (based on diameter) using the velocity field measurements of Kovasznay (9). Kovasznay had measured the velocity field downstream in the near wake of a circular cylinder and found he could express it in the functional form

$$u(y_1,y_2,t) = F_1(y_1,y_2)\cos 2\pi[\zeta_1(y_1)+nt] + F_2(y_1,y_2)\cos 4\pi[\zeta_2(y_1)+nt]$$

Phillips wrote the drag and lift forces using the momentum equation (integral form) for incompressible flow. For the drag

$$D = \rho \frac{d}{dt}\int u_1 dy_1 dy_2$$

Drag could be computed directly from the velocity field data but the lift computation would require the normal component of turbulence which had not been measured. Phillips used the vorticity equation along with continuity to obtain the lift fluctuation. He obtained

$$L = 0.38\rho_o \bar{U}^2 D \cos 2\pi nt$$

The axial length scale was found to be very large for Re 100 and for the range $100 < Re < 160$ to be about 17D (D = cylinder diameter). Using this, the radiated dipole sound was expressed

$$\overline{p^2}(r) \simeq 0.27\cos^2\theta \frac{\rho_o^2 l D \bar{U}^6 S^2}{a_o^2 r^2}$$

where l = cylinder length, D = diameter, and S = Strouhal number (~ 0.2).

When higher Reynolds numbers were tested a similar expression was derived but with a numerical factor of 0.037 rather than the 0.27 used in the above. Also, the span correlation

was found to decrease to a value of about 3D at the highest Reynolds numbers tested.

Measurements which gave extensive data on the Strouhal number have been presented both by Kovasznay and by G. H. Gerrard (10). Gerrard measured lift and drag fluctuations on circular cylinders using a pressure transducer mounted on the top on the cylinder. He concluded that the drag fluctuations are an order of magnitude smaller than those of the lift. The radiated sound intensity is given without derivation as

$$I \propto \frac{\rho_o}{a_o^3} \frac{\cos^2\theta}{r^2} \bar{U}^6 S^2 l_c^2 C_L^2$$

where $(C_L^2)^{0.5}$ is the lift coefficient which was determined experimentally to be 0.8 at Re = 7×10^4 and 0.01 at Re = 4×10^3. It appears that the expression is incorrect as written since there is no provision for total cylinder length. Probably the l_c^2 should be replaced by Sl_c, the product of the correlation length and the cylinder length. The trend with Reynolds number of the lift coefficient seems reversed to this writer since one would expect a higher intensity at the lower Reynolds number. This is due to the decrease in the correlation length with an increase in Reynolds number.

The chronology of the above research was such that each investigation was done at a different time so that each had access to the results of the previous investigators. The development is perhaps more systematic than that which has been done more recently when the various workers were proceeding in parallel.

The next three programs to be discussed were all directed

to the airfoil wake noise problem. Each of the three was done in a different part of the world and was done independently of the others. It is interesting to compare the approaches as they are completely different although they started at a common point which was the technology level in 1965.

I. Kavrak used a hydrogen bubble flow visualization technique (11) in water to observe the wake of both circular cylinders and airfoils. Through still photographs and films, he was able to qualitatively estimate the flow field. Based upon these observations, he assumed pressure waveforms and computed the spectrum of the static pressure in the wake. Kavrak noted that vortices shed from the airfoil were neither regular in size or shape. They tended to grow while being convected downstream but did not change shape. The vortex cross section appeared to be elliptical with an axis ratio ranging from 2 to 6. The vortex pattern for an airfoil wake was like that of a rectified signal, not thealternating vortex pattern typically seen in flow around cylinders.

In a later paper (12), Kavrak measured the fluctuating static pressure in the wake using a probe designed for the purpose. He observed the most intense pressure fluctuations in the regions of maximum shear stress. The observations were used to develop a model based on curve fits to the various measured parameters. The vortices were assumed to be elliptic waveshapes. Pressure-time histories were fitted using least squares methods and the resulting functions were Fourier transformed to yield spectra of the pressure. Once the various curve fits required were completed, the maximum pressure in the wake was expressed

in the functional form

$$\frac{P_{max}}{\frac{1}{2}\rho_o \bar{U}^2} = F(Re)\frac{Y_2}{b}\exp\left(-\sigma\frac{Y_2}{b}\right)$$
$$\left\{\exp\left[-.05(\alpha-\alpha_o)^2\right] + 0.02(\alpha-\alpha_o)^2\right\}$$

where F(Re) is a Reynolds number dependent function, α = angle of incidence, α_o = incidence angle at minimum drag, b is the transverse distance from the center of the wake to the 1/2 maximum velocity point. Sound measurements were made with a rotor made up of four airfoils located with their spans parallel to the axis of rotation. A microphone placed on this axis measured the radiated sound. Comparisons of wave shapes between the radiated sound and the pressure in the wake were made. No actual quantitative comparisons were presented comparing source pressure to radiated sound levels. For such a geometry, one would expect significant interaction effects due to the wakes acting as an inflow turbulence mechanism. The frequency content of these interactions may be such as to avoid the problem.

While the above research was being carried out in Istanbul, B. D. Mugridge was approaching the problem somewhat differently in England. Mugridge (13) attempted to relate sound generation to the covariance of static pressure on one side of an airfoil. He obtained a relationship for the power spectrum of the force fluctuation on the blade and identified the fluctuations with eddy shedding. Assuming the eddies to be convected along at some fraction of the free stream velocity, he was able to express the force spectrum for the airfoil. In any method of this type, some measure of the spatial extent of the correlation must

be made. In this case it is the correlation area on the airfoil surface. The method used by Mugridge was to compare the radiated sound to the autospectrum of the static pressure at one point on the airfoil surface. By forming a ratio of these two quantities in a way which would account for the geometry of the radiation path, an estimate of the correlation area could be obtained. The idea was to measure the cause (the surface pressure) and the effect (the radiated sound), then determine the correlation area required to get the correct answer. The experimental measurements were made on a custom airfoil design (which appears to have a thickness to chord ratio of 0.20) mounted in a wind tunnel. The airfoil was cambered so that the boundary layer turbulence would be most confined to the suction surface. This would validate the one sided integration procedure. Radiated sound was taken as that picked up by a pressure transducer mounted on the wall of the wind tunnel. Area ratios based upon the ratio were

$A_c/A = 1/5$ at 1 kHz, and $A_c/A = 1/45$ at 2.5 kHz

When compared with results taken by Schloemer (14) for boundary layers with adverse pressure gradients, some estimate of what might expected was obtained. These estimates were

$A_c/A = 1/15$ at 1 kHz, and $A_c/A = 1/90$ at 2.5 kHz

No explanation was advanced for the differences. Mugridge concluded the problem would be resolved when experimental measurements of A_c could be made directly using two surface mounted static pressure transducers. The measurements were made with a cambered airfoil and efforts were made to insure the bulk of the turbulence would be generated on the suction side of the

airfoil. One way to eliminate the integration on the back side is to make the boundary layer very thin on that side. That was apparently the aim in Mugridges's method.

In a later paper (15), Mugridge presented cross correlation measurements between the surface static pressure at 84% of the chord with the longitudinal component of turbulence in the boundary layer near the trailing edge of the airfoil. He found substantial correlation between the surface static pressure and the velocity in the outer edge of the boundary layer. This correlation had not been seen in similar measurements taken on wall boundary layers. The large eddy structure in the outer region was felt to be relatable to the higher pressure levels measured for airfoil surfaces as compared to those pressure levels measured in wall boundary layers at similar flow conditions. The airfoil surface pressure levels were typically 15 dB above those for the wall boundary layer. Obviously there was something significant about the trailing edge.

Some measurements of overall turbulence length scales were made in the wake of the airfoil using spatial correlations. These were found to collapse fairly well if the wake momentum thickness was used in the normalization.

The third approach to the airfoil sound generation problem was made by the present author (16). In this program the net force fluctuation on the airfoil was related to the momentum fluctuations in the airfoil wake. The relation was established using the unsteady form of the integral momentum equations. The component of momentum normal to the airfoil chord was taken as the forcing function for the sound generation. This required

measurement of the transverse component of turbulence. In this model the correlation required was the volume of correlated momentum in the wake of the airfoil. This was obtained through measurements of the correlation lengths in the three coordinate directions. The correlation volume was taken as that defined by the two point velocity correlations measured using two single wire sensors. This meant that the volume for the transverse component would be assumed to be identical to that for the stream component. The spectrum of the normal component was determined using an x-probe hot wire sensor. In this way even if the volume was determined using the longitudinal component the magnitudes would be correctly measured. These results were then combined to predict the spectrum of the radiated sound. The resulting expression was

$$\overline{p^2}(\vec{x},f) = \frac{4f^2\rho_0^2\bar{U}^4 l_{y_3}^2 l_{y_2}^2}{a_0^2 r^2}\left(\frac{u_2'}{\bar{U}}(f)\right)^2\left[16\pi^2\left(\frac{f\,l_{y_1}}{\bar{U}}\right)^2\right]$$

When this prediction was compared with measured sound radiation data for the same airfoils, fair agreement was obtained. The experimental sound radiation data was obtained for the airfoils located in the potential core of a free jet discharging through an anechoic chamber. In the facility both the magnitude and the radiation pattern could be obtained. The predicted levels were usually lower than those measured over the entire frequency range. The prediction has now been seen to contain an error in the formulation. The same mistake was made as that mentioned before by Gerrard. The dependence on the span correlation should be on the product of the span correlation length

and the actual span length not on the square of the span correlation length as was shown above. For the particular model above and the data with which it was compared, the difference would add 6 dB to the entire spectral level predicted. This increases the predicted spectra to levels having better agreement with those measured.

The major failing of the model was the poor prediction of the spectral levels at higher frequencies. There was a consistent tendency to overpredict these levels. This was known to be due to the usage of a constant value for the correlation lengths where in fact the correlation length is expected to decrease with increasing frequency. It was the development of this more complete model where the correlation lengths would be measured for the particular velocity component of interest and the lengths would be determined as functions of frequency which formed the basis for the present study.

Measurements of radiated sound from single airfoils have been recently presented by a group at the United Aircraft Research Laboratories (17). This laboratory has built a very complete facility for the measurement of sound radiation from airfoils. The facility consists of a large open throat wind tunnel having its test section in an anechoic chamber. At the time of the present report the background noise levels were quite high, hopefully these will be reduced to levels allowing better resolution in test results. In the data reported, a pure tone was observed over a wide range of Reynolds numbers, in fact several pure tones were observed at various operating

conditions. No explanation other than vortex shedding was advanced. This tone phenomenon was observed to be dependent upon the incidence angle, increasing the incidence angle increased the probability of appearance of the tone(s). Surface pressure correlations in the form of two point space correlations were made using transducers. In the fully turbulent, no tone, region no correlation was observed in the span direction. The transducers used were 1/2 inch diameter microphones located on a 9 inch chord airfoil. The diameter of the transducers is larger than the correlation length. Because of this the auto-spectra taken must be held suspect since the response is surely an average of the pressure over the face of the microphone. This might be expected to substantially underestimate the surface static pressure.

It was because of the small correlation lengths which this author had observed in previous work (16) that the approach of relating the net force fluctuation on the airfoil to the momentum fluctuation in the wake was taken. The greater spatial resolution and ease of probe placement versus the problems associated with positioning and calibration of surface transducers was felt to justify the more indirect wake momentum approach.

3.0 Models for the Prediction of Sound Radiation

In this section the models used for prediction of sound radiation by both single airfoils and rotors are outlined. The motivation for the development of a single airfoil model is twofold. As a component of a rotor, understanding the sound generation characteristics of the airfoil can help in understanding similar mechanisms on the rotor. Secondly, if sufficient confidence can be established in the concept of relating net force fluctuation to near wake turbulence, then this approach may be useful in studying noise generation by the airplane itself exclusive of the engine noise.

The rotor model is based upon a rotating array of fluctuating forces simulating the forces on the blades. The force on each blade is defined in terms of the experimental measurements and the single airfoil model.

3.1 Single Airfoil Model

It may be seen from the Curle solution to the wave equation that three possible mechanisms exist for the generation of sound by a stationary airfoil in a smooth turbulence free flow. These are the boundary layer related pressure fluctuations, force fluctuations due to some net effect like vortex shedding, and turbulent stress fluctuations of the boundary layer and wake turbulence. The second mechanism has been chosen as the dominant one for the present case. Boundary layer noise has been discounted based on results of both Sharland and Mugridge which indicate boundary layer noise to yield too small a sound level (down approximately 15 dB from measured results. Direct radiation from wake turbulence has been discounted because of

measured radiation patterns and velocity dependencies of SPL. Experimental results for several surface contours, incidence angles, and Mach number range indicate a dependence of overall radiated SPL on velocity to the 5.5 to 6th power. The examples of these dependencies may be seen in Figures 2 and 3. Direct radiation from the turbulent stresses would result in an 8th power dependence on velocity. The fact that the sound radiation is observed to occur at the same frequency as the transverse component of turbulence in the wake further supports the dominance of this dipole mechanism. This similarity in the spectra may be seen in the results presented in reference 16.

If the sound generation mechanism is accepted as some form of surface wake interaction, what can be done to relate it to aerodynamic performance? Recall the far field solution for a net force fluctuation on a body immersed in a flow was

$$\rho(\vec{x},t)-\rho_0 = \frac{1}{4\pi a_0^3}\frac{x_i}{|\vec{x}|^2}\int_S \frac{\partial p}{\partial t}(\vec{y},t)\,dS(\vec{y})$$

The most natural approach might be to form the density covariance then observe that the forcing function is the covariance of the surface static pressure. The primary reason that this approach was not taken in the present investigation was the concern that the correlation lengths required for determination of the correlation areas would be smaller than the spatial resolution capabilities of the transducers which would be available for the measurements. It was thought that if a method relating sound generation to the aerodynamics of the wake directly could be established then perhaps a simpler relationship for the mechanism in terms of normal aerodynamic performance would result.

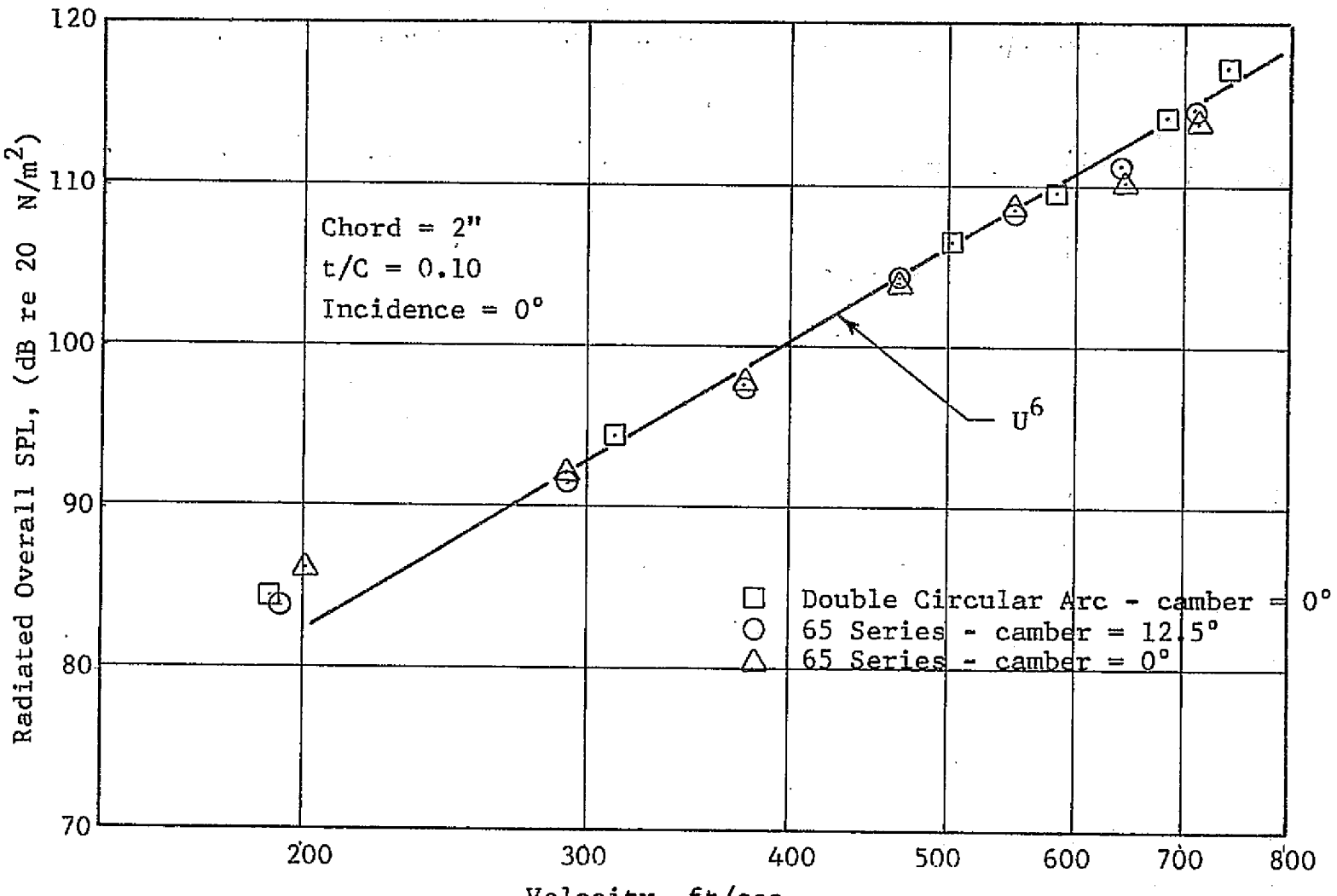

Figure 2 Dependence of Overall SPL on Velocity for Different Airfoil Shapes

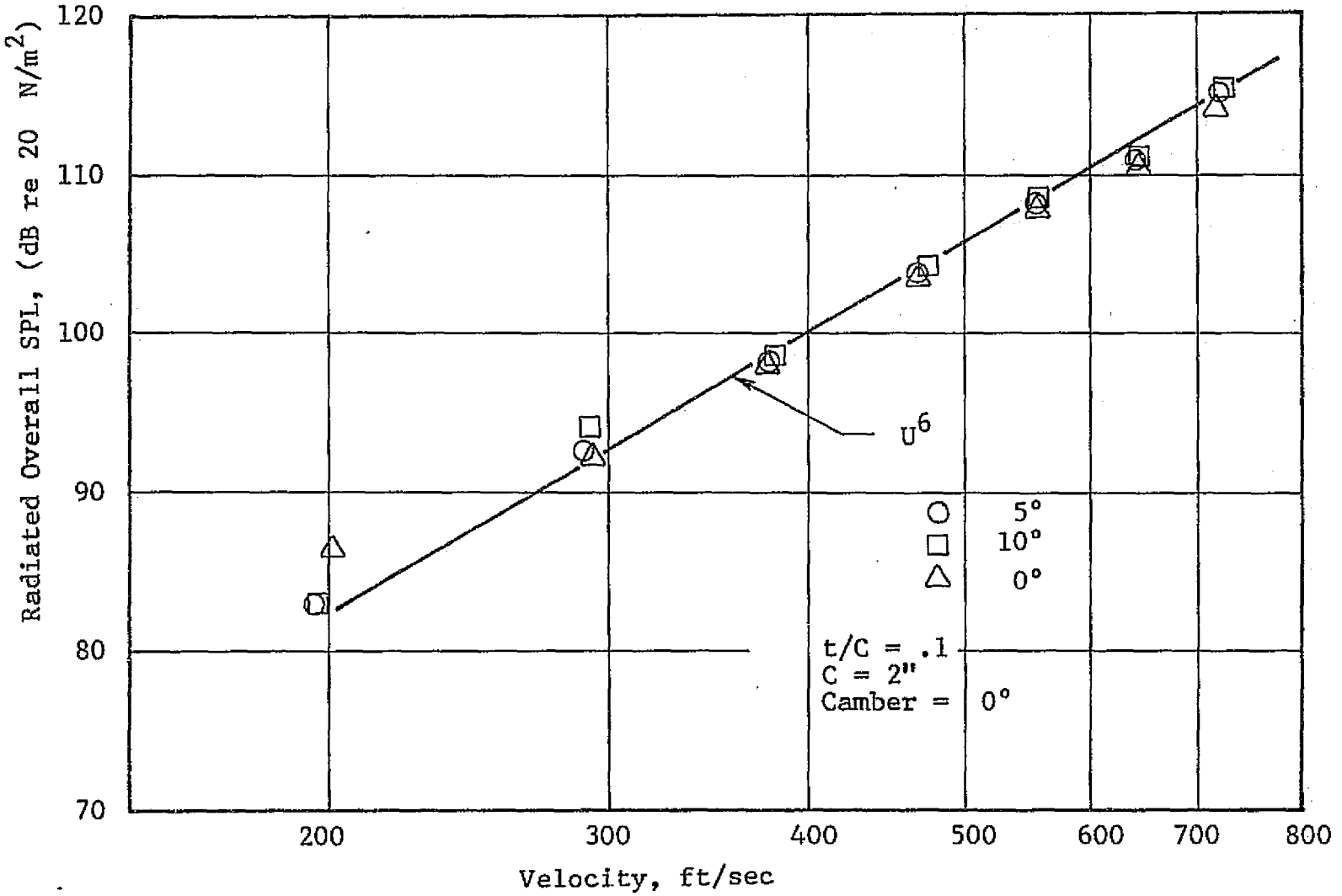

Figure 3 Dependence of Overall SPL on Velocity and Incidence Angle for 65 Series Airfoil

In addition, the measurement of the turbulence structure of the wake could be carried out using hot wire sensors thereby allowing reasonably good spatial resolution of the correlation lengths.

Since the sound generation has been shown to be relatable to the net force fluctuations on the airfoil, a simple method can be used to relate these force fluctuations to wake turbulence. If the Gauss divergence theorem is applied to the above integral for the pressure on the body and the momentum equation is used to relate the resulting pressure gradient to velocity, the following correspondence can be written:*

$$\int_S \frac{\partial p}{\partial t}(\vec{y},t)\,dS(\vec{y}) = \int_{\vec{y}} \frac{\partial^2}{\partial t^2}\rho\vec{u}(\vec{y},t)\,d\vec{y}$$

This states that the net force fluctuation is equal to the net momentum fluctuation in the airfoil wake.

The idea of the model is the wake immediately following the airfoil will reflect the net momentum on the blade since it is here that the boundary layers from both sides will mix, static pressure variations on both sides will balance and the resultant effect will be reflected in the momentum in the wake in the region of mixing. If one takes surface integrals on one side of an airfoil and then predicts the sound generation based upon that, in effect, it is assumed that the two sides are uncorrelated. It seems to be more reasonable to allow the effects of the two sides to average out in the near wake then use that averaged effect as the measure of the net force fluctuation on

*Details are presented in Appendix A.

on the airfoil.

The net force fluctuation on the airfoil is then to be approximated by the momentum in the wake volume immediately downstream of the airfoil. Details of the development are somewhat lengthy and are presented in detail in the appendix. The near wake is taken as the correlation volume nearest the trailing edge of the airfoil. This volume is defined as the product of the correlation lengths in the three coordinate directions. The integration for the resulting covariance of the two point velocity correlations would be the wake thickness, the airfoil span, and the total correlation length in the stream direction. The particular correlation was found to be somewhat different for the longitudinal and transverse components of turbulence. This is expected since the integral scales for the longitudinal and transverse components are different even for isotropic turbulence; see for example the discussion in reference 24.

Using the above assumptions, the spectrum of sound radiation can be related to the spectra of two point velocity correlations as

$$G_p(\vec{X},\omega) = \sum_{i=1}^{2}\sum_{j=1}^{2} 16\, L_1^2(u_iu_j,\omega)\, L_2(u_iu_j,\omega)\, L_3(u_iu_j,\omega)$$

$$\int_{Y_2}\int_{Y_3} A_i A_j\, \overline{u_iu_j}(Y_1,Y_2,Y_3,\omega)\, dY_3\, dY_2\, dY_1$$

With:

$$A_1 = \frac{\rho_o \bar{U}_1}{4\pi a_o^3 |\vec{X}|}\sin\Psi \quad , \quad A_2 = \frac{\rho_o \bar{U}_1}{4\pi a_o^3 |\vec{X}|}\cos\Psi$$

and Ψ is the angle of the observer relative to a normal to the chord of the airfoil, Figure 4.

The variables L_1, L_2, and L_3 are correlation lengths defined as the frequency dependent integral scales in the three coordinate directions. These lengths are obtained from spatial integrations of a coherency function for the two point velocity correlations. In the experimental part of the program measurements of $L_i(u_1u_1,\omega)$ and $L_i(u_2u_2,\omega)$ were made directly but because of the amount of data reduction the lengths for the cross terms were not done. These lengths were taken as the arithmetic mean of the lengths determined for the longitudinal and transverse components. They were approximated by

$$L_i(u_1u_2,\omega) = L_i(u_2u_1,\omega) = 1/2(L_i(u_1u_1,\omega) + L_i(u_2u_2,\omega)) \qquad i = 1,2,3$$

There is contribution from the cross terms for non-zero incidence angles. When the wake is not symmetric, the integrals containing the cross terms do not vanish. For the data obtained in this investigation the cross terms made very little contribution to the radiated sound.

There results four terms in the expression for the radiated sound:

(1) $i = 1$, $j = 1$ corresponds to a dipole oriented along the stream direction. This term has been neglected in previous analyses based upon observations that the alternate shedding of vortices from opposite sides of the body would give a quadrapole in the stream direction. This appears to be valid for low Reynolds

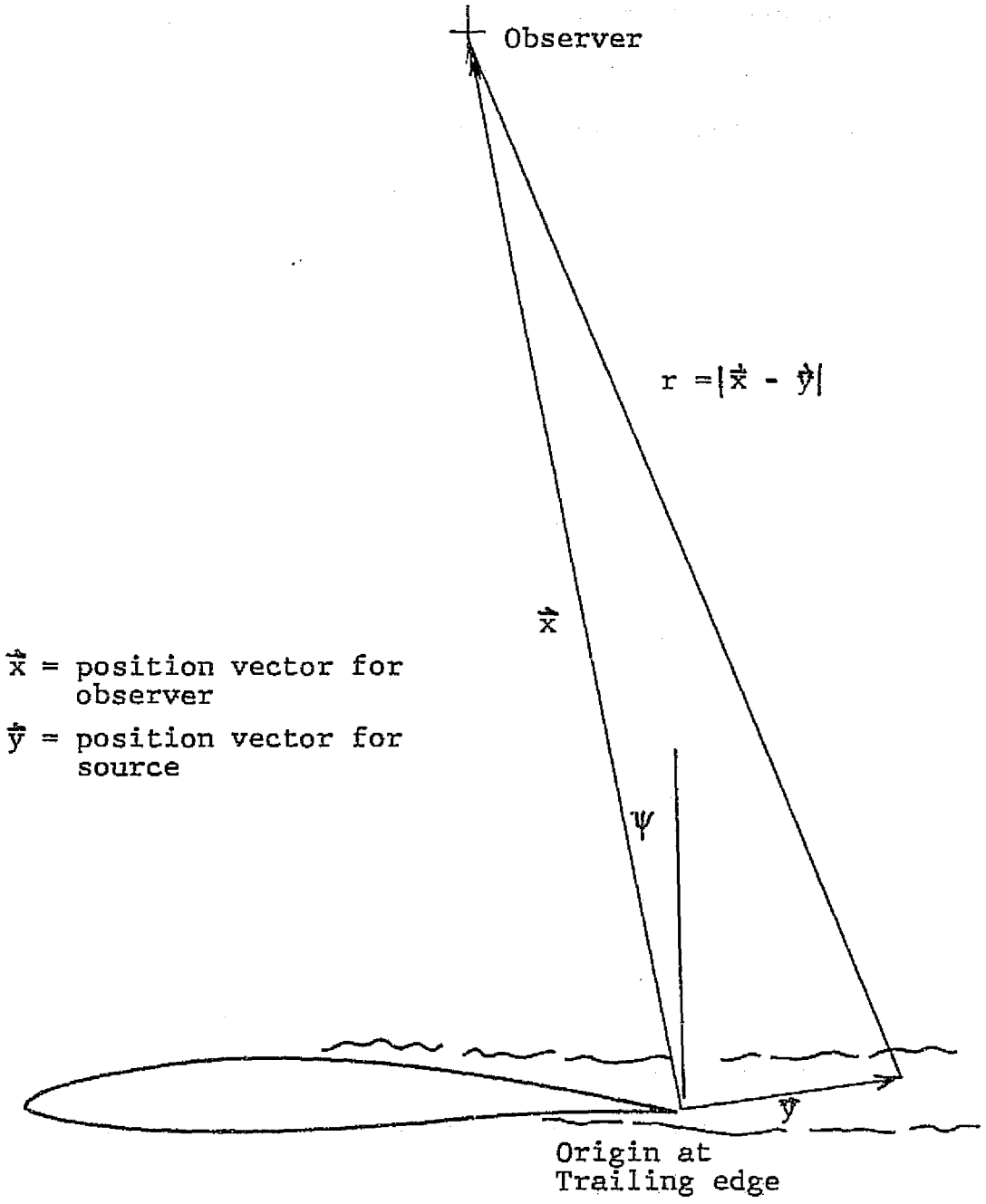

Figure 4 Illustration of Nomenclature Used in Single Airfoil Model

number flows where pure vortex shedding exists; however, for high Reynolds number flows and particularly with non-zero incidence angles it appears that longitudinal momentum fluctuations will be present.

(2) i = 2, j = 2 corresponds to the fluctuation in the transverse direction due to the transverse momentum. This is the mechanism used in previous models of vortex sound generation. It will yield a dipole aligned in the direction of a normal to the airfoil chord.

(3) i = 2, j = 1 or i = 1, j = 2 are the cross terms which are present when the airfoil operates at non-zero incidence angles. Because of the sign on the radiation angle these two terms will always subtract from the sum of the other two terms. The effect is to render the radiation pattern non-symmetric.

Contributions of these various effects will be illustrated in the results section of this report. In this section, the way the model includes the effects of non-zero incidence angles will be shown along with other aerodynamic effects. This basic model forms a starting point for the development of an engineering model which will eventually allow scaling effects to be determined. The extension of these results to the rotor is the next subject to be considered here.

3.2 Rotor Model

The analytical model chosen for extension of the single airfoil results to a rotor geometry was that presented by Ffowcs Williams and Hawkings (21). They solved the non-homogeneous wave equation for an array of sources (simple, dipole,

and quadrapole) moving in a circular path. Details of the development of their analysis into a model for the present application are presented in Appendix B.

The equation to be solved is

$$\frac{\partial^2 \rho}{\partial t^2} - a_o^2 \nabla^2 \rho = Q(\vec{x},t).$$

It has the general solution

$$\rho(\vec{x},t) - \rho_o = \frac{1}{4\pi a_o^2 |\vec{x}|} \iint_{\vec{y}} Q(\vec{y},t') \, \delta\left(t' - t + \frac{r}{a_o}\right) d\vec{y} \, dt'$$

which may also be written in terms of its generalized Fourier transform:

$$\rho(\vec{x},\omega) = \frac{e^{-i\omega \frac{r}{a_o}}}{4\pi a_o^2 |\vec{x}|} Q\left(-\frac{\omega}{a_o} \frac{\vec{x}}{|\vec{x}|}, \omega\right).$$

For the case of point forces, the source term reduces to

$$Q\left(-\frac{\omega}{a_o} \frac{\vec{x}}{|\vec{x}|}, \omega\right) = -i \frac{\omega}{a_o} \hat{r}_k D_k \left(-\frac{\omega}{a_o} \frac{\vec{x}}{|\vec{x}|}, \omega\right)$$

where D_i is the magnitude of the dipole force.

These general results are reduced for the particular case of an evenly distributed array of blades each with its force uncorrelated with the others. The forces on the blades are assumed to be stationary random processes. With these assumptions, the radiation of sound from a multibladed rotor can be approximated as

$$G_p(\vec{x},\omega) = \frac{1}{16\pi^2 a_0^4 |\vec{x}|^2}\left(\frac{\omega}{a_0}\right)^2 \sum_{n=-\infty}^{+\infty} \sum_{k=1}^{B} d_r(\theta_k, t-n\Omega) d_r(\theta_k, n\Omega - t)$$

$$J_n^2\left(\frac{-\omega R_s \sin\phi}{a_0}\right)$$

where d_r is the component of the force in the direction of the observer.

Notice that the assumption that the entire blade span may be approximated by a single force vector is quite restrictive in that the blades of practical interest are usually long and the aerodynamic properties vary significantly along the span. A span distributed result can be obtained by breaking the rotor into annular segments then adding the sound radiation which results from each segment to get the total radiation from the rotor. The reason this simple procedure worked is because the correlation which exists in the span direction is small. Each radius along the blade span radiates essentially independently of the others so the use of a simple summation is valid.

3.2.1 Relation to Single Airfoil Results

The next step is to use the single airfoil wake model to describe the force on the individual blades of the rotor. The total force on the blade is taken as the integral of the pressure over the blade surface. This is the same procedure used in the single airfoil model development. The force is

$$d(\theta_k, t) = \int_{S(\theta_k)} -p(\vec{y},t)\, dS(\vec{y})$$

From the single airfoil model write

$$\int_S p(\vec{y},t)\, dS(\vec{y}) = \int_{\vec{y}} \frac{\partial}{\partial t} \rho \vec{u}(\vec{y},t) d\vec{y}$$

Now transform to express this in terms of frequency:

$$d(\theta_k,\omega) = i\omega\rho_o \int_{\vec{y}} u_k(\vec{y},\omega)\, d\vec{y}$$

The result for the modulus of the force fluctuation is

$$d_r(\theta_k, f-n\Omega)\, d_r^*(\theta_k, f-n\Omega) = (\omega - 2\pi n\Omega)^2 \rho_o^2\, \hat{r}_k \hat{r}_l$$

$$\int_{\vec{z}} \int_{\vec{y}} G_{u_k u_l}(\vec{y},\vec{z},\omega-2\pi n\Omega)\, d\vec{y}\, d\vec{z}$$

The results have been left in terms of the power spectrum of the two point velocity correlations. These correlations can now be expressed within the assumptions of the single airfoil model as

$$\hat{r}_k \hat{r}_l \int_{\vec{z}} \int_{\vec{y}} G_{u_k u_l}(\vec{y},\vec{z},\omega-2\pi n\Omega)\, d\vec{y}\, d\vec{z} =$$

$$\sum_{k=1}^{3} \sum_{l=1}^{3} \hat{r}_k \hat{r}_l\, 16\, L_1^2(u_k u_l, \omega-2\pi n\Omega)\, L_2(u_k u_l, \omega-2\pi n\Omega)$$

$$L_3(u_k u_l, \omega-2\pi n\Omega) \int_{Y_2} \int_{Y_3} \overline{u_k u_l}(Y_1, Y_2, Y_3, \omega-2\pi n\Omega)\, dY_3\, dY_2$$

This result was programmed to form a prediction of the radiated sound from a rotor due to the random force fluctuations experienced during operation in a smooth turbulence free flow.

3.2.2 Computer Program for Rotor Sound

Discussion of the computer program developed for the rotor sound prediction will be brief; the approach was fairly straight forward. The complexities in coding the model results in a fairly substantial effort to get the computer program checked

out.

Characteristics of the sound mechanisms are known relative to the individual blades as given by the single airfoil model. These blades are arrayed to form a rotor; each blade is set at an angle to the rotor axis to properly align with the relative velocity vector (stagger angle plus incidence). In order to express the properties on the individual blades in the rotor coordinate system, two changes of basis were required. The first was to unrotate the stagger angle and the second was to go from the blade to the observer coordinate system.

Details of the algebra are not presented here. It is sufficient to state that the program was checked out using constant force vectors on the blades and comparing the resulting tone noise generation with other available methods. Another check of the method was made by setting the rotor speed to zero so that the rotor degenerated to a set of stationary airfoils. The spectra for this case agreed with the single airfoil model. It was felt the rotor program was functioning correctly.

4.0 Experimental Program

The experimental program consisted of two parts. Initially tests were made using a 25.4 cm chord airfoil located in the potential core of a free jet tunnel at the University of Washington. Correlations of wake turbulence using two single sensors were made to provide some information on the physical dimensions of the correlations to be measured in the larger test facility at the NASA Ames Research Center. These measurements in the Ames 7 by 10 subsonic wind tunnel #1 using a 91.4 cm chord airfoil will form the major part of the experiemntal results.

The purpose of the experiment conducted at Ames was to determine the power spectra of the two point velocity correlations in the wake of a single airfoil. The airfoil used was representative of contours used in helicopter rotors (NACA 63-009). A large airfoil, 91.4 cm chord, was used to insure the measurements would be made at a high Reynolds number and thereby avoid the uncertainties existant in the transitional flow regime.

Estimates of the two point velocity correlations, u_1u_1, u_1u_2, u_2u_1, and u_2u_2 were made using two x-probe hot wire sensors. Cross power spectral densities of signals from these four hot wire sensors were used to obtain the required spectral data. Notice that correlations of the velocities in the span direction were not studied. The two point correlations in the span direction would be expected be strictly a volume turbulence effect since there is no surface for them to exert a force on. They are parallel to the airfoil. A single traverse was made in order to estimate the magnitude of this turbulence component

and as expected it was found to be comparable to the other two components.

As a check of the accuracy of the four wire method additional cross power spectra were taken using two single wire sensors. This yielded the u_1u_1 spectrum. It was felt that data from these single wires are probably more accurate than those from the x-probes because of the reduced possibility for probe interference effects. It was expected this increased scope in the experiment would help in evaluating the confidence limits of the four wire method.

Data reduction was performed from data stored on magnetic tape. Details of the test facility, instrumentation, and test procedure are given below.

4.1 Test Facility

As mentioned above the Ames 7 by 10 subsonic wind tunnel #1 was used for this investigation. This tunnel is normally used to measure forces and moments needed to evaluate aerodynamic performance of flow models. The tunnel is a recirculating type driven by electric fans. Speeds in excess of 60 m/sec are readily available, although in this test a fixed speed of 45.6 m/sec was used. The entire two story building in which the test section is located is sealed while the tunnel is running which means the control room pressure is equal to the static pressure in the test section. Leaks do not cause any particular difficulty with this arrangement since there is little or no flow through them. Control of the test section velocity is simply done using a rheostat. The tunnel held its setting quite

well for most of these tests. However, when the airfoil was set to the 6 degree angle of attack, some drift was experienced.

The airfoil used was a 91.4 cm (36 inch) chord NACA series 63-009 contour having zero camber angle. The aspect ratio of this airfoil was approximately 1.5 so that care had to be exercised to insure the flow was straight and parallel. Tufts were attached along both sides of the airfoil above and below the projected traverse plane and the flow was observed to be acceptably parallel in the region of the measurements when the angle of incidence was at zero degrees. Only one survey point was taken at 6° incidence because it was expected that the flow would be three dimensional and unreliable for an airfoil of such a low aspect ratio.

Velocity in the test section was set using a pitot static probe mounted in the test section upstream of the model. Readout was made on a vertical water manometer. Pressure variation was less than 2.5 mm of water for the tests reported here.

Turbulence levels of the test section were measured with the movable probe traversed out into the potential flow. The level was found to be very low. The longitudinal component was measured to be 0.5% on an RMS basis and the transverse component was less than this. The measurements were made by recording the peaks of the autocovariance functions and the levels were too low for the transverse component to load the SAICOR Correlator used for the measurement. The level could have been determined using a true RMS meter had it been convenient and necessary to the purpose of the experiment.

The Reynolds number corresponding to the test airfoil and

flow condition was approximately 2 x 10^6(91.4 cm chord and 45.6 m/sec velocity).

Two x-type hot wire sensors were used, one stationary and the other movable relative to the stationary one. The stationary probe was attached to a floor mounted strut which had an elliptical cross section. The photograph in Plate I shows the installation. The stationary probe used a right angle adapter in order to get the correct wire orientation while the movable probe was on a sting mount allowing it to be positioned very close to the stationary probe. The movable probe was mounted on the tunnel traverse mechanism. This mounting allowed all three coordinate directions to be traversed by remote control. Backlash problems required that probes be always positioned from one direction. This was done throughout the testing and offered no particular operational difficulties. Estimated position uncertainties for the three directions were:

stream: -.01 cm + .01 cm

span: -.012 cm +.012 cm

normal: -.012 cm +.012 cm

Backlash in the span and normal directions was about .05 cm but this error was avoided by the test procedure described above. The stream direction traversing was done with a DISA traversing mechanism which had no discernible backlash.

4.2 Instrumentation

Data flow for the experiment was from the hot wire anemometers to magnetic tape then later from magnetic tape to the time series analyzer. A list of the instrumentation is given

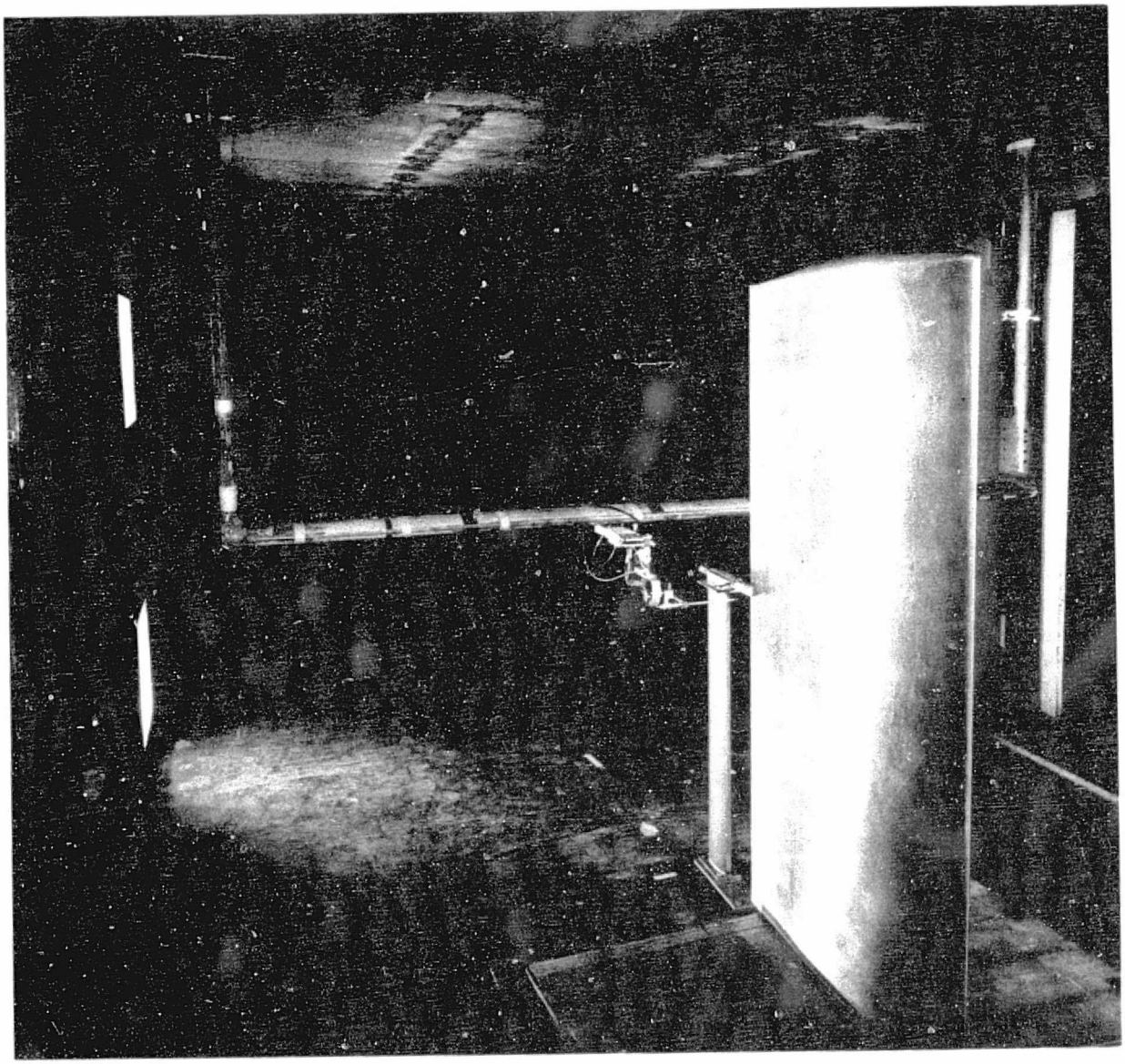

NASA Photograph

Plate I Photograph of Test Section

below and a flow chart of the data flow is shown in Figure 5.

Hot Wire Anemometry and probes:

constant temperature anemometer	DISA 55D01
linearizer unit	DISA 55D10
stationary x-probe	DISA 55A39
movable x-probe	DISA 55A38
single wire probe	DISA 55A22
DC voltmeter	DISA 55D30

Tape Recorder: Ampex FR-1300A, 14 channel
IRIG single extended, bandwidth 10 kHz at 30 ips

Time Series Analyzers:

Correlator: SAICOR model SAI-43A

Time Series Analyzer: Time Data model 1923

4.3 Test Procedure

Test procedure consisted of calibrating the probes, setting the wire sensitivities, positioning the probes and recording the data on magnetic tape. More details follow.

4.3.1 Probe Calibration

Calibration was carried out in the test section by locating the probe in the free stream away from the airfoil and varying the velocity over a range of test speeds anticipated (24 m/sec to 48 m/sec). The exponent required to set into the linearizer was then determined and set into the linearizer to yield an output proportional to velocity in the test range. The effectiveness of the linearization was checked by performing another calibration on the linearized output. The responses were found to be linear over the test velocity range.

4.3.2 Operation

Typically the sensitivity of a hot wire will vary a small amount from wire to wire. In this test the gain on the linearizers was adjusted so that all the wires were equal sensitivity.

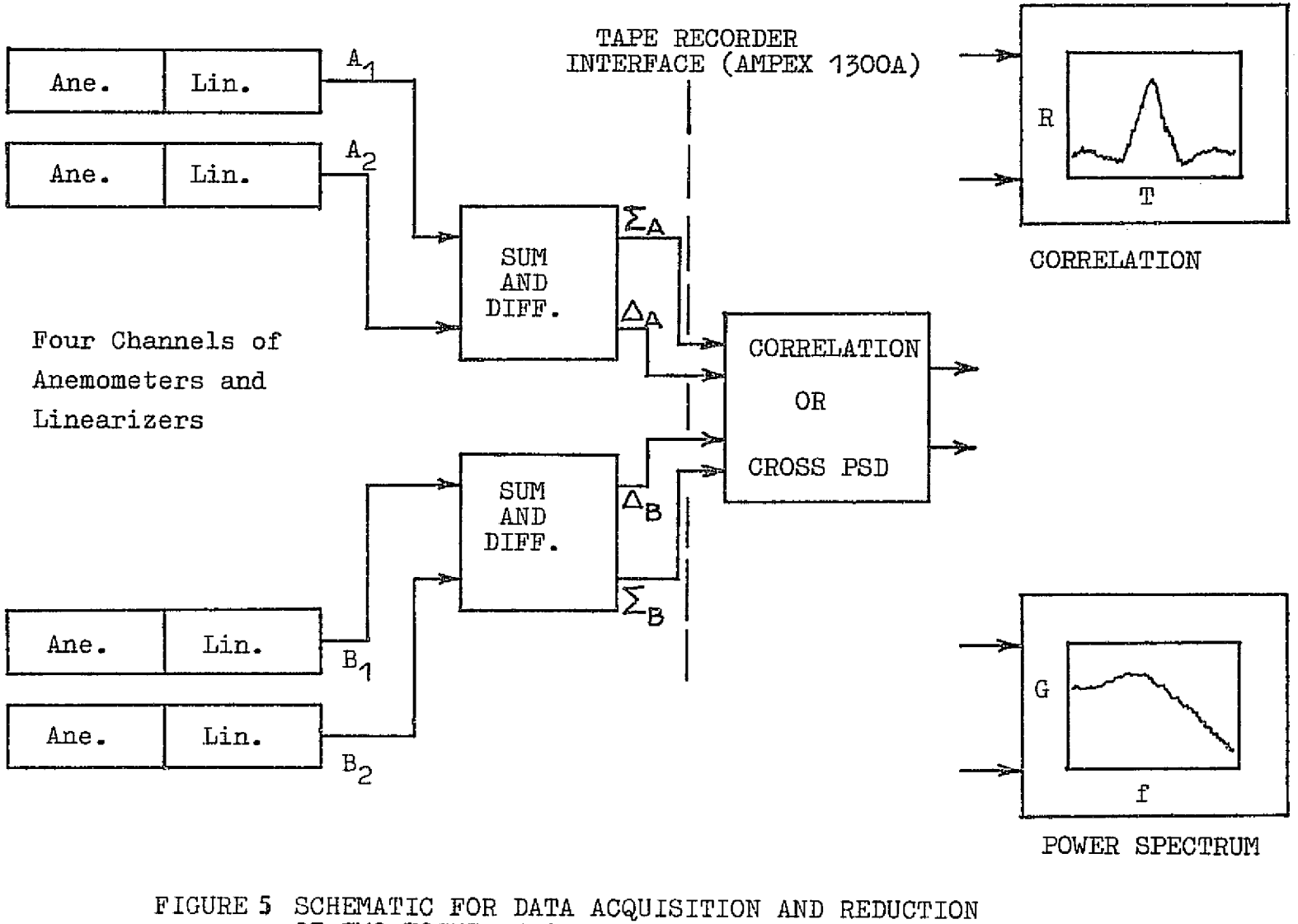

FIGURE 5 SCHEMATIC FOR DATA ACQUISITION AND REDUCTION OF TWO POINT VELOCITY CORRELATIONS

Initially the wires were set at the same overheat ratio and temperature compensation probes were used on all four hot wire circuits so the adjustment to achieve equal sensitivity was very small. This adjustment was done by locating the movable probe in the free flow region and setting the linearizer gain so that the DC levels of each of the two wires was equal. Then this probe was moved into position directly downstream of the stationary probe, that is, so the x-arrays were located in line at an axial separation of approximately 2 mm. The DC levels of the stationary probe were then set to match those of the movable one. In this way all four wires would respond to the same steady velocity with the same voltage. We observed that moving the downstream probe spanwise until it was clear of the wake of the other probe made no difference in the DC levels and concluded that the procedure was sufficient for setting probe sensitivities equal. When making correlation volume measurements, the movable probe was placed manually close to the fixed probe. The procedure used was to position the movable probe directly behind the fixed probe which had been located on the center line of the wake and a given distance downstream of the trailing edge. Spacing between the centers of the x-probes was set at approximately 2.5 mm. From this position, traverses were made in the three coordinate directions. Actual selection of spacing was made through the on-line use of the SAICOR correlator. With the cross correlation displayed on the scope, we could select separations which would provide a smooth decrease in the correlation between the two probes. If this on-line capability were missing, positioning would have been

very much more trial and error.

Once the probes were positioned, a sample of data was recorded on magnetic tape. Sample lengths varied from one to two minutes. Data recorded were:

$$e_{A1},\ e_{A2},\ e_{A1} + e_{A2},\ e_{A1} - e_{A2},$$

$$e_{B1},\ e_{B2},\ e_{B1} + e_{B2},\ e_{B1} - e_{B2}$$

where,

e_{A1} = voltage from probe A wire 1

e_{A2} = voltage from probe A wire 2

e_{B1} = voltage from probe B wire 1

e_{B2} = voltage from probe B wire 2

These data could then be analyzed to yield the cross power spectral densities of the two point velocity correlations.

Data were recorded at four axial positions for the stationary probe and an array of correlations were made at each of these positions. The axial positions used were: 3.5, 8.3, 16.7, and 36% of the chord downstream of the airfoil trailing edge and on the center line of the wake. The wake centerline was located as the point of minimum mean velocity.

The two probes were positioned as shown in Plate II. As mentioned earlier, the steady flow direction was perpendicular to the stationary probe body. This is not an ideal condition, but for these correlation measurements there was little choice if close spacings between the two probes were to be obtained without wake interference problems. One difficulty with such a mounting method is the strain gauge effect in the wire resistance which results as an effect of vortex shedding induced forces on the wire supports. If this occurs the supports

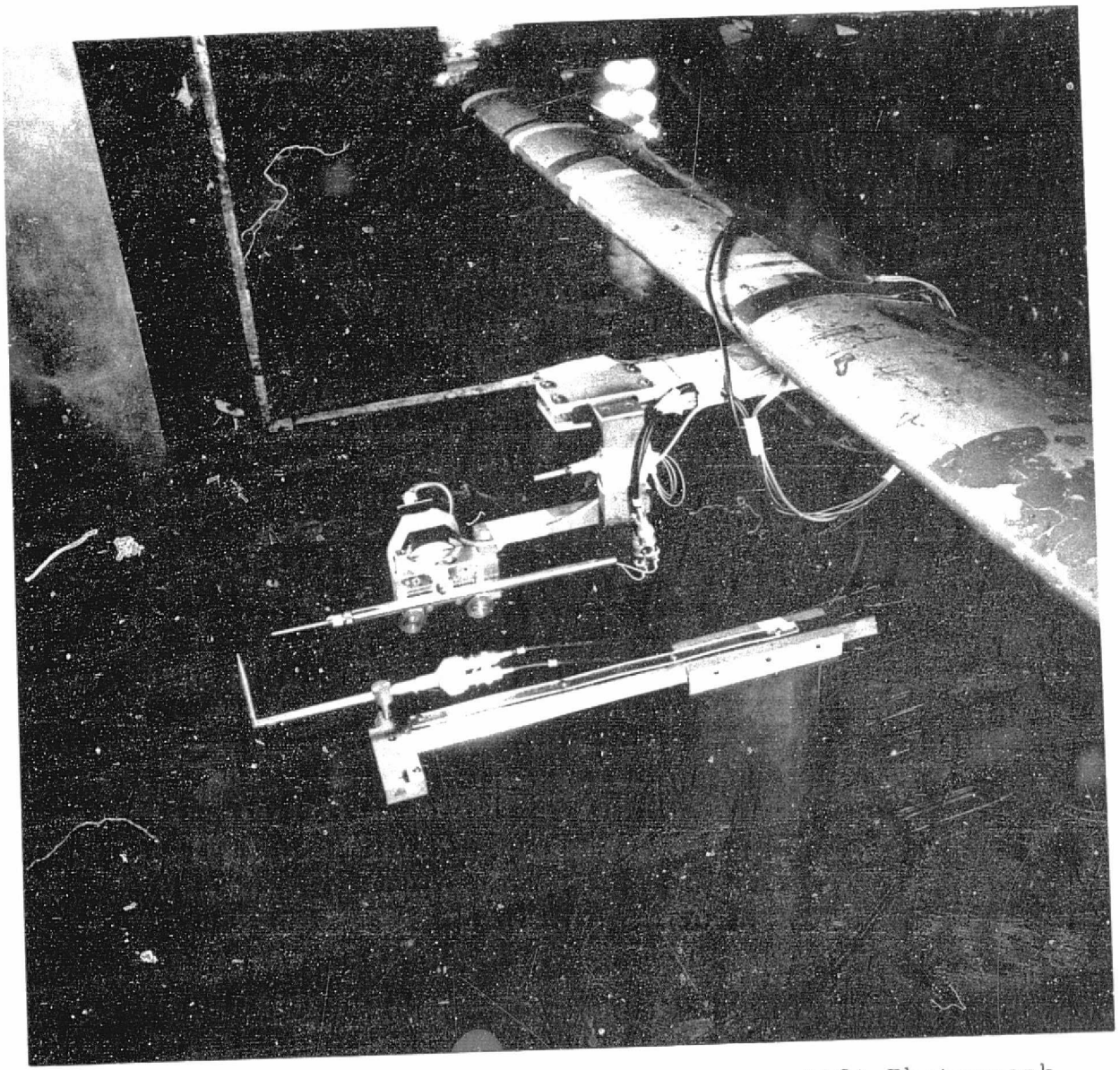

NASA Photograph

Plate II Photograph of Probe Placement

vibrate and one receives false signals at frequencies near 15 kHz. For the present case these signals were outside the frequency range of interest and masked by the levels of wake turbulence. Correlations taken on data where the probe was outside the wake did indicate the vortex shedding mentioned. The tape recorded was band limited at 10 kHz so this did not appear in the recorded data.

It was observed that one very good way for locating the wake centerline would be to use the zero shear stress since this was available on-line as the cross correlation of the "sum" with the "difference" signals taken on a single x-probe.

4.3.3 Data Reduction

Data reduction was carried out on two different time series analysis instruments. The on-line instrument, the SAICOR, was also used for data reduction of the final recorded data. This was primarily for the single x-probe data to determine the wake property distributions and cross correlations of the data from the two single wires to be used as a data check of the four wire method. The settings used on the SAI-43A were:

> Full linear averaging with 128 summations of 1024 points each. The work position was varied in order to fill the frame on the X-Y plotter. Very smooth correlations resulted from this instrument used in this way.

The cross power spectral densities were performed directly on the Time Data 1923 using its Fast Fourier transform capability. By cross correlating the sum and difference signals from the two probes, the spectra of the two point velocity correlations were obtained. The form used was the magnitude of the power spectrum.

The forms may be summarized as:

$u_1(y,\omega)\ u_1^*(y,\omega)$

$u_1(y,\omega)\ u_2^*(y,\omega)$

$u_2(y,\omega)\ u_1^*(y,\omega)$

$u_2(y,\omega)\ u_2^*(y,\omega)$

An alternate procedure to the usage of the Time Data Analyzer was to directly Fourier transform the correlation functions obtained on the SAI-43A correlator. This was done using a time series analysis program developed as part of this program. The program developed would give cross power spectra, autospectra, and present magnitude and phase information.

For data presentation the various plots were digitized using a graphics machine at the UW Computer Center which allows plots to be accurately transcribed to binary tape. The transcribed data was then conditioned to the proper physical units using further programs and plotted using a CalComp Plotter. A parabolic fit package was used for the correlation functions and a simple straight line plot was used for the spectra.

4.4 Sources of Errors in Measurements

Errors in the experimental data are larger than had been expected. The most significant errors are not due to the uncertainties in probe placement as had been expected or in the accuracy of the reading, but to what are thought to be operator errors in the data reduction and probe interference errors inherent in the two probe correlation method.

As was mentioned earlier, data reduction was carried out using both a Time Data Analyzer and a SAICOR Correlator. Reduction using the Time Data Analyzer was not performed by the

author but by a professional operator employed for that purpose. This was the only way that data could be reduced using the machine. Reduction on the SAICOR was done by the author. We were never able to make the Time Data results agree quantitatively with either the SAICOR results or with meter readings of the true RMS levels. The RMS levels computed from the correlation functions reduced on the SAICOR agreed very closely with those measured using true RMS meters.

Reduction was carried out using the Time Data Analyzer on two different occasions and significantly different results were obtained. When comparisons were made between spectra reduced by Fourier transforming the covariance functions obtained on the SAICOR analyzer and those done on the Time Data Analyzer, a disagreement of 10 dB was observed. This was for the first set of data reduced. When the second set was done disagreement of 3 dB between the two sets of data, both reduced by the same operator on the same machine, occurred.

As a result of the uncertainty in the actual levels, an alternate procedure was used to determine the correlation length estimates from this data. The cross spectra were normalized with the autospectra of the velocity at the stationary probe. This formed a kind of coherency function. Spatial integration of this function yielded the correlation lengths as a function of frequency which was the proposed use of the data. All data finally used in the airfoil wake model were reduced in the first set of Time Data results. These are thought to be self consistant. The same gain error appears to be present in all this data. The normalized data should not reflect the gain setting

error. The results are in good agreement with the correlations measured using the SAICOR derived spectra.

Another uncertainty in the data appears to be due to interference between the probes. Notice in Figure 25 that the coherence function falls off rapidly as the probes are very close to each other then as the spacing increases the correlation increases again. This effect appears to be due to some sort of probe interference. It seems to be present for the stream correlations where the probes are located downstream of each other and the effect was not observed when measurements with two single wire sensors were used to repeat the correlations. The integrations tended to reduce the error in terms of final effect on the correlation length. A similar interference probably exists for the transverse component but there was no way to check the x-probe measurements for this component. Future measurements of this type might be better done using two single wires slanted at 45° to provide the various components rather than the x-probes used here. The time for the experiemnt would be four times as long but the results should be sufficiently more accurate to justify the method. The best estimate of the error in the correlation lengths at each frequency is 15% based on comparisons between the single wire measurements and the x-probe results.

In the results presented here, the Time Data values are corrected for the suspected 10 dB error by normalization with the autospectra. For the SAICOR reduced data, in that excellent agreement was obtained with various data checks it is thought that these data are correct.

Finally, it should be noted that these measurements are somewhat involved and time consuming and errors of the magnitudes noted appear to be somewhat common in this type of data. For the purposes of the acoustic predictions, the expected maximum scatter is $\pm$ 3 dB which is sufficient although not as good as would be desired.

4.5 Experiments with a 25.4 cm Airfoil

Some preliminary testing was done using a 25.4 cm chord airfoil at the University of Washington. This airfoil was also an NACA series 63-009 contour. The test facility used was a free jet of rectangular cross section 20.4 cm by 45.7 cm. Shaping of the nozzle was done so that the wall curvature decreased uniformly to zero curvature at the exit plane thereby insuring straight parallel flow in the jet discharge. The airfoil was mounted in the potential core of the jet.

Correlation measurements were made using two single wire sensors. Space time correlations for the longitudinal component of turbulence was measured in the three coordinate directions and at four positions in the wake.

General comments regarding technique and data reduction are similar to those for the 91.4 cm airfoil except that all reduction was done using a SAICOR model 43A correlator. The primary purpose of this experiment was to establish a test plan for the program using the large airfoil. As it turned out the data were able to be used in the scaling law development described later in this report.

5.0 Experimental Results

The primary experimental results obtained in the program are the measurements of the wake turbulence for the 91.4 cm chord NACA series 63-009 airfoil. Test conditions common to the data presented for this airfoil are sumarized below:

Airfoil type: NACA series 63-009, 91.4 cm (36 inch)
Total temperature: 65° F
Static pressure: 1 atmos.
Velocity, free stream: 46.2 m/sec (150 ft/sec)
Incidence angles: 0° and 6°

5.1 Overall Wake Properties

Wake surveys were made atfive downstream positions using the movable x-probe hot wire sensor. Signals from this sensor were reduced to yield mean velocity, the longitudinal component and the transverse component of turbulence.

Mean velocity profiles are presented in Figure 6, RMS turbulence profiles for the longitudinal component in Figure 7, and for the transverse component in Figure 8. These distributions were used in the airfoil prediction model. In addition, some data were checked with longitudinal turbulence component measurements made with a single wire sensor. RMS levels between the two probes, the x-probe and the single wire, agreed to within 6%.

A mean velocity profile was taken 1.2 mm downstream of the airfoil trailing edge. This was obtained using a single wire probe so that very fine spatial resolution would be obtained. The profile is shown in Figure 9. This profile was used to compute the wake momentum and displacement thicknesses used in the data evaluation. Drag coefficients based on the measured momentum thickness agreed with published results very closely. This

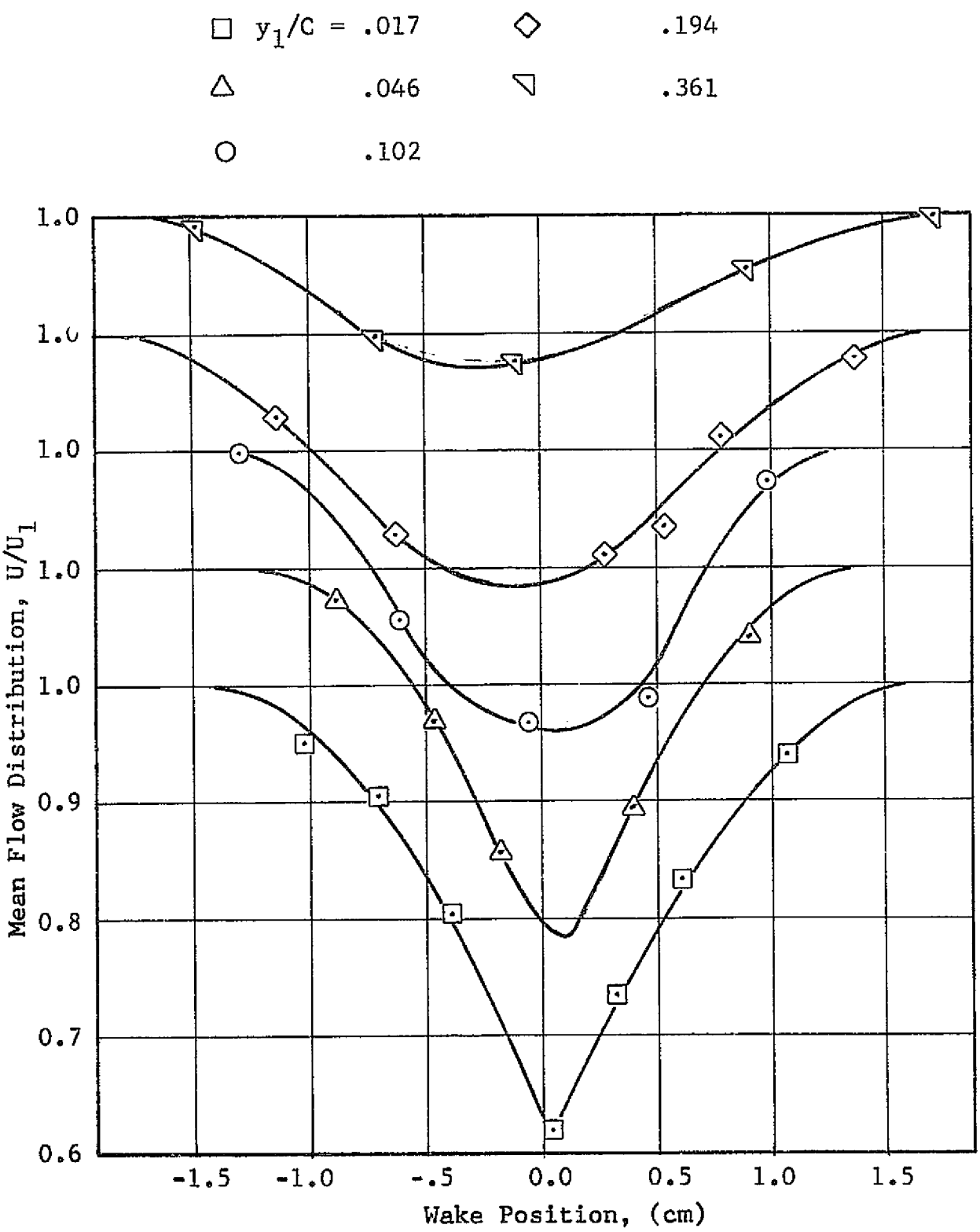

Figure 6 Distribution of Mean Velocity in the Wake of the 36 Inch Chord Airfoil - Nondimensional

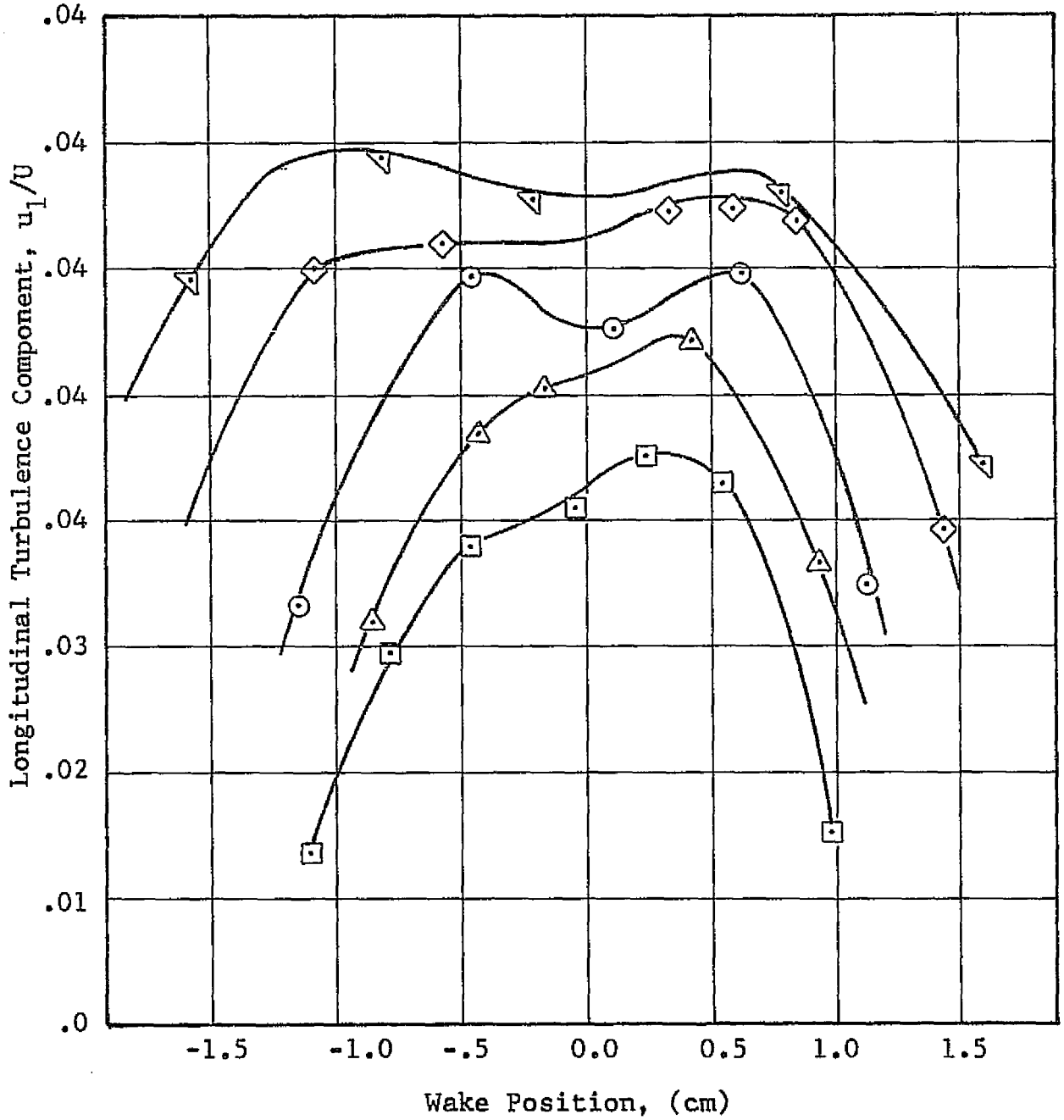

Figure 7 Distribution of Longitudinal Component of Turbulence in Airfoil Wake (RMS Level)

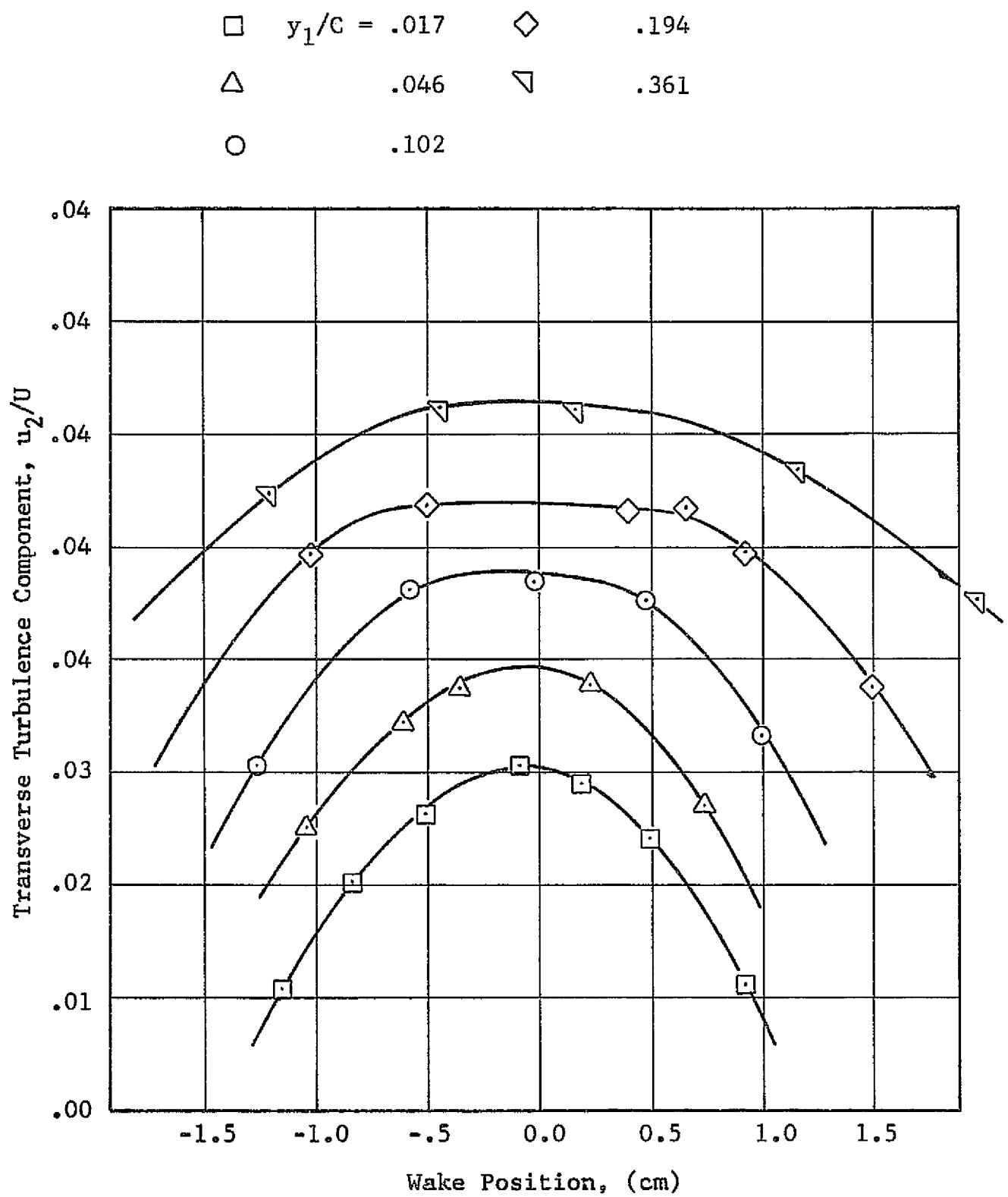

Figure 8 Distribution of the Transverse Component of Turbulence in Airfoil Wake (RMS Level)

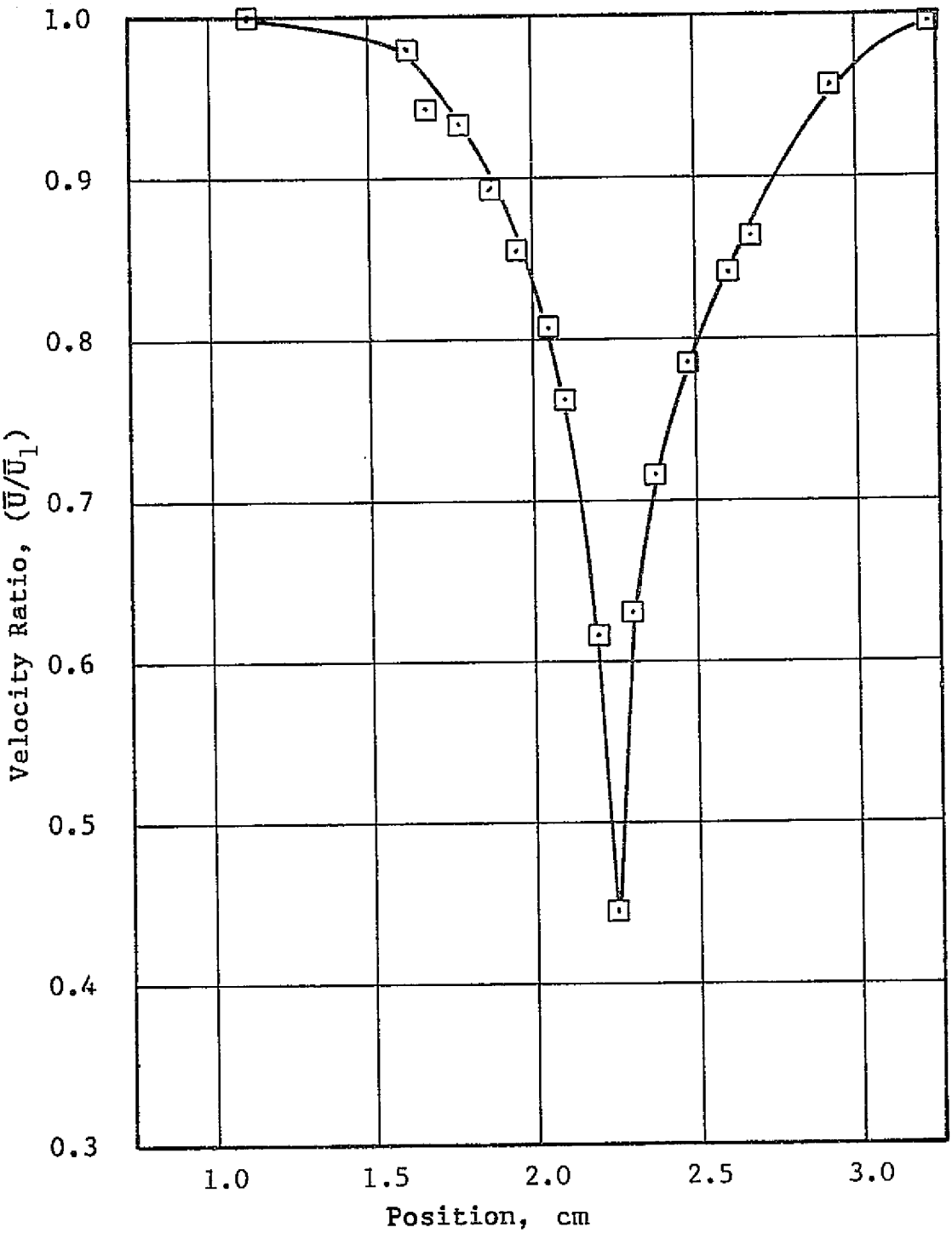

Figure 9 Mean Velocity Profile in Airfoil Wake, 91.4 cm Chord, $y_1/C = .014$

helps provide confidence in the measured profile.

An indication of the wake development can be seen from the centerline changes of the properties along the stream direction. Centerline distributions of the mean velocity and the two turbulence components are shown in Figures 10 and 11. Notice that beyond 0.10 chord downstream the mean velocity defect is decreasing at a 0.5 power as would be expected for a wake in the self preservation range. In terms of displacement thickness this corresponds to 70 thicknesses. Reference to turbulence literature suggests that self preservation does exist by this distance, but only for the mean velocity not higher moments.

5.2 Power Spectra of the Turbulence Components

The power spectra for the longitudinal and transverse turbulence components were obtained by a Fourier transform of covariance functions determined using the SAICOR correlator. These power spectra are presented for each of the five stream positions for the wake centerline. This centerline spectrum was observed to be representative of the turbulence in the main part of the wake.

Power spectra for the longitudinal component are presented in Figures 12 through 16. Notice that there appear to be three spectra on each figure. The data shown are a Fourier transform of both sides of the measured auto covariance function and a cross spectrum of the entire function (two sided). This method gives a measure of the error in the entire procedure used in the data reduction from the auto covariance measurement through its manual digitization and Fourier transform. Notice that errors are negligible except for the high frequencies where the

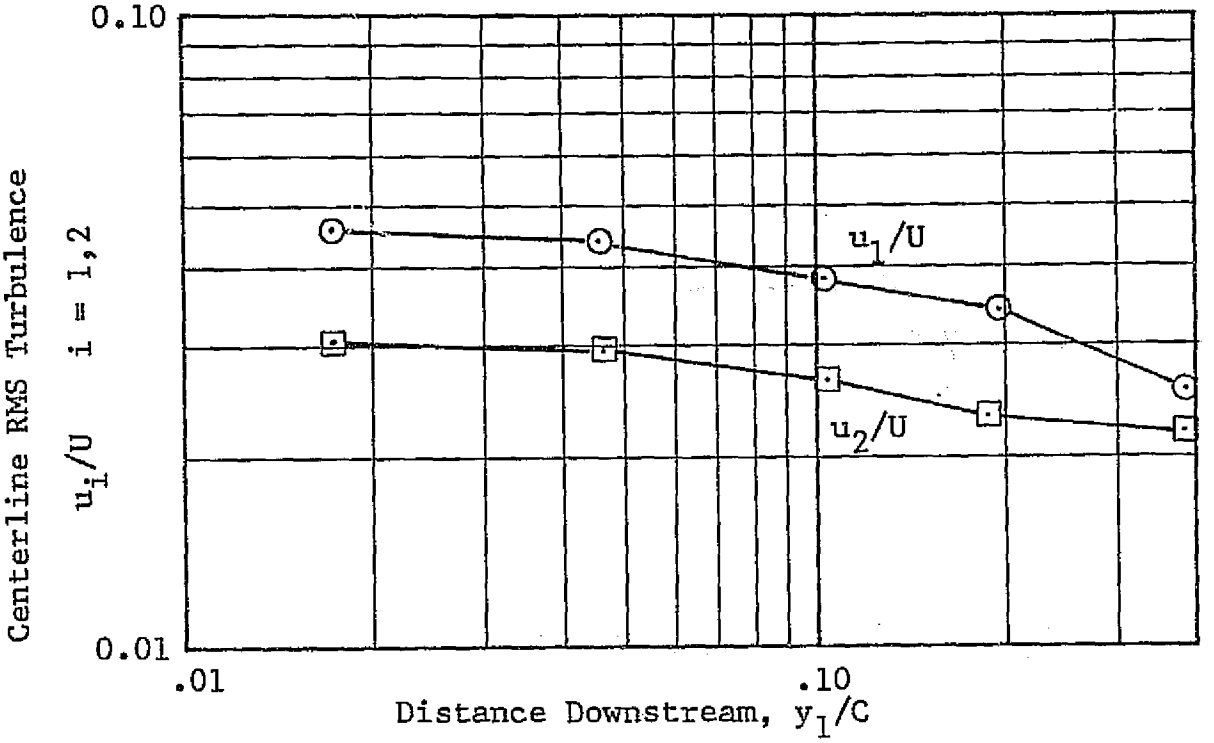

Figure 10 Distribution of RMS Turbulence in the Stream Direction - Stream and Normal Components

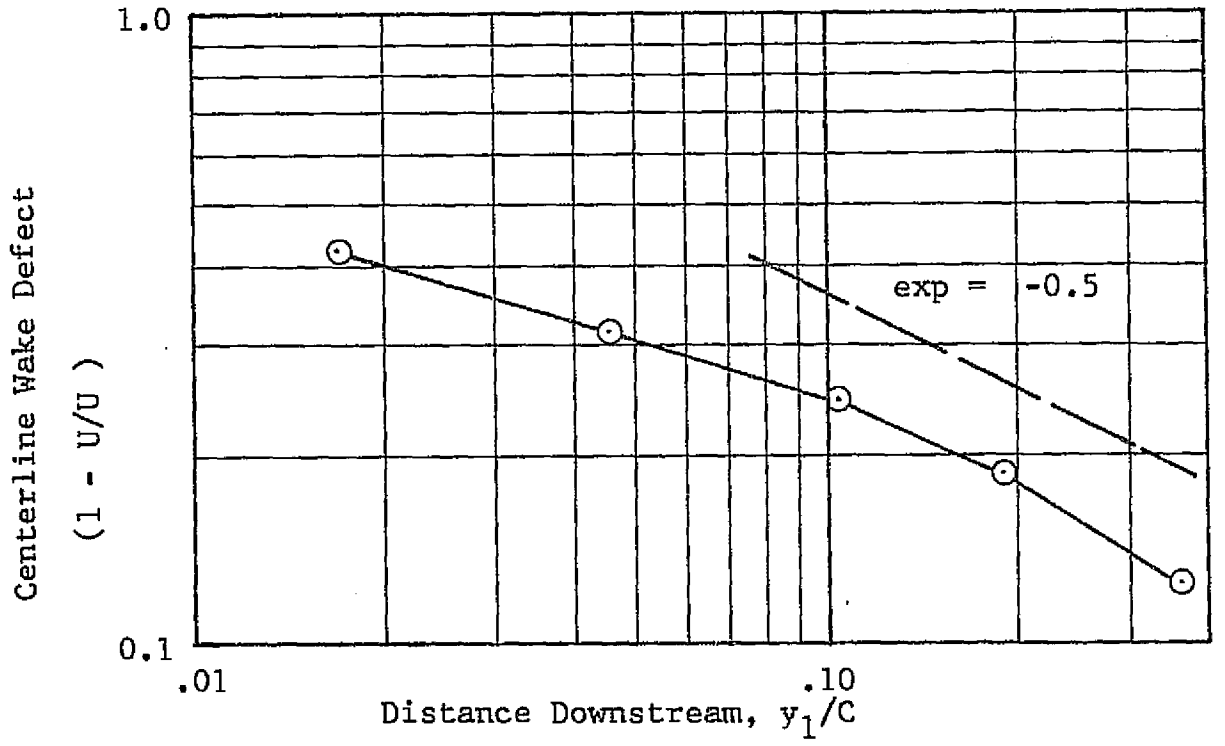

Figure 11 Distribution of Centerline Velocity Defect in the Stream Direction

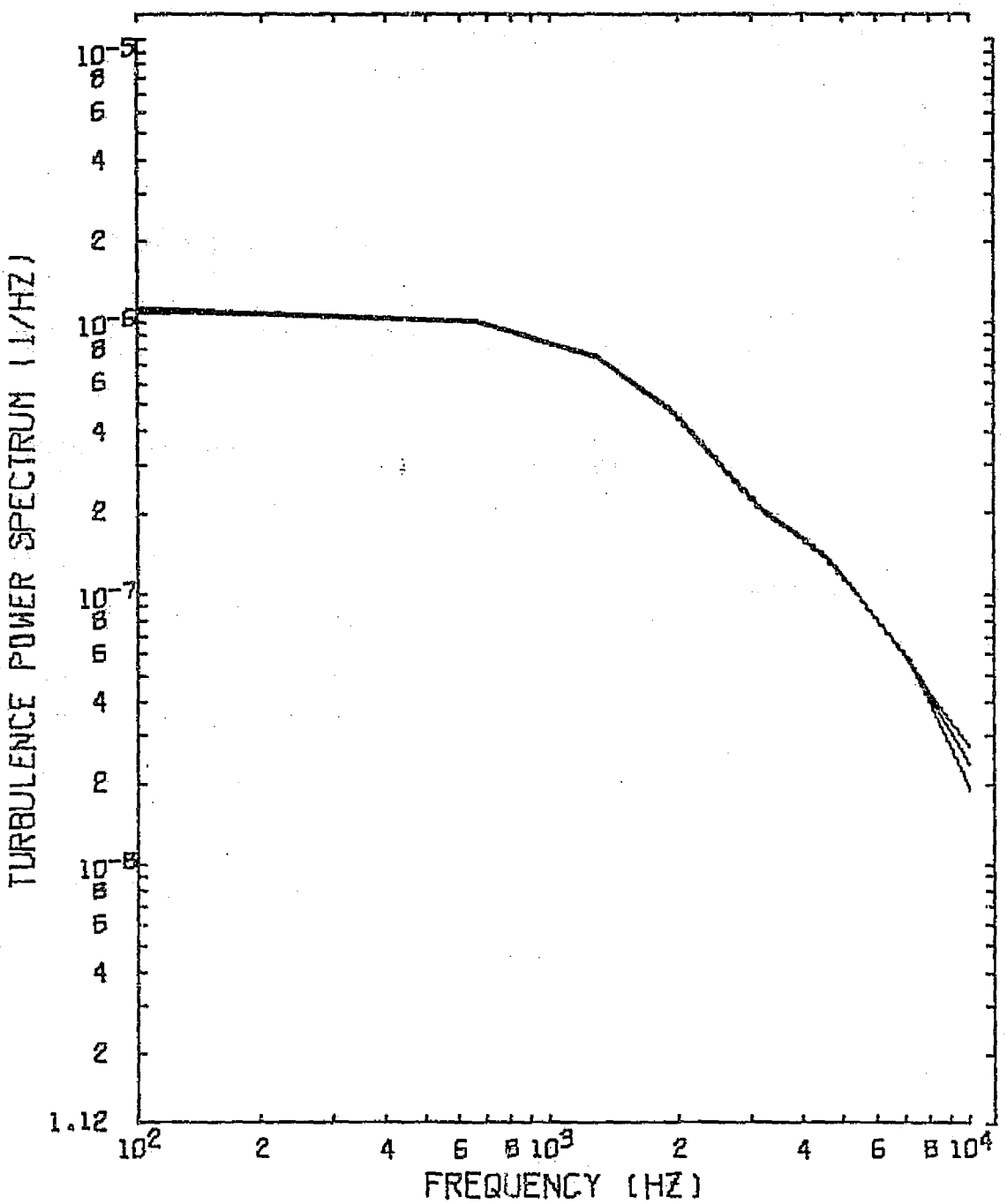

Figure 12 Auto-Spectrum for the Longitudinal Component on the Wake Centerline, $y_1/C=.017$

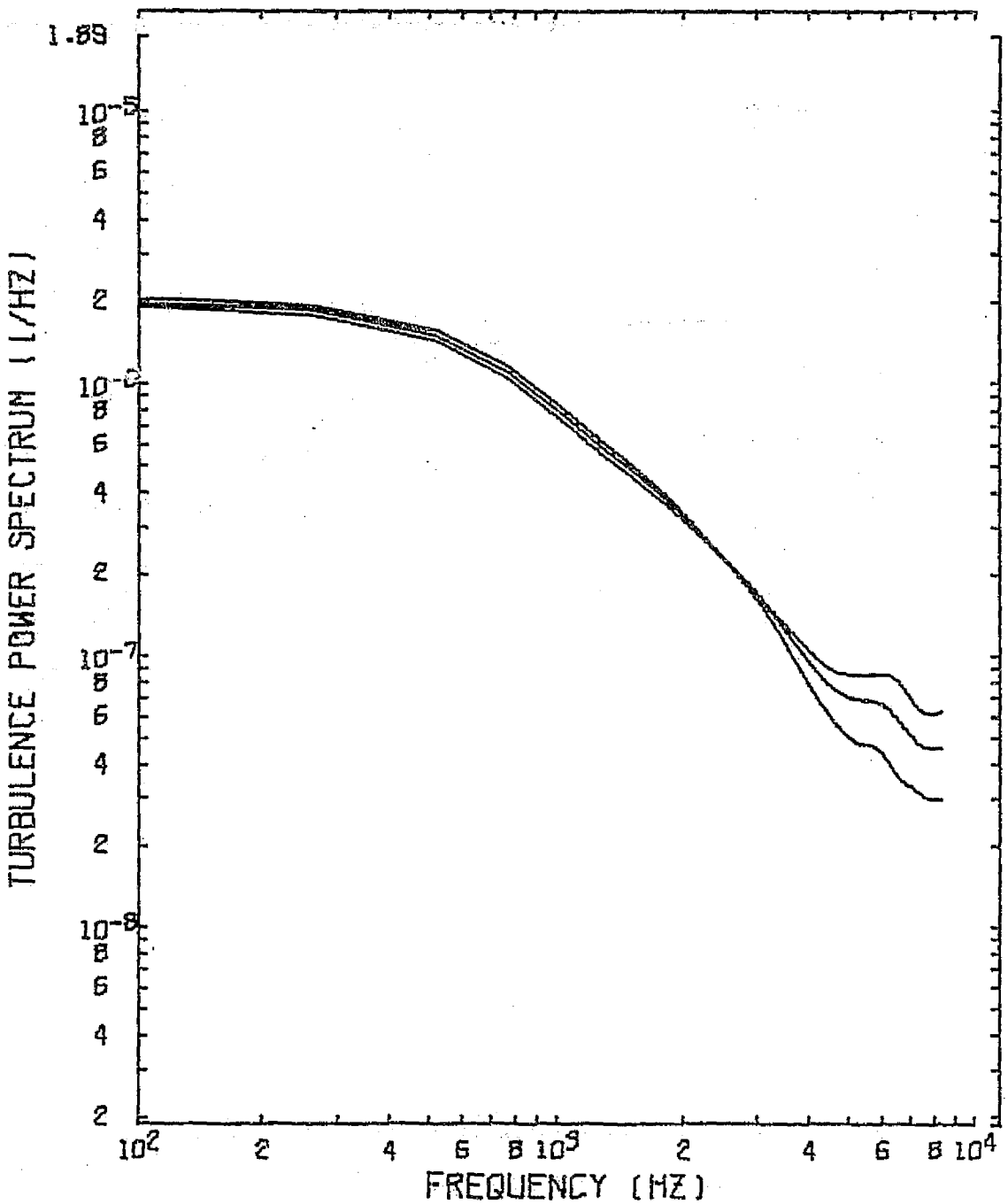

Figure 13 Auto-Spectrum for the Longitudinal Component on the Wake Centerline, $y_1 / C = .046$

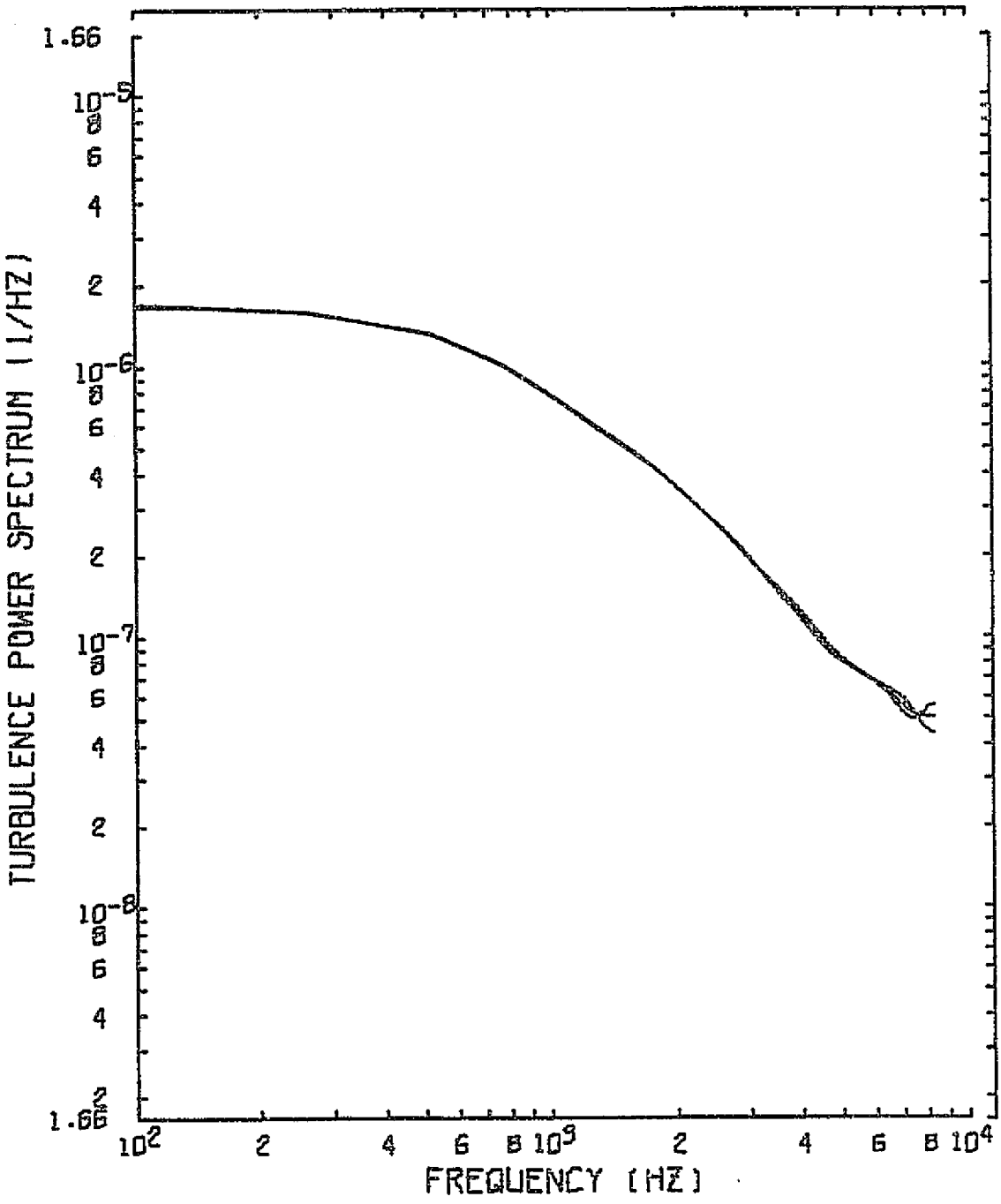

Figure 14 Auto-Spectrum for the Longitudinal Component on the Wake Centerline, $y_1/C = .102$

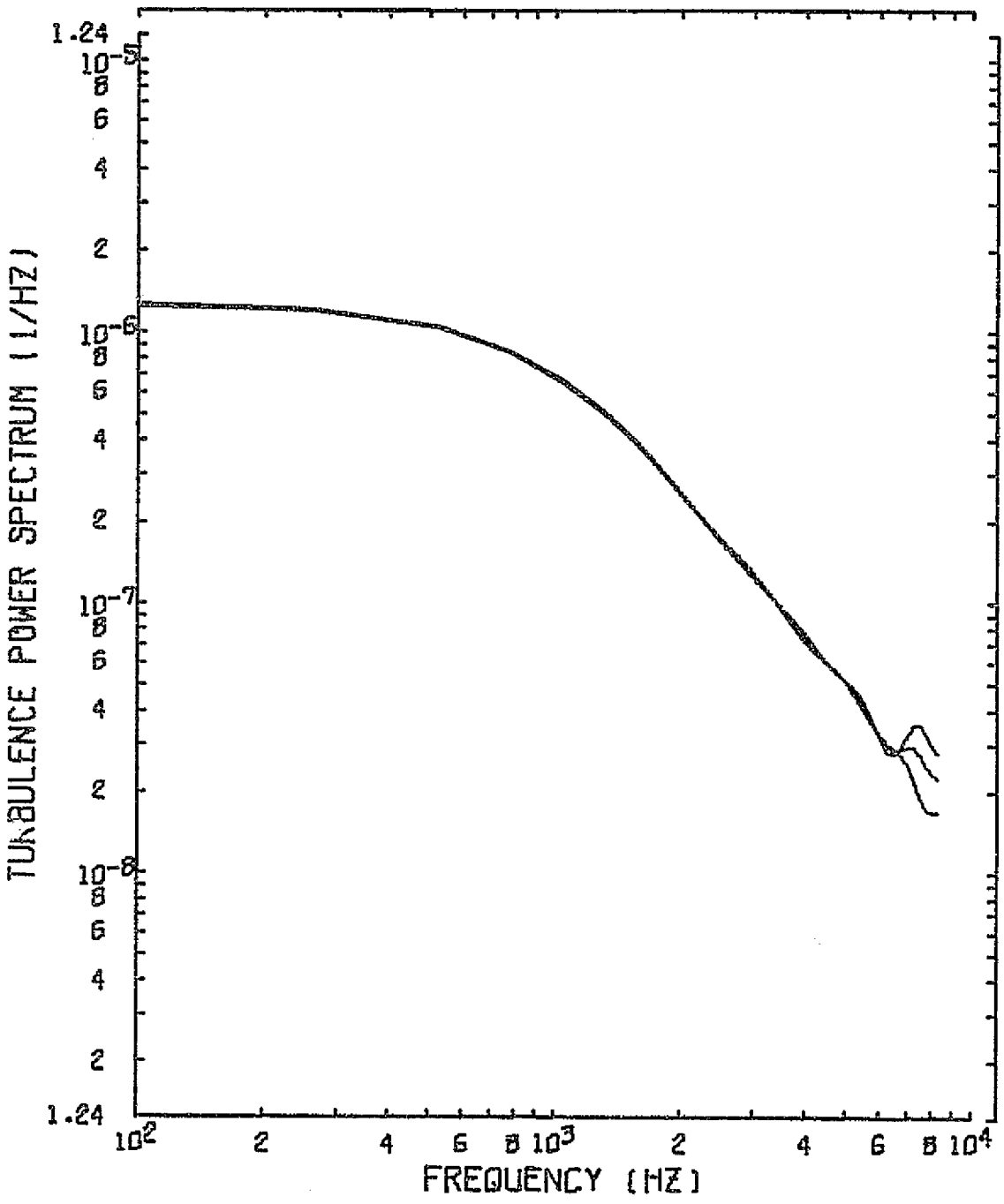

Figure 15 Auto-Spectrum for the Longitudinal Component on the Wake Centerline, $y_1/C = .194$

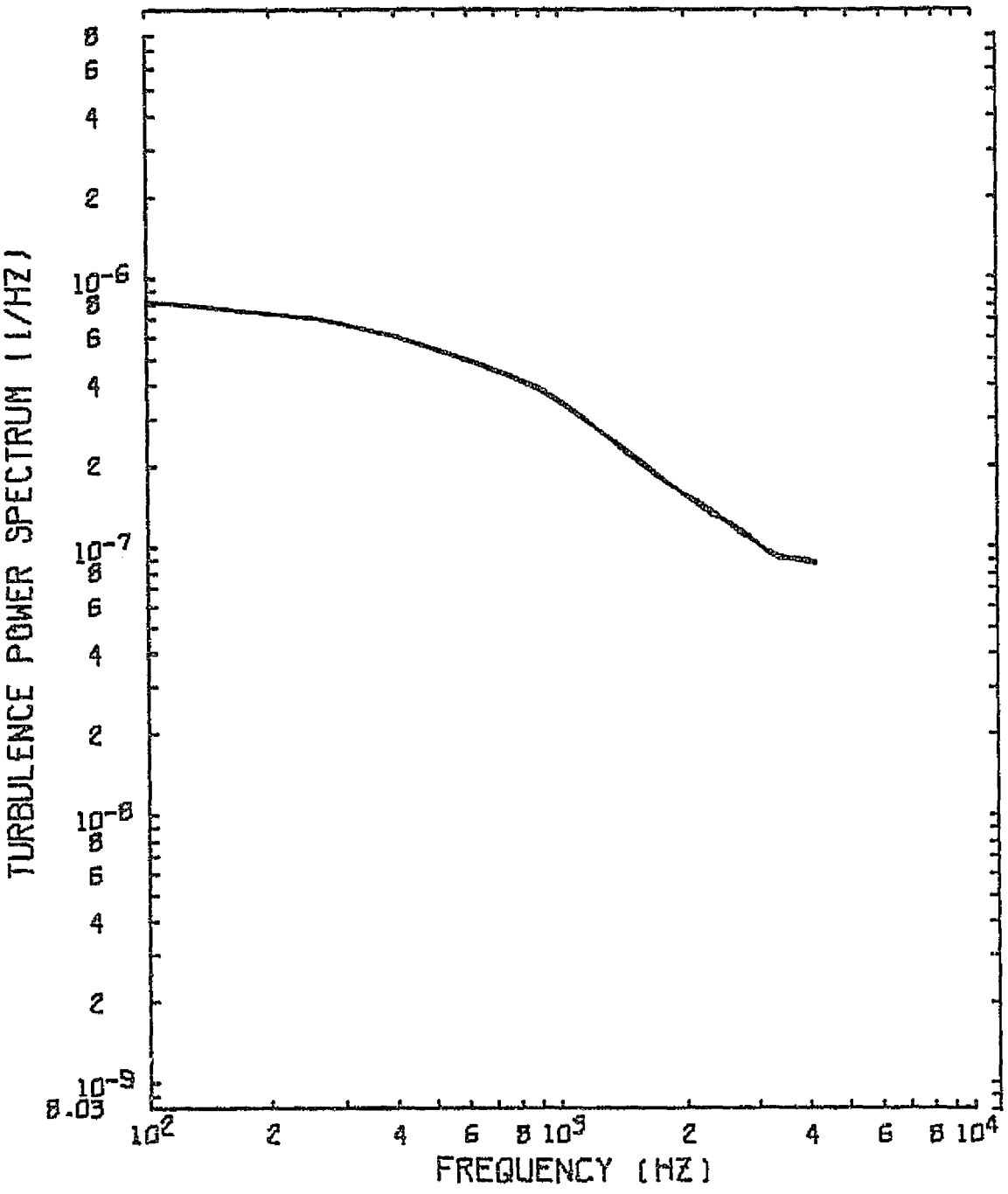

Figure 16 Auto-Spectrum for the Longitudinal Component on the Wake Centerline, $y_1/C = .361$

effects of the noise floor are becoming apparent.

The bandwidths(uncorrelated Fourier coefficients) for the data are 520 Hz. This tends to flatten the spectra in the low frequency range. The Time Data results have a bandwidth of 41 Hz so better describe the details of the low frequency spectrum.

Notice in the spectra for the longitudinal component that there is monotonic decrease in the level with frequency. For the transverse turbulence, Figures 17 through 21, the energy does not exhibit this behavior but peaks at a higher frequency then decreases beyond this point. This is the general behavior noted by Tennekes and Lumley (24) for isotropic turbulence.

Autospectra for the two turbulence components for the 6° incidence angle are presented in Figures 22 and 23. The major effect of the increase in incidence angle is to shift the energy to lower frequencies as would be expected.

5.3 Spectral Distribution of the Two Point Velocity Correlations

The purpose of the measurements of the spectra of the two point velocity correlations was to determine the spatial correlation of the various frequency components.

A measure of the spatial correlation was required as a function of frequency for the two turbulence components in each of the three coordinate directions. The way this measure was established was to normalize the magnitude of the cross power spectra with the autospectra for the signal from the stationary probe. This resulted in a spatial correlation function at each frequency and in each coordinate direction. This was essentially a cross plot of the space time power spectra. A spatial integration of each of these frequency dependent correlation

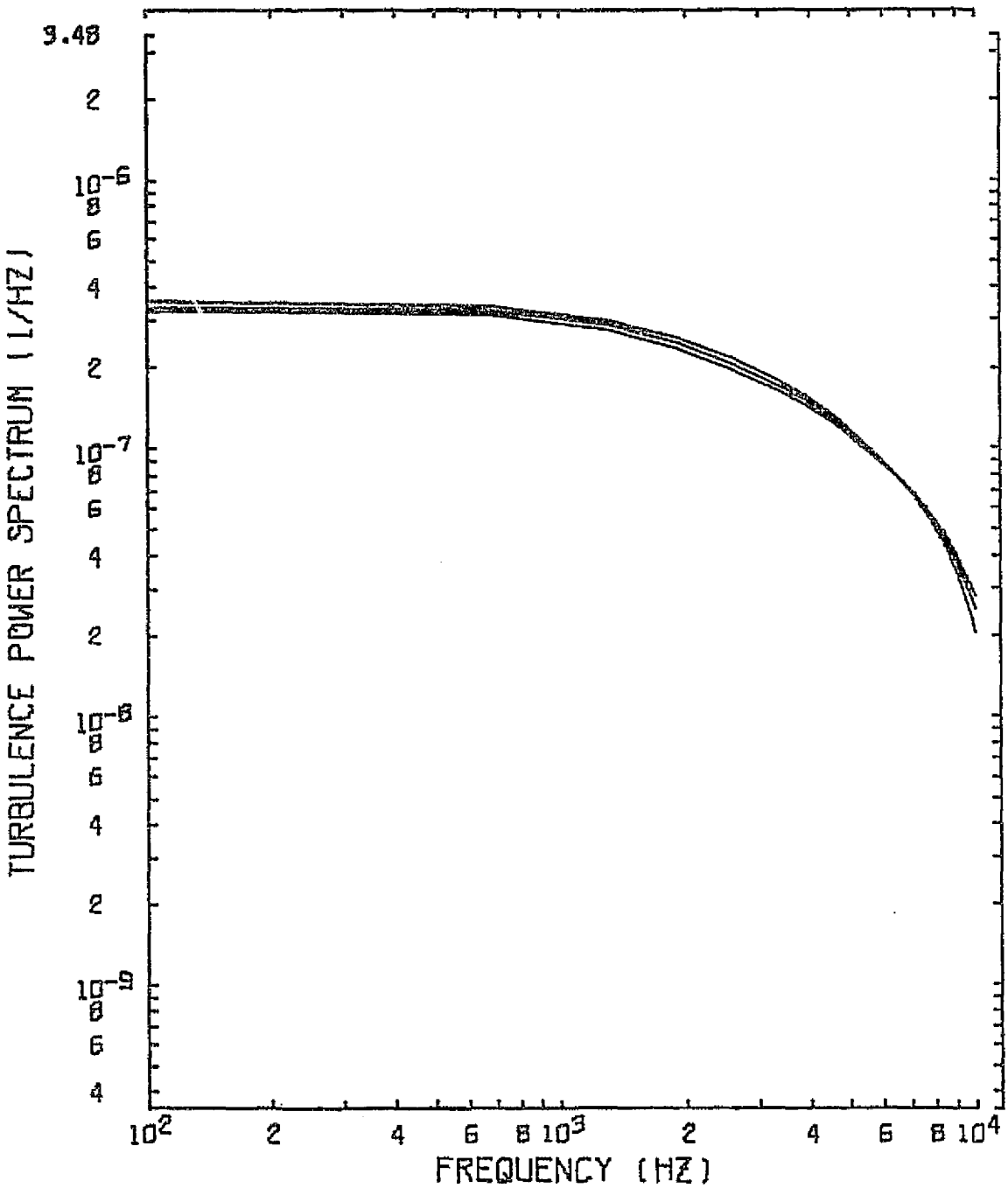

Figure 17 Auto-Spectrum for the Transverse Component on the Wake Centerline, $y_1/C = .017$

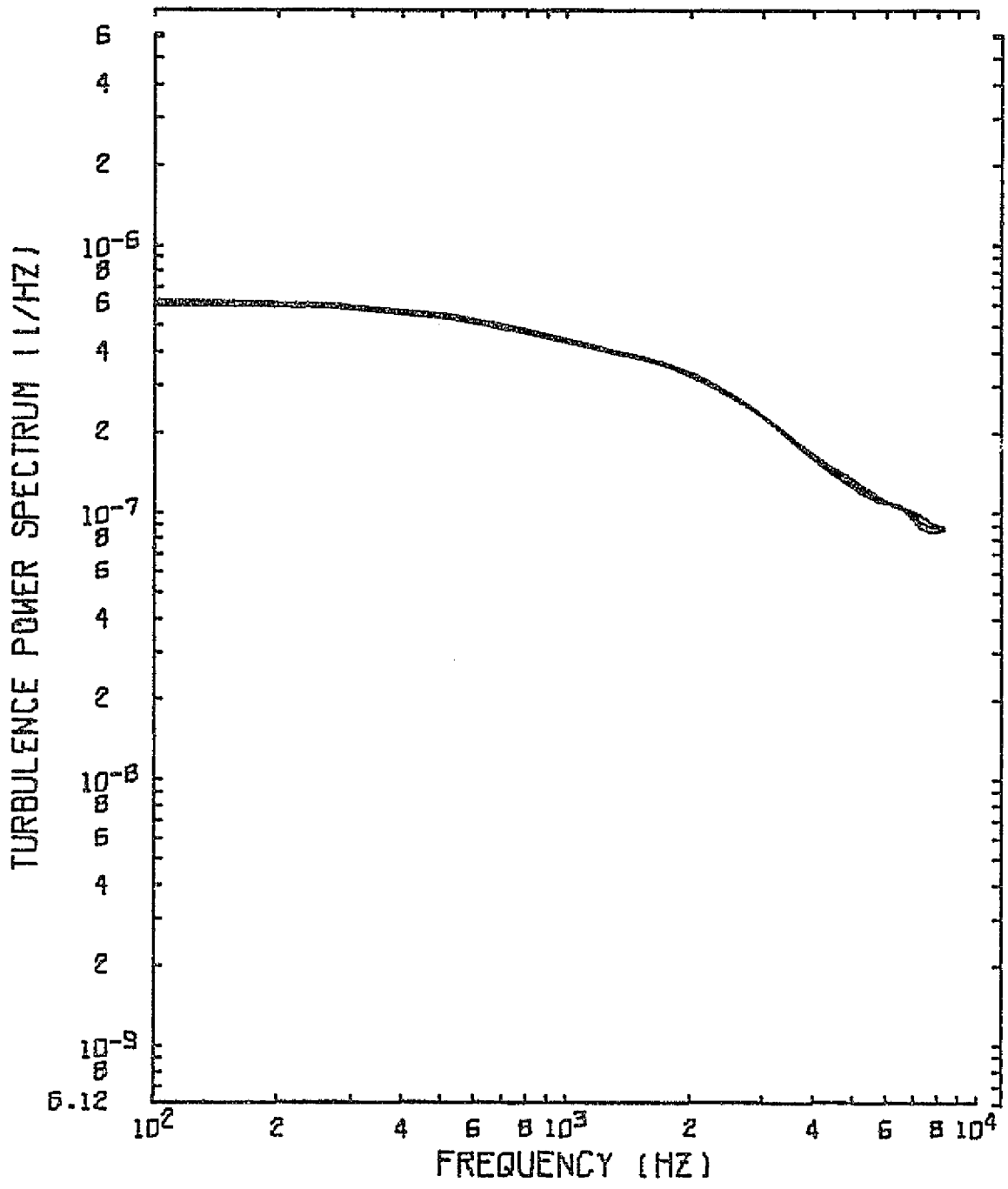

Figure 18 Auto-Spectrum for the Transverse Component on the Wake Centerline, $y_1/C = .046$

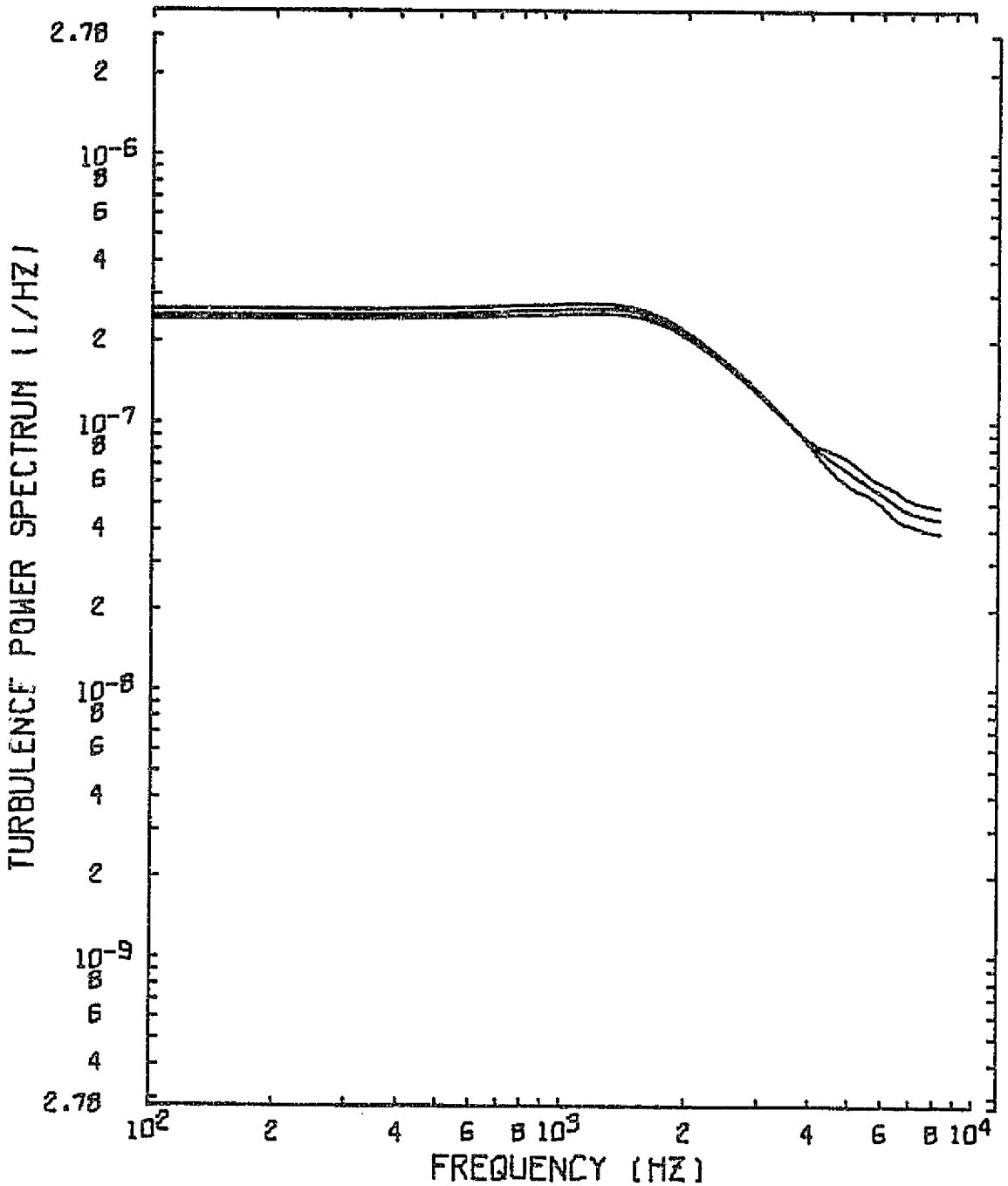

Figure 19 Auto-Spectrum for the Transverse Component on the Wake Centerline, $y_1/C = .102$

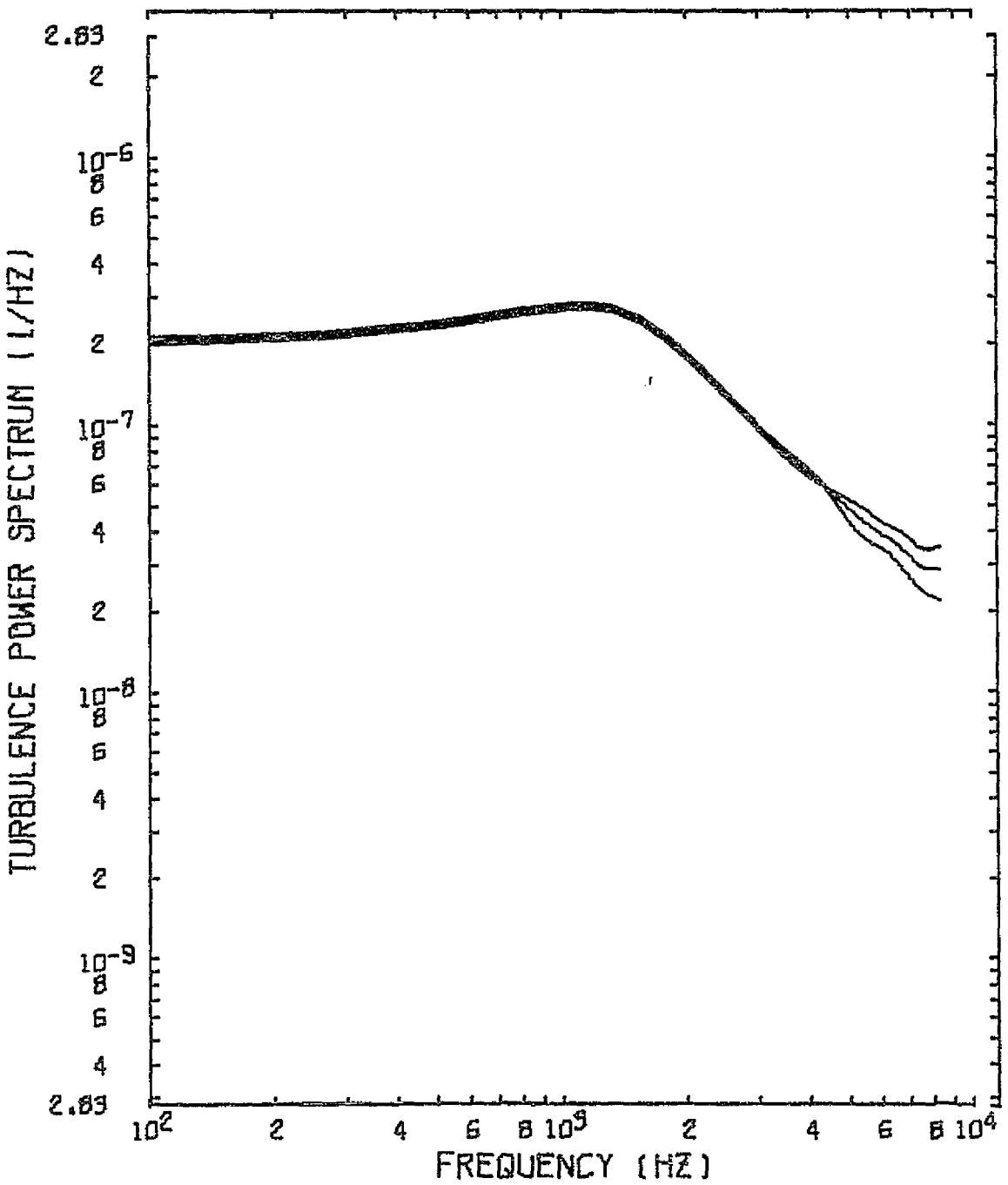

Figure 20 Auto-Spectrum for the Transverse Component on the Wake Centerline, $y_1/C = .194$

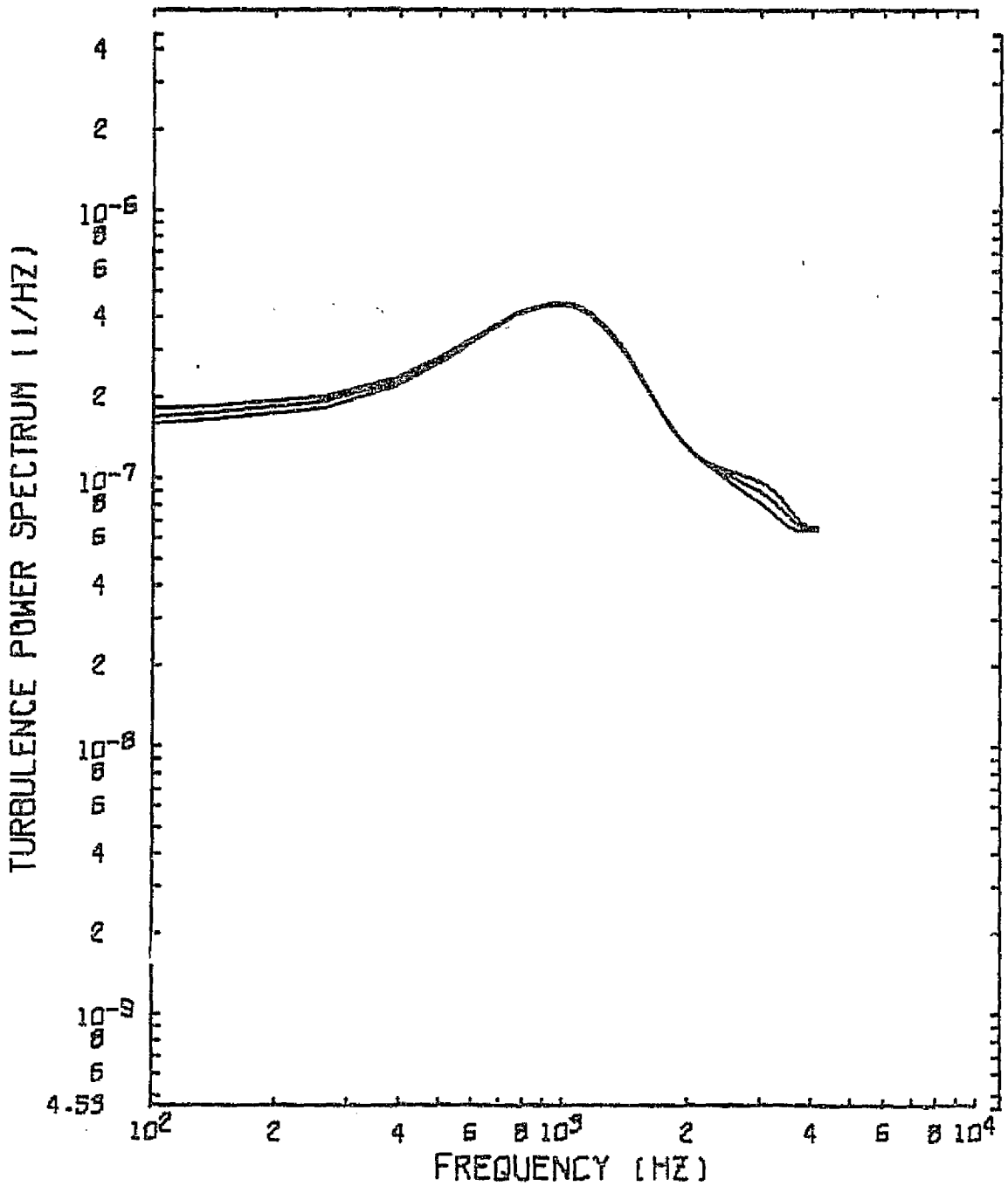

Figure 21 Auto-Spectrum for the Transverse Component on the Wake Centerline, $y_1/C = .361$

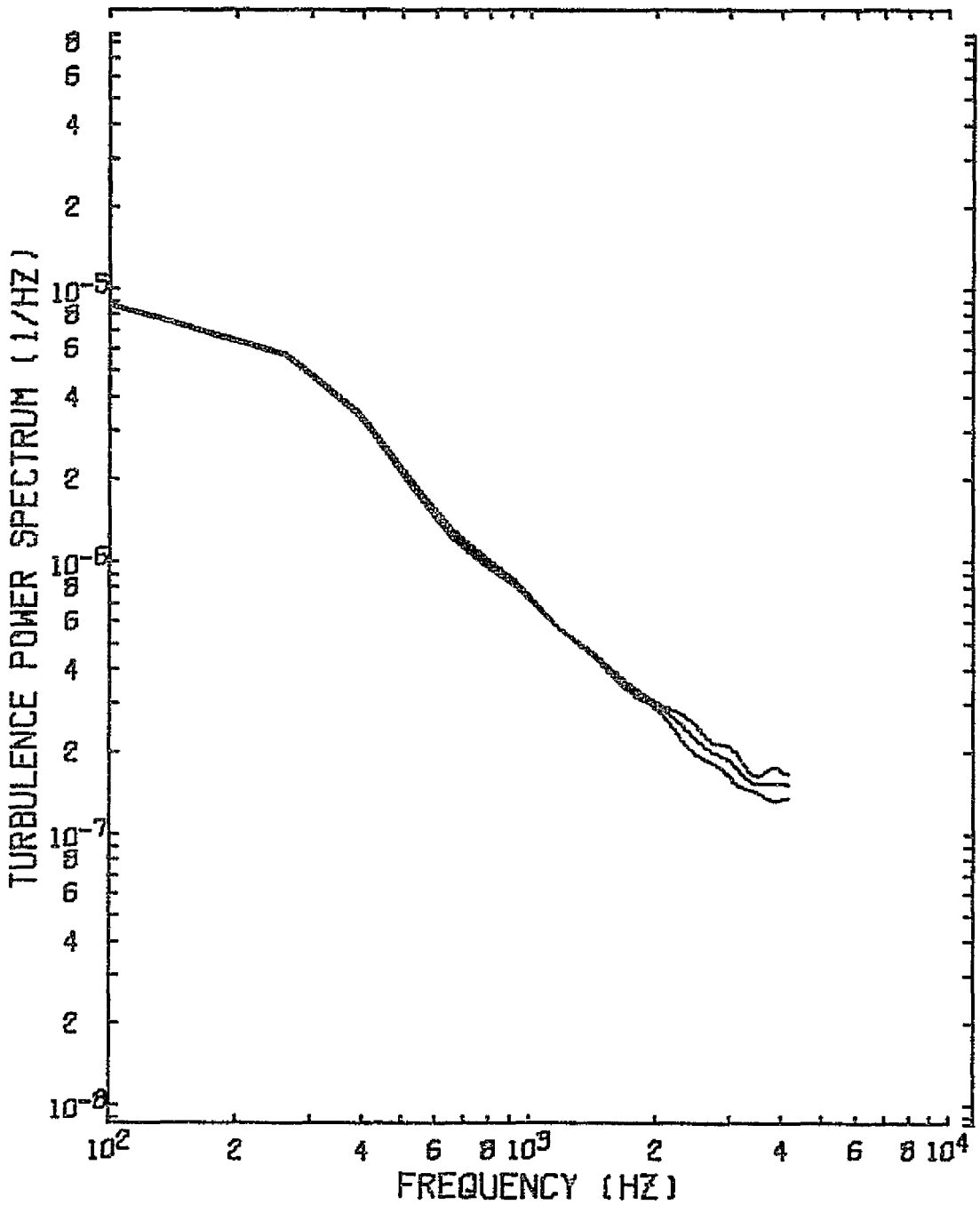

Figure 22 Auto-Spectrum for the Longitudinal Component on the Wake Centerline, i = 6°, y_1/C = .035

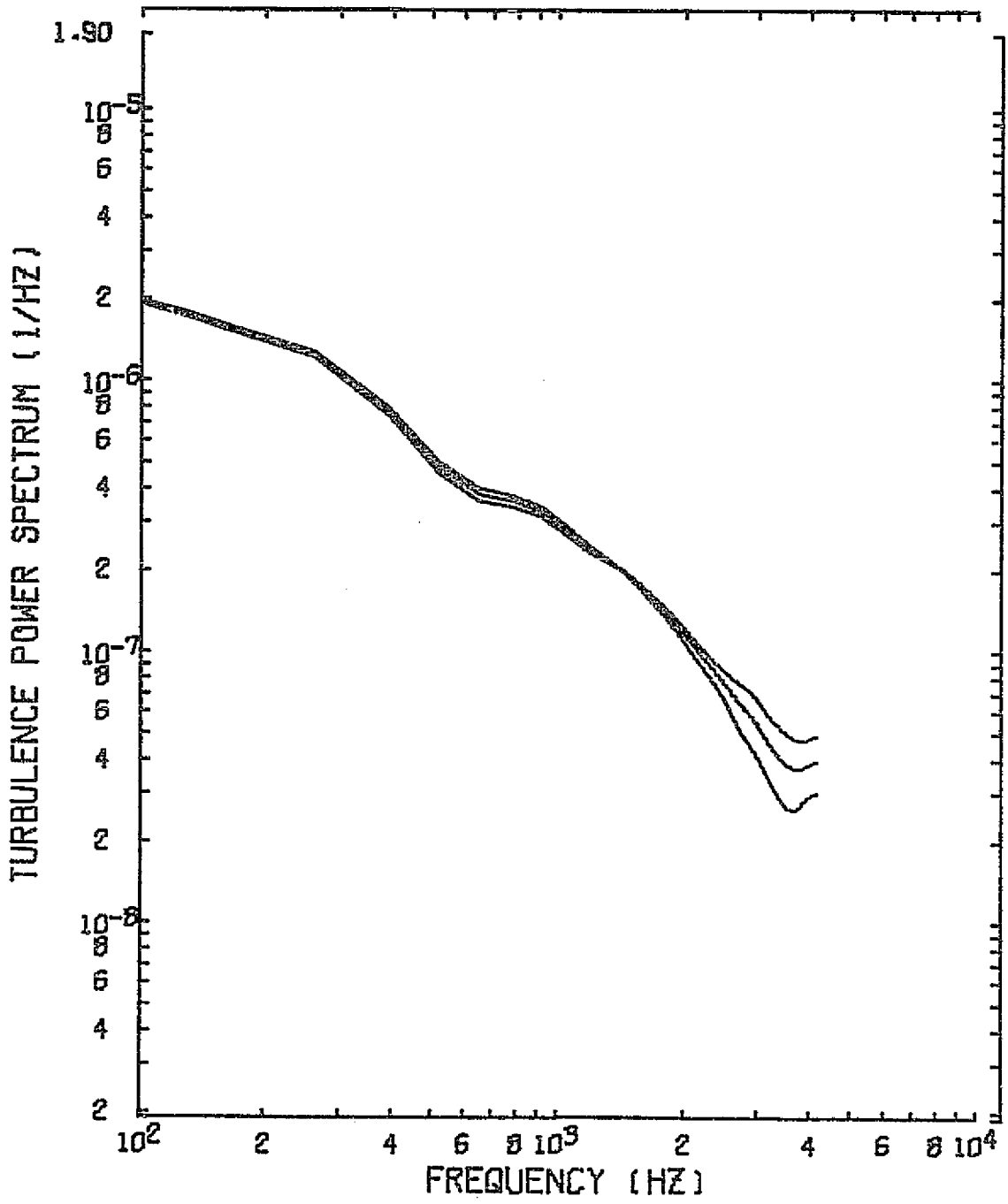

Figure 23 Auto-Spectrum for the Transverse Component on the Wake Centerline, i = 6°, y_1/C = .035

functions would yield an integral length scale as a function of frequency.

The cross spectra data will be presented in the form of the spatial correlation functions at each of the frequencies. This cross plotting procedure is somewhat lengthy so only enough data will be shown to illustrate the method.

The spatial correlations for the longitudinal component at 0° incidence are shown for the stream direction in Figure 24, for the span direction in Figure 25, and for the normal direction in Figure 26. Correlation plots for the 6° incidence case are presented in Figures 27, 28, and 29 in the same order as the 0° incidence data.

The spatial correlation functions for the transverse component are shown in the three directions in Figures 30, 31, and 32 for the 0° incidence data and in Figures 33, 34, and 35 for the 6° case.

The numerical integration of plots of this type was carried out on the CDC 6400 to yield a spectral distribution of the integral lengths in the different directions. Because of the few points in the spatial coordinates, the method used for the integration was the trapezoidal rule. A more sophisticated quadrature formula appeared to introduce more uncertainties because of the scarcity of data points.

5.4 Frequency Dependent Correlation Lengths

The correlation lengths measured through the above described integration for the stream direction are shown in Figures 36 and 37. Data are presented for both components of turbulence and each of the two incidence angles studied. Notice that the

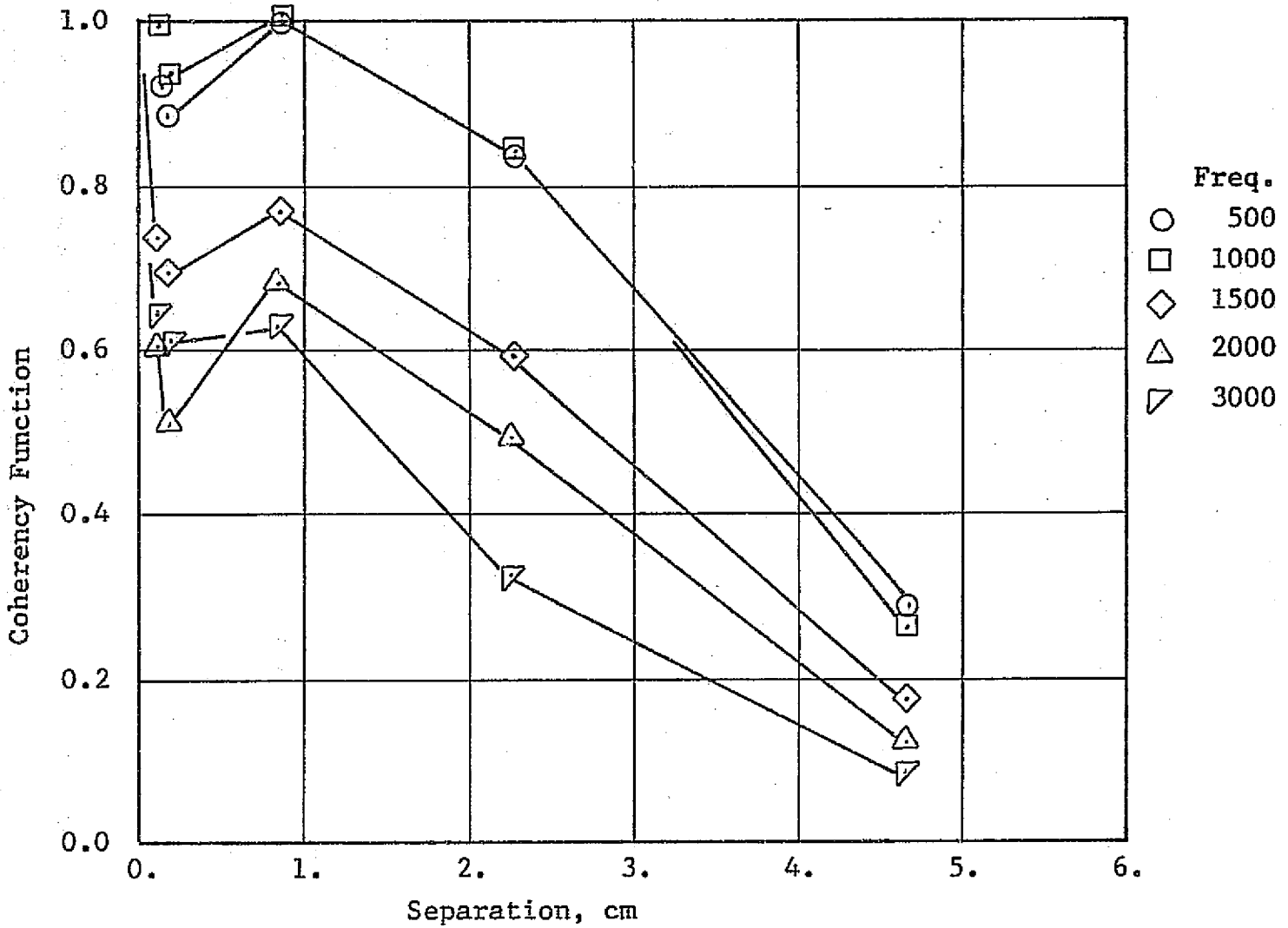

Figure 24 Coherence Function in Stream Direction - Longitudinal Component - Incidence = 0°

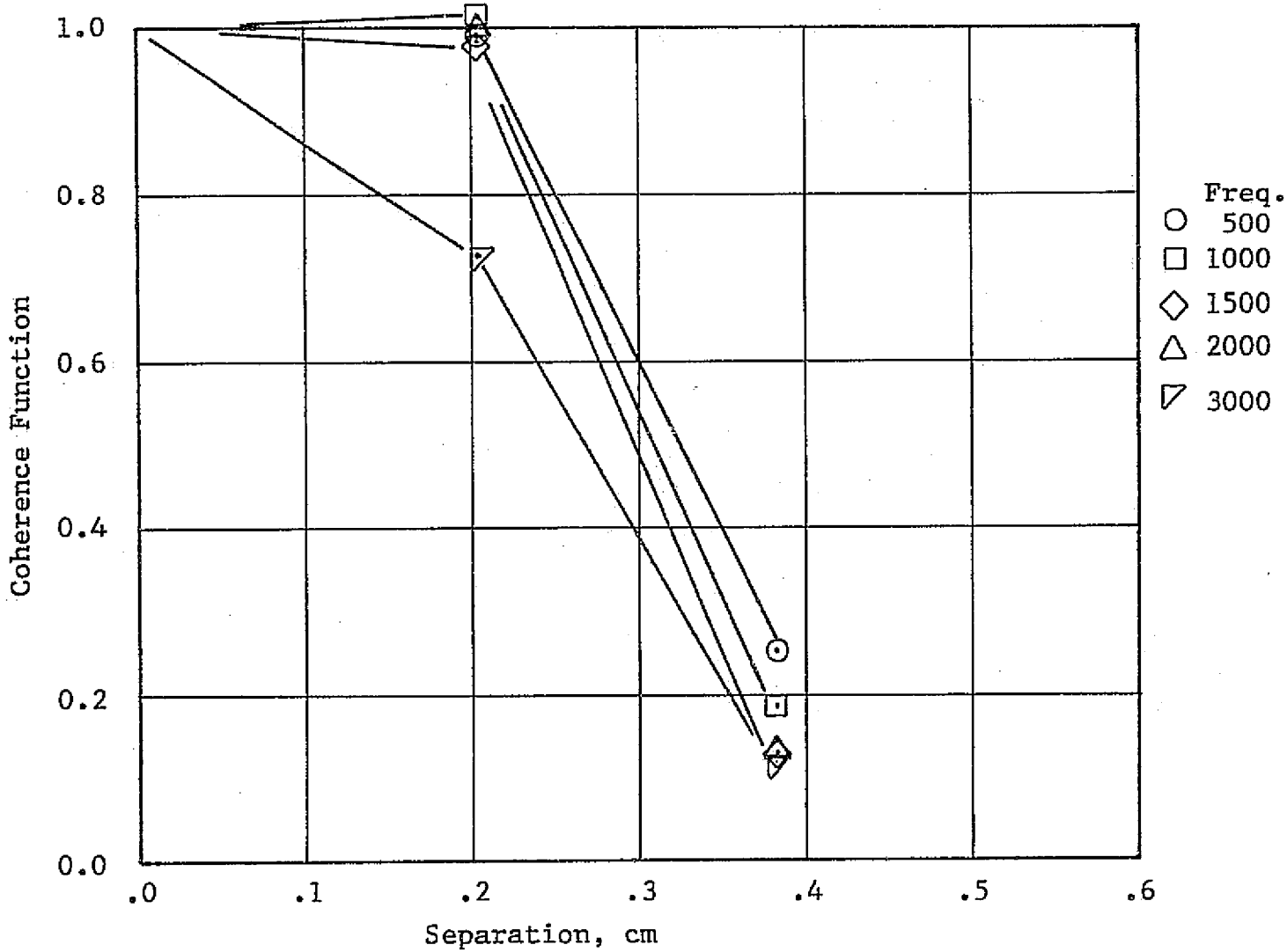

Figure 25 Coherence Function in the Span Direction - Longitudinal Component - incidence = 0°

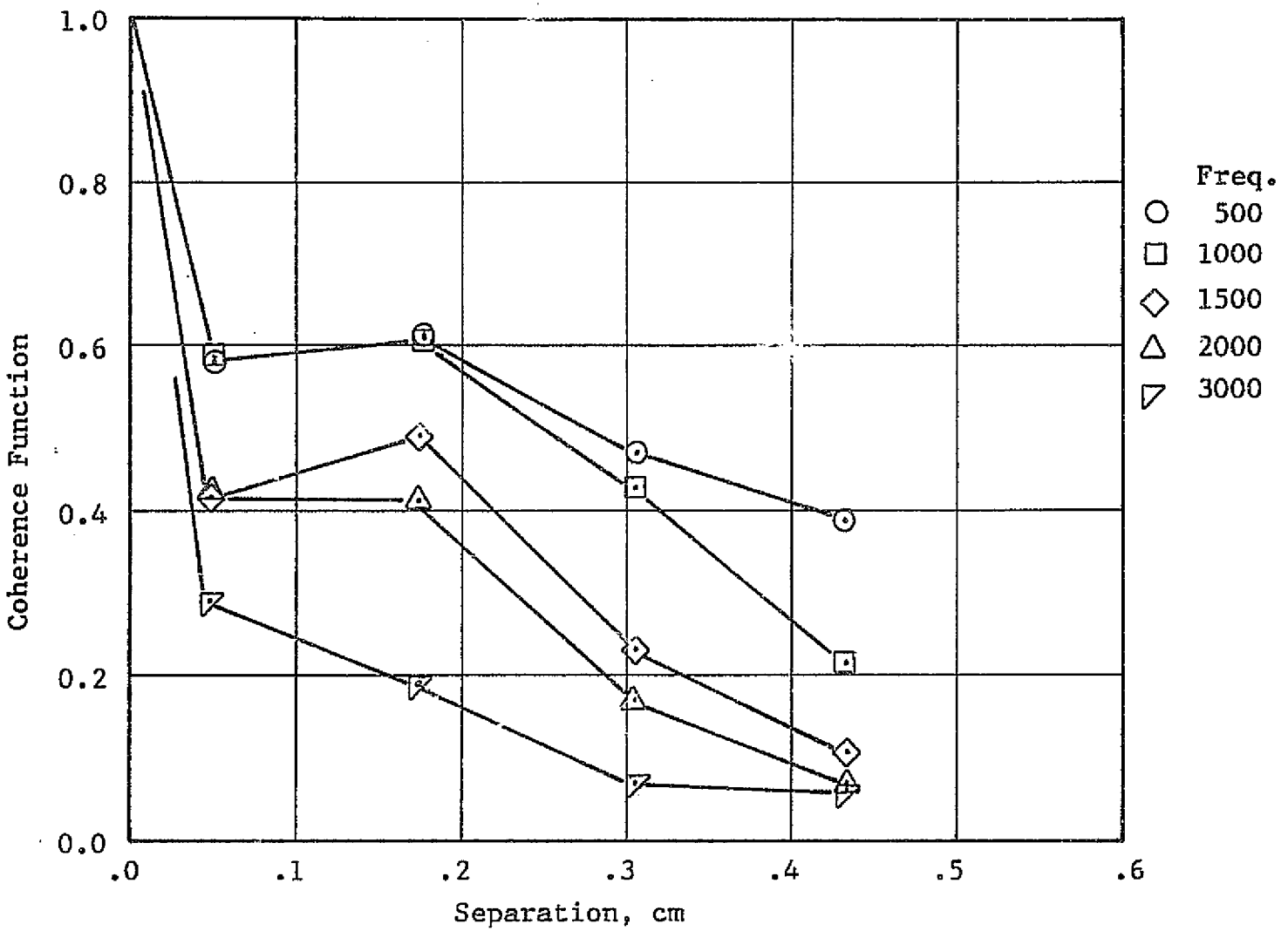

Figure 26 Coherence Function in the Normal Direction Longitudinal Component - Incidence = 0°

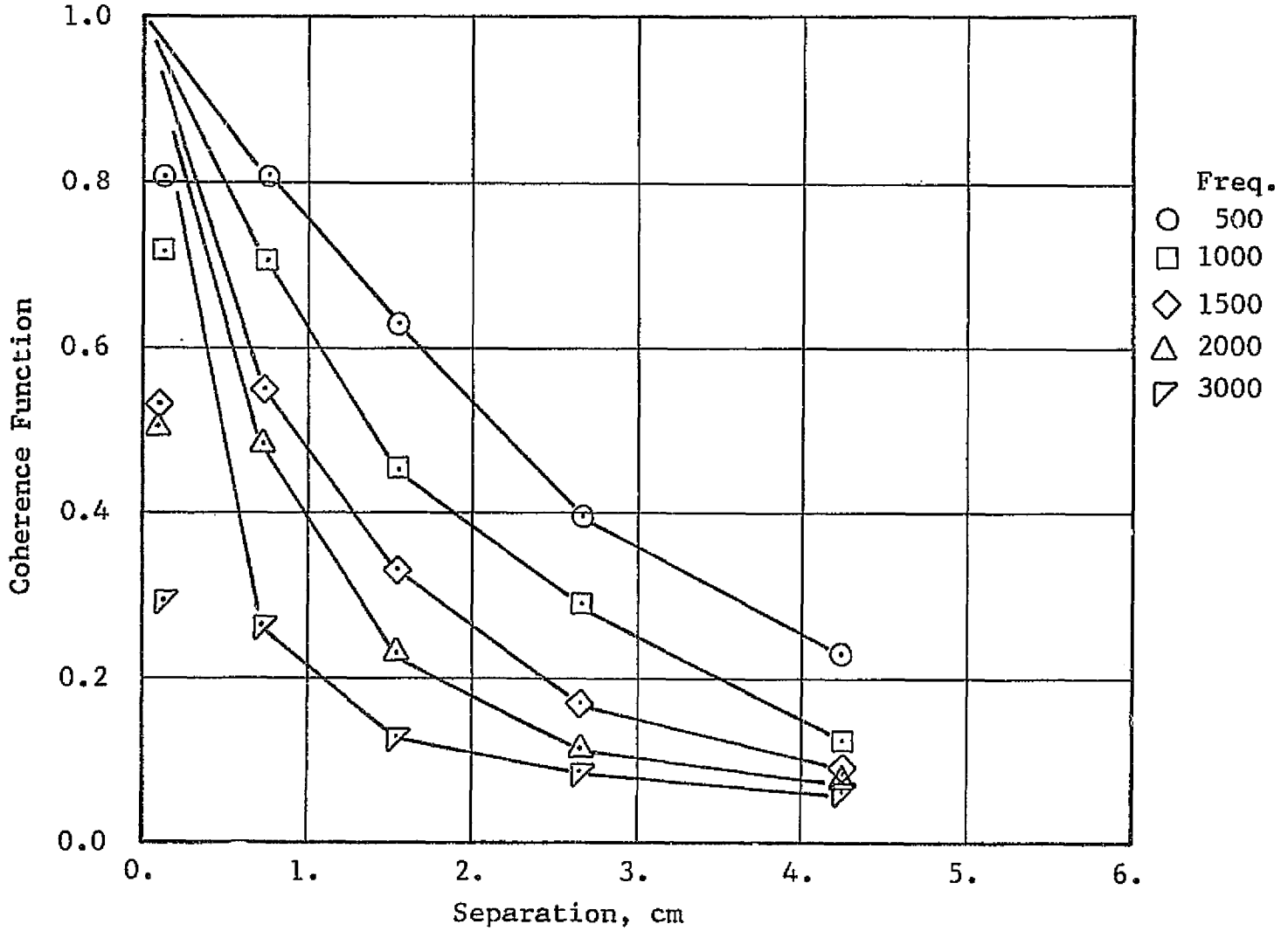

Figure 27 Coherence Function in the Stream Direction - Longitudinal Component - Incidence = 6°

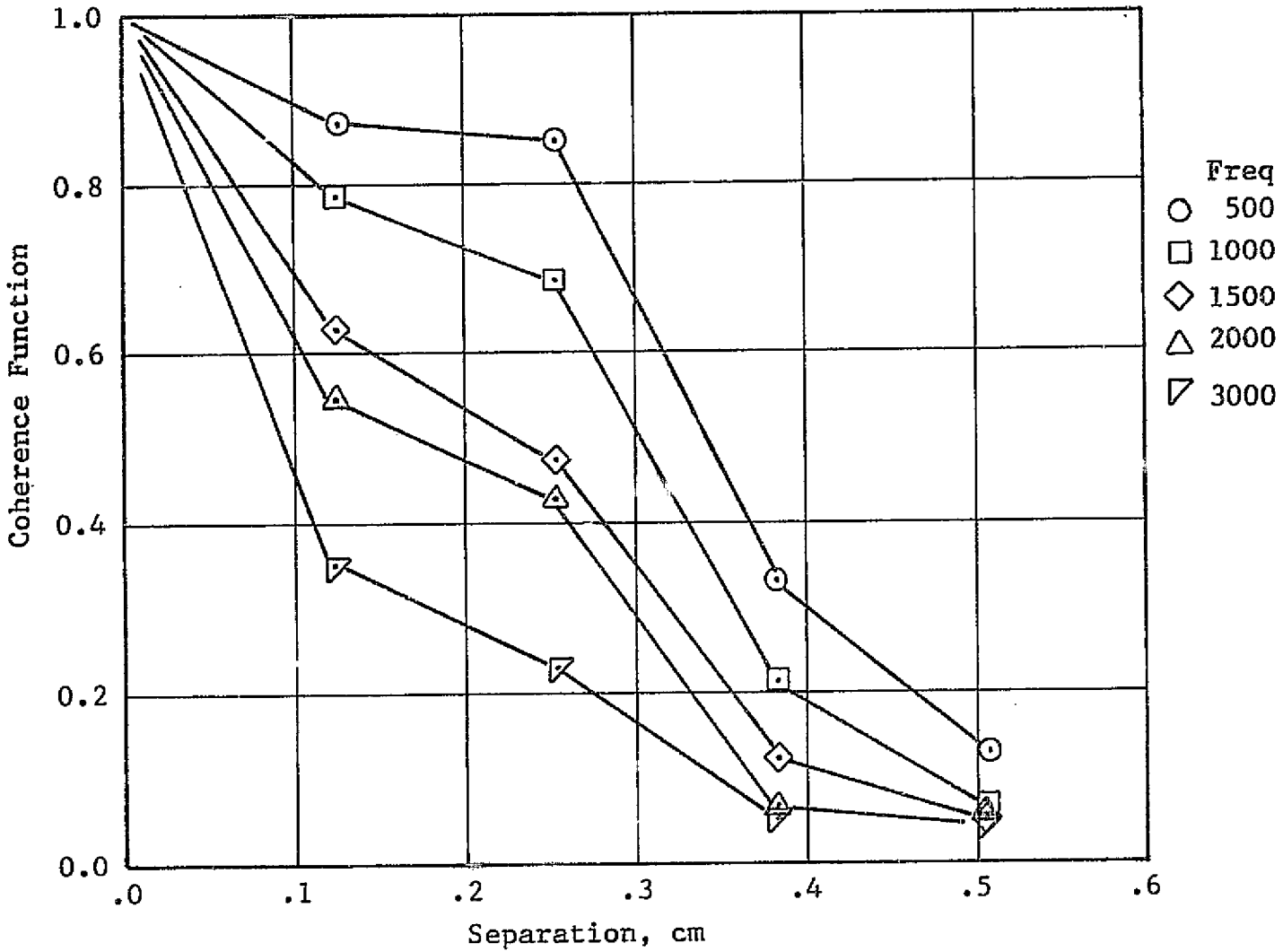

Figure 28 Coherence Function in the Span Direction - Longitudinal Component - Incidence = 6°

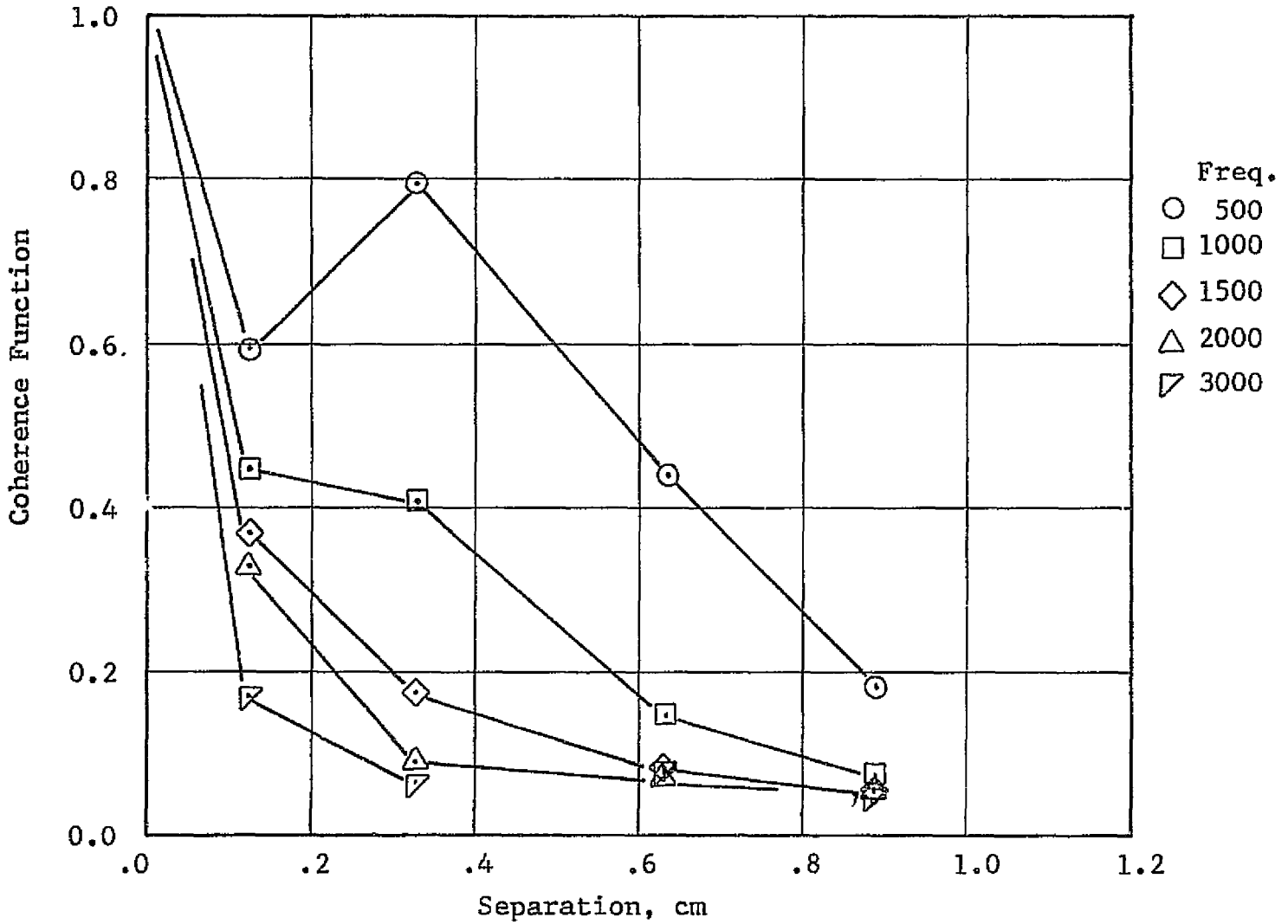

Figure 29 Coherence Function in the Normal Direction Longitudinal Component - Incidence = 6°

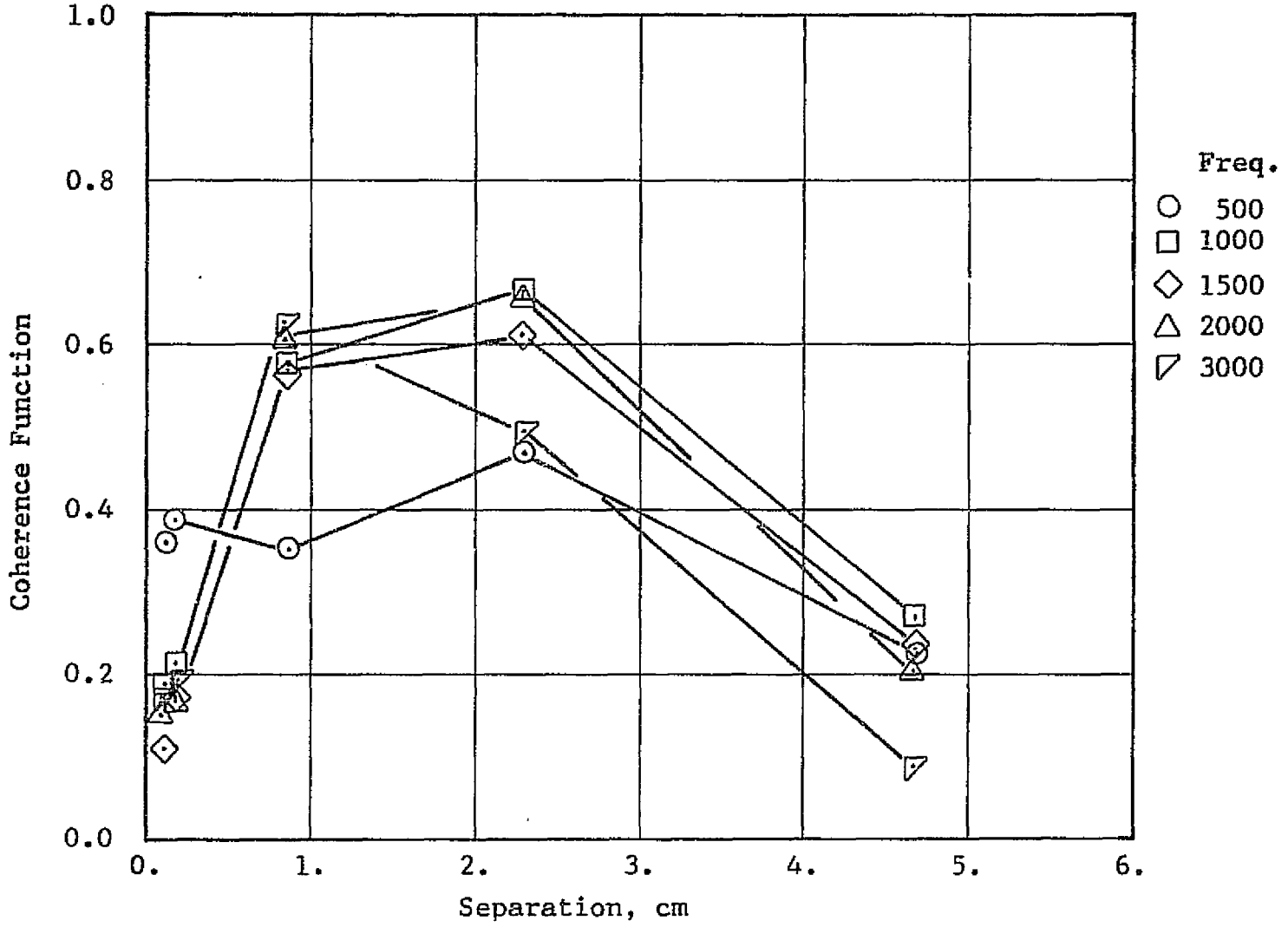

Figure 30 Coherence Function in the Stream Direction - Transverse Component - Incidence = 0°

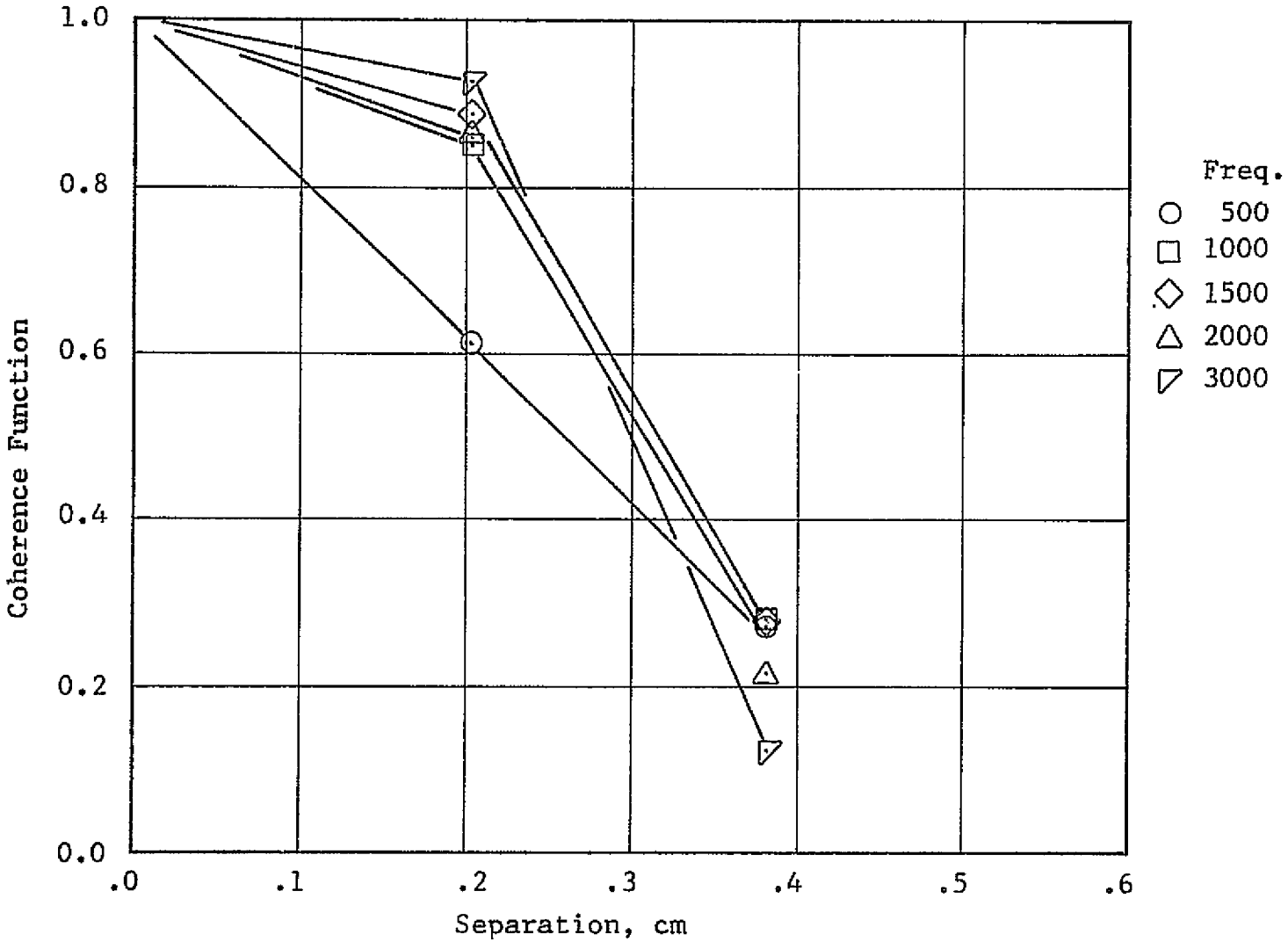

Figure 31 Coherence Function in the Span Direction - Transverse Component - Incidence = 0°

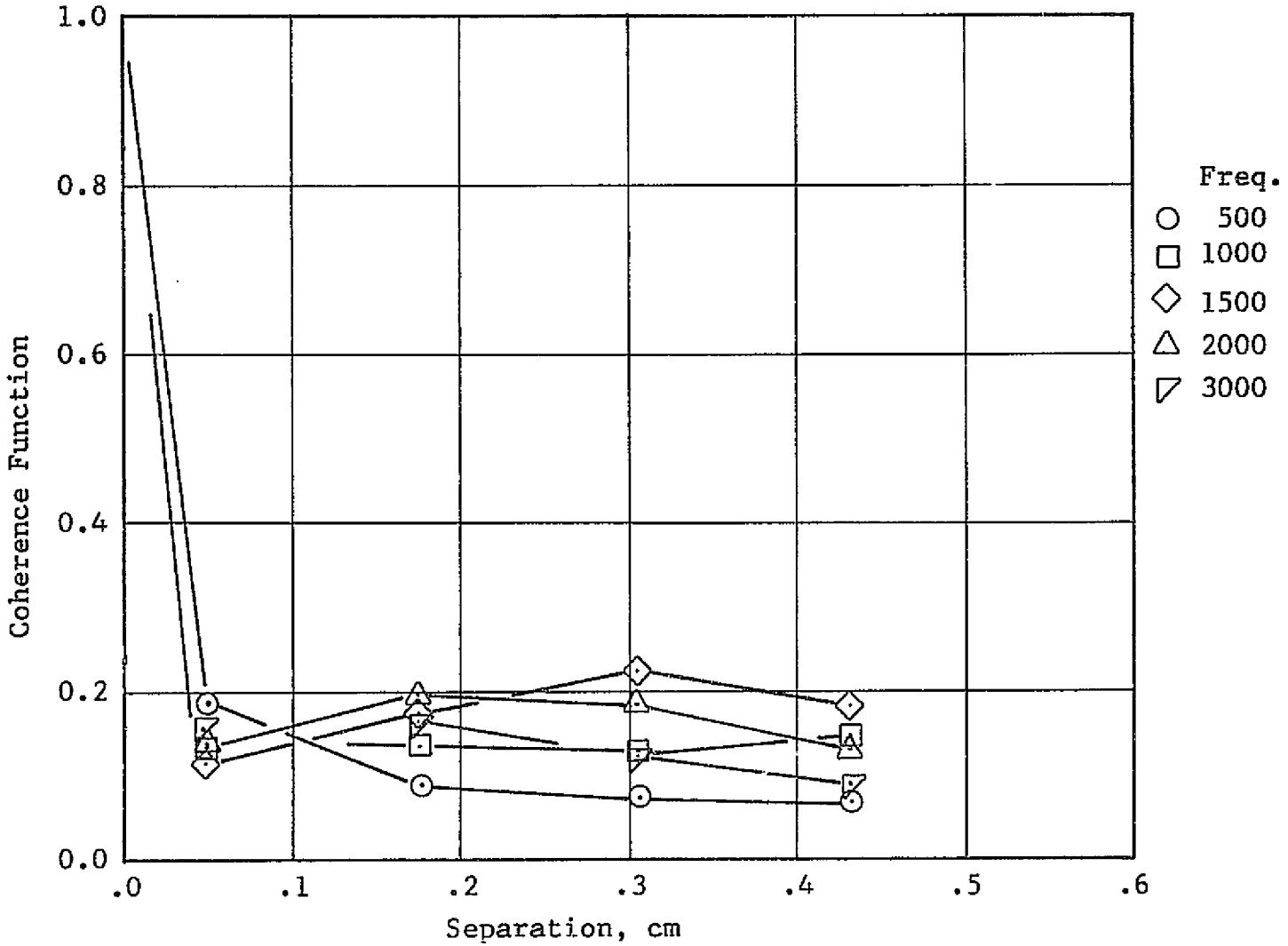

Figure 32 Coherence Function in the Normal Direction Transverse Component - Incidence = 0°

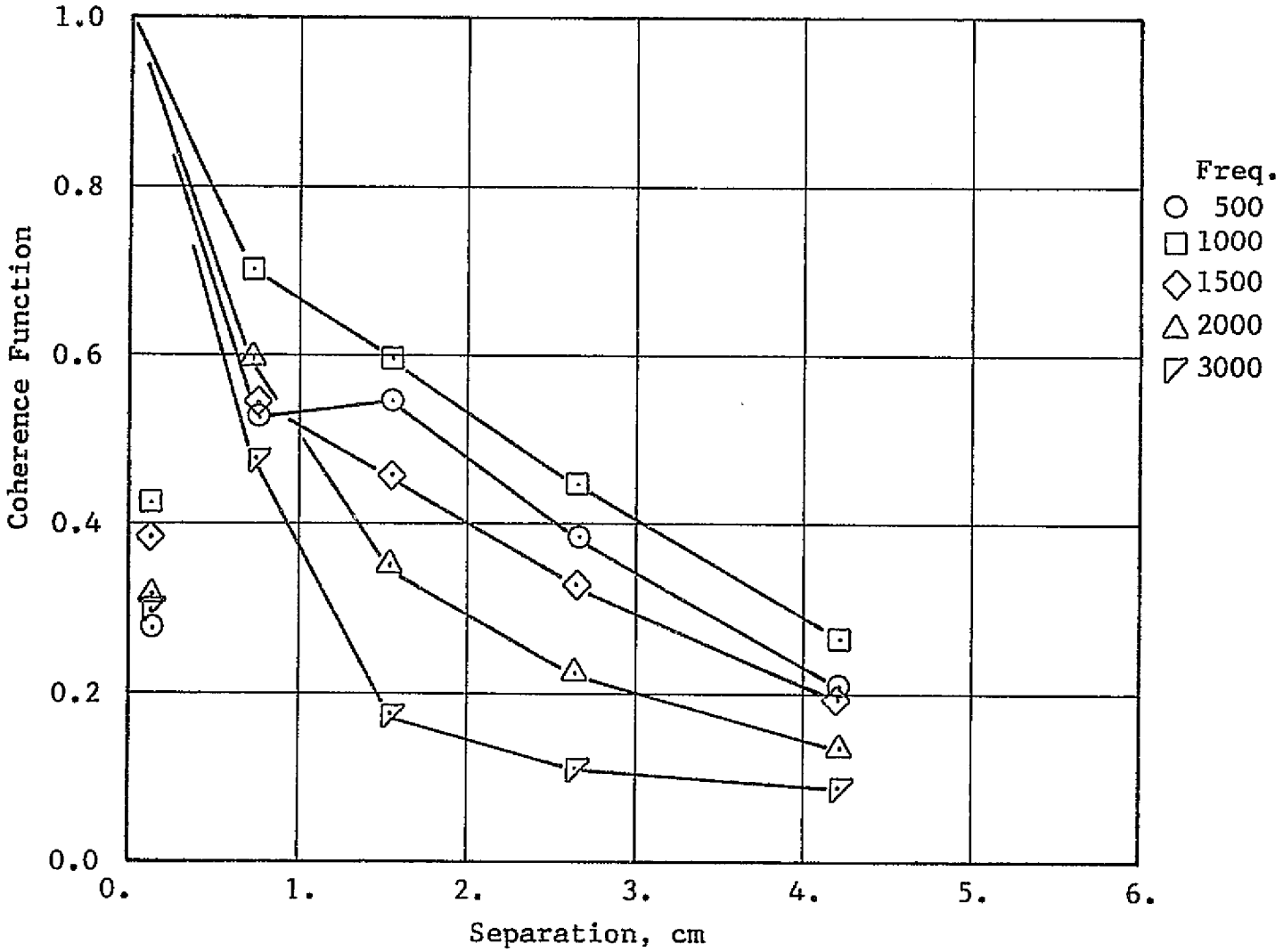

Figure 33 Coherence Function in the Stream Direction - Transverse Component - Incidence = 6°

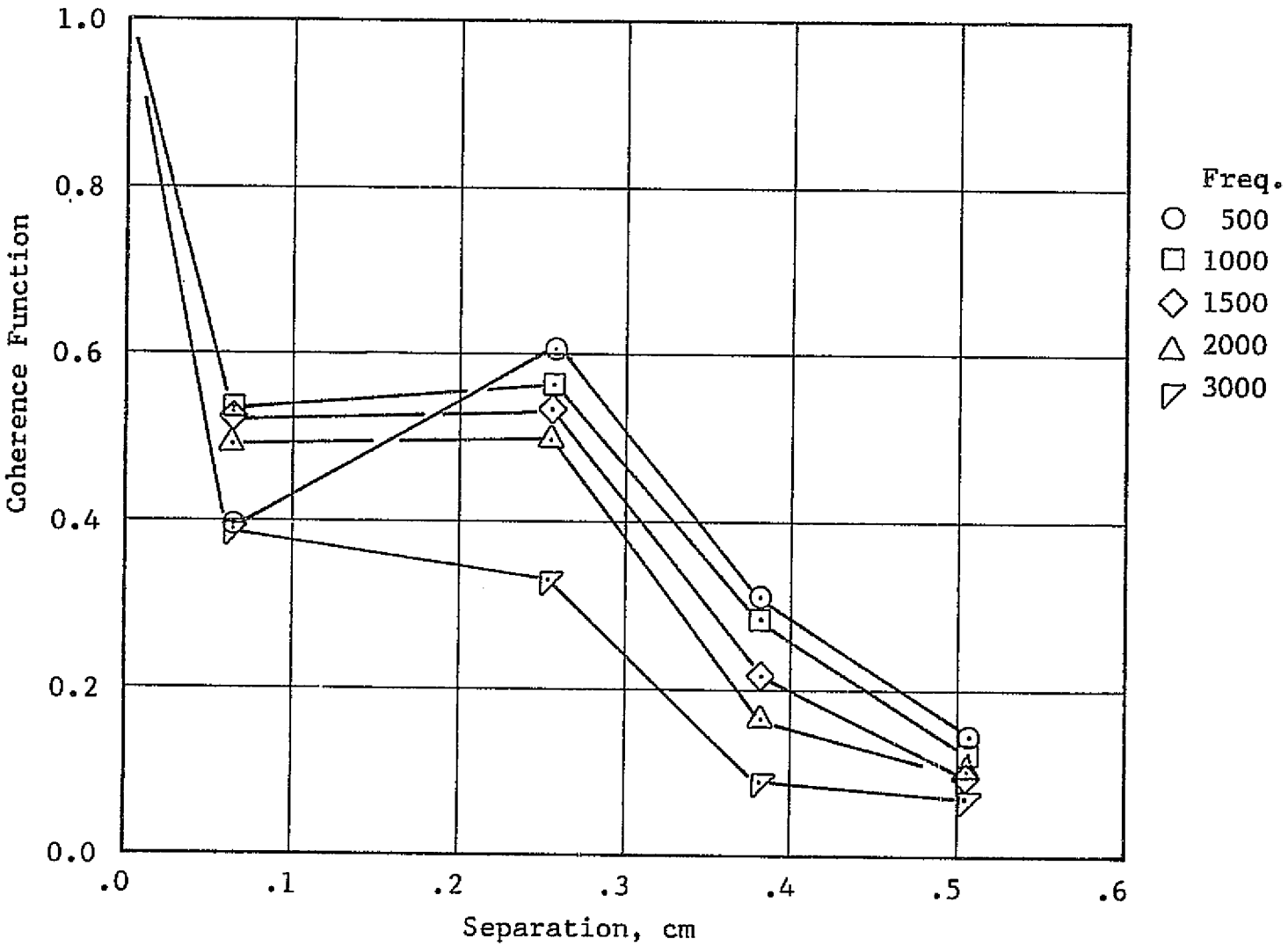

Figure 34 Coherence Function in the Span Direction - Transverse Component - Incidence = 6°

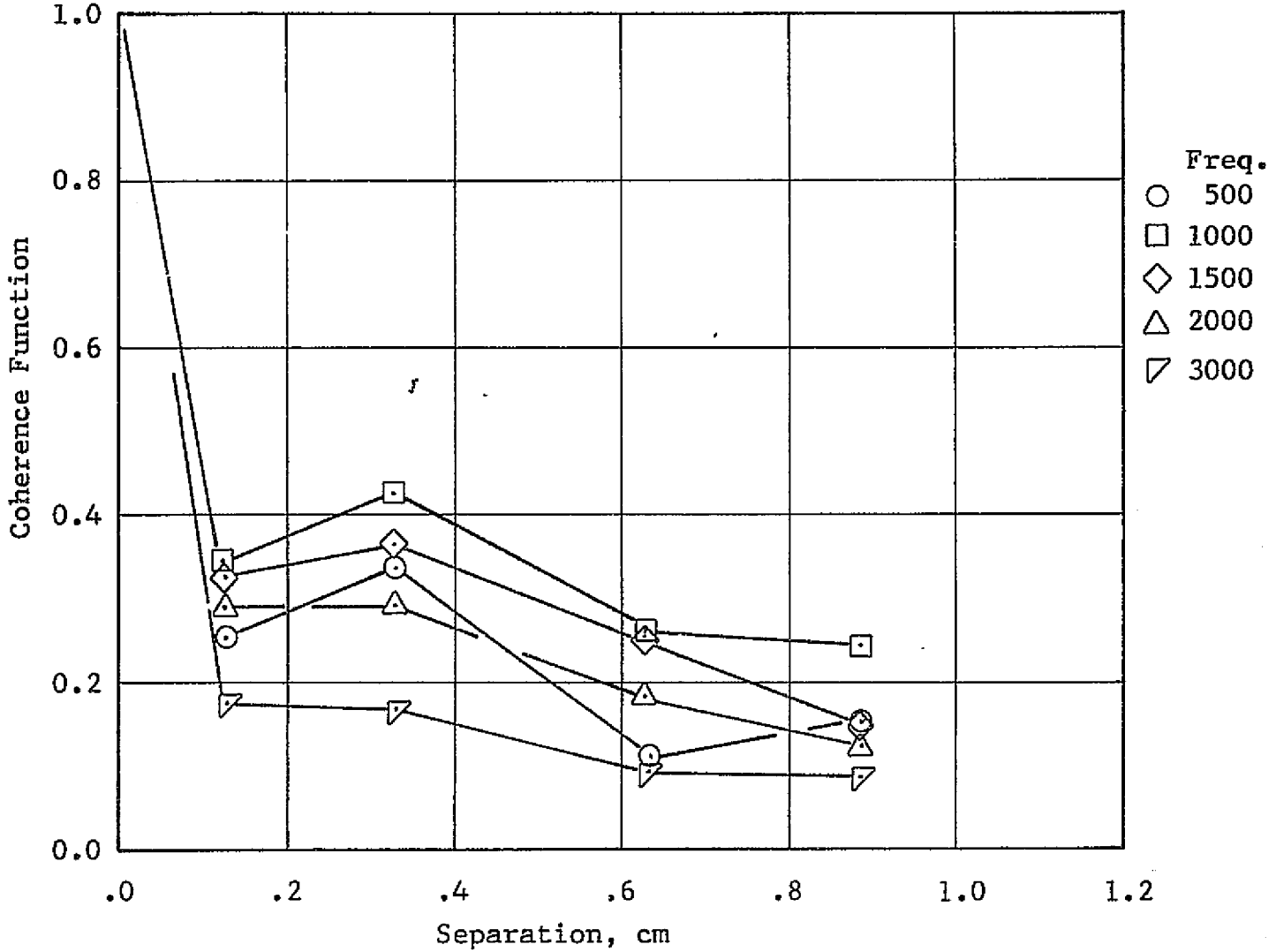

Figure 35 Coherence Function in the Normal Direction Transverse Component - Incidence = 6°

lengths for the 6° case are larger at lower frequencies but smaller at the higher frequencies for the longitudinal component. For the transverse component the lengths are about the same up to 1 kHz where the 0° lengths become as much as twice those for the 6° data.

In the span direction the correlation lengths of both components are nearly the same over the entire frequency range for the 0° data, Figures 40 and 41. The same general behavior noted for the longitudinal component can also be seen here. The lengths are about the same at low frequency for both incidence angles with the 6° data rolling off at a lower frequency than the 0° data.

The greatest differences occurred with the normal direction data. Substantially larger correlation lengths were observed in the 6° data for both components of turbulence. Ratios of 3 to 4 times the 0° lengths were observed at different frequencies as may be seen in Figures 38 and 39. Notice that the normal correlation length for the 0° case was found to be .15 cm for the transverse component; this seems very small for a wake of this size.

In general, the lengths measured for the transverse component are substantially different in the three coordinate directions. The extent of correlation in the stream direction is more that ten times that in the normal direction. An eddy length of 2 cm does not seem physically unreasonable for this flow since one half the wake width is about this size. The 0.15 cm normal length seems small; however, examination of both the cross power spectra and the cross correlation functions support this

length as correctly measured.

A rough check of the general magnitude of the stream correlation length can be made through a comparison with some eddy size estimates. Those suggested by Tennekes and Lumley (24) will be used. On page 259 of this reference a measure of the eddy size is taken as

$$l_e = 2\pi/k$$

where k is the wave number which is defined for the present data as $k = \omega/U_c$ with U_c the convection speed in the centerline region of the wake. One half this eddy size, to be consistent with the definition of the correlation lengths, is plotted in Figure 38. As may be seen the eddy size estimate is of the same order as the correlation lengths plotted but with substantial spectral differences.

Another measure which can be made is to compute the integral scale for each of the directions using the spatial correlation functions which are the values of the correlation function at zero time lag. These results are shown in Figures 38, 39, 40, and 42 since these were the only cases for which spatial correlation functions were available. The spatial integral scale is close to the zero frequency value of the correlation lengths. This is expected since the zero wave number for a generalized Fourier transform does correspond to the integral scale.

The greatest differences occurred with normal direction correlation lengths. Substantially larger lengths were observed in the 6° data for both components of turbulence. This

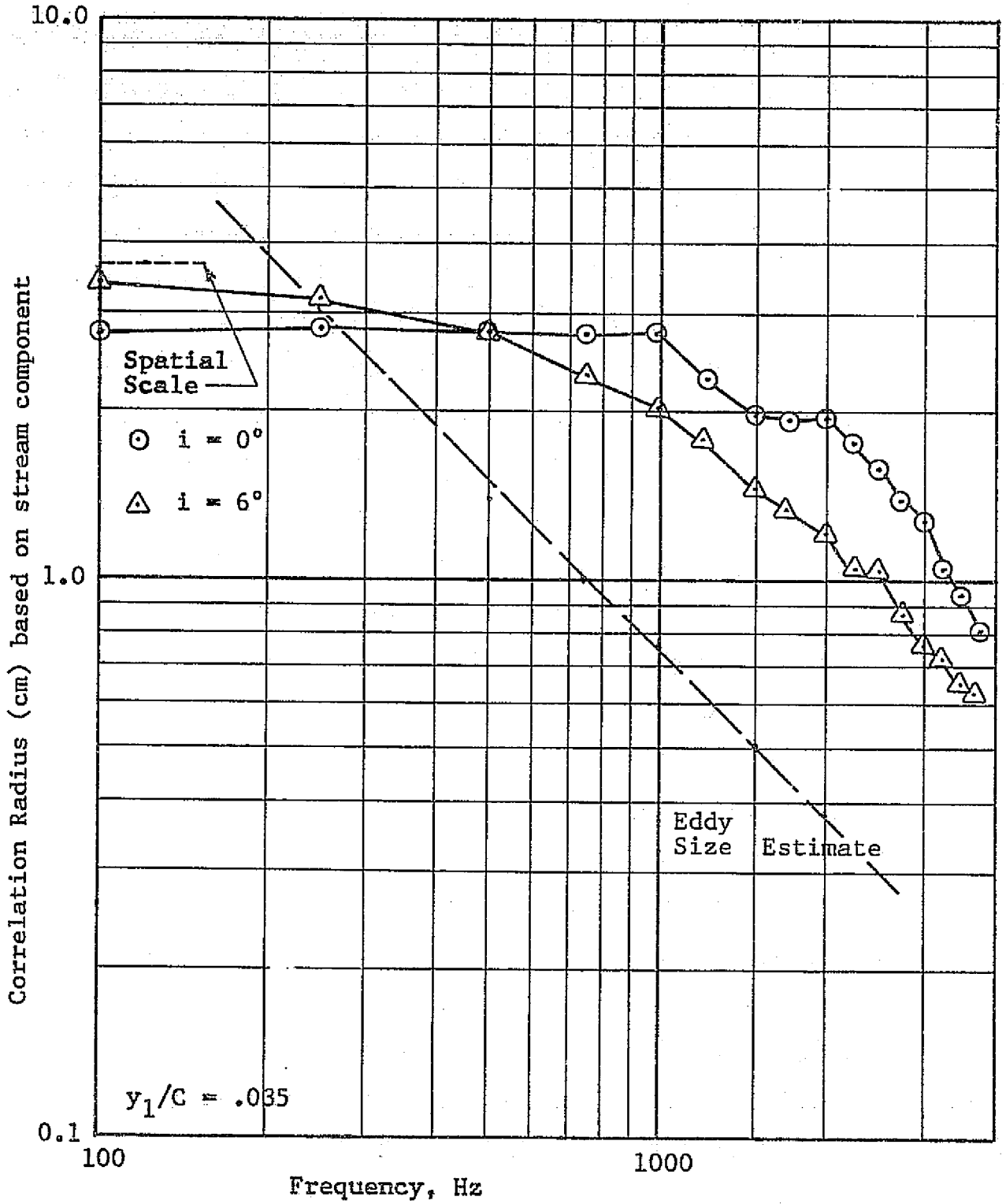

Figure 36 Frequency Dependence of the Correlation Length in the Stream Direction - Stream Component

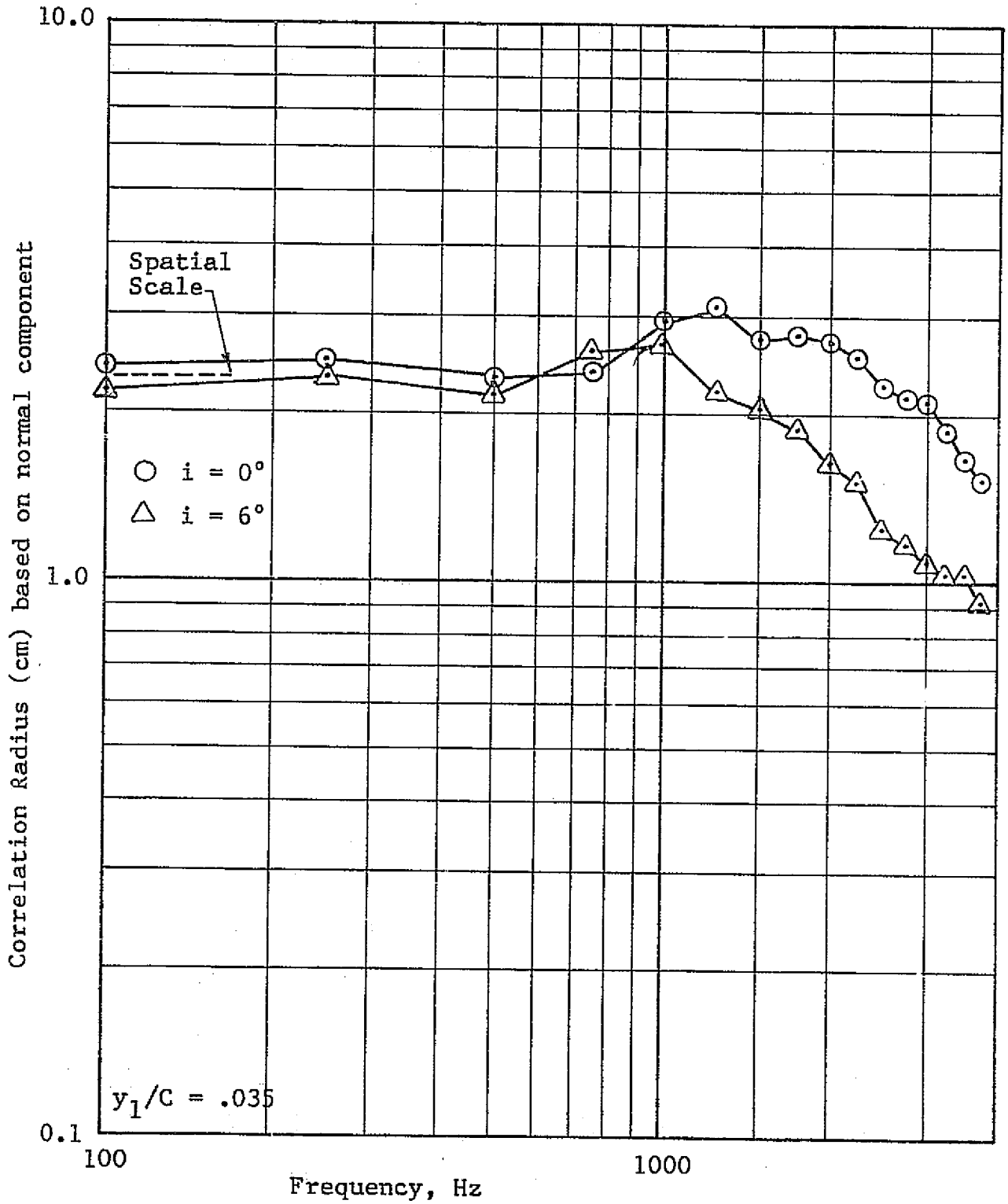

Figure 37 Frequency Dependence of the Correlation Length in the Stream Direction - Normal Component

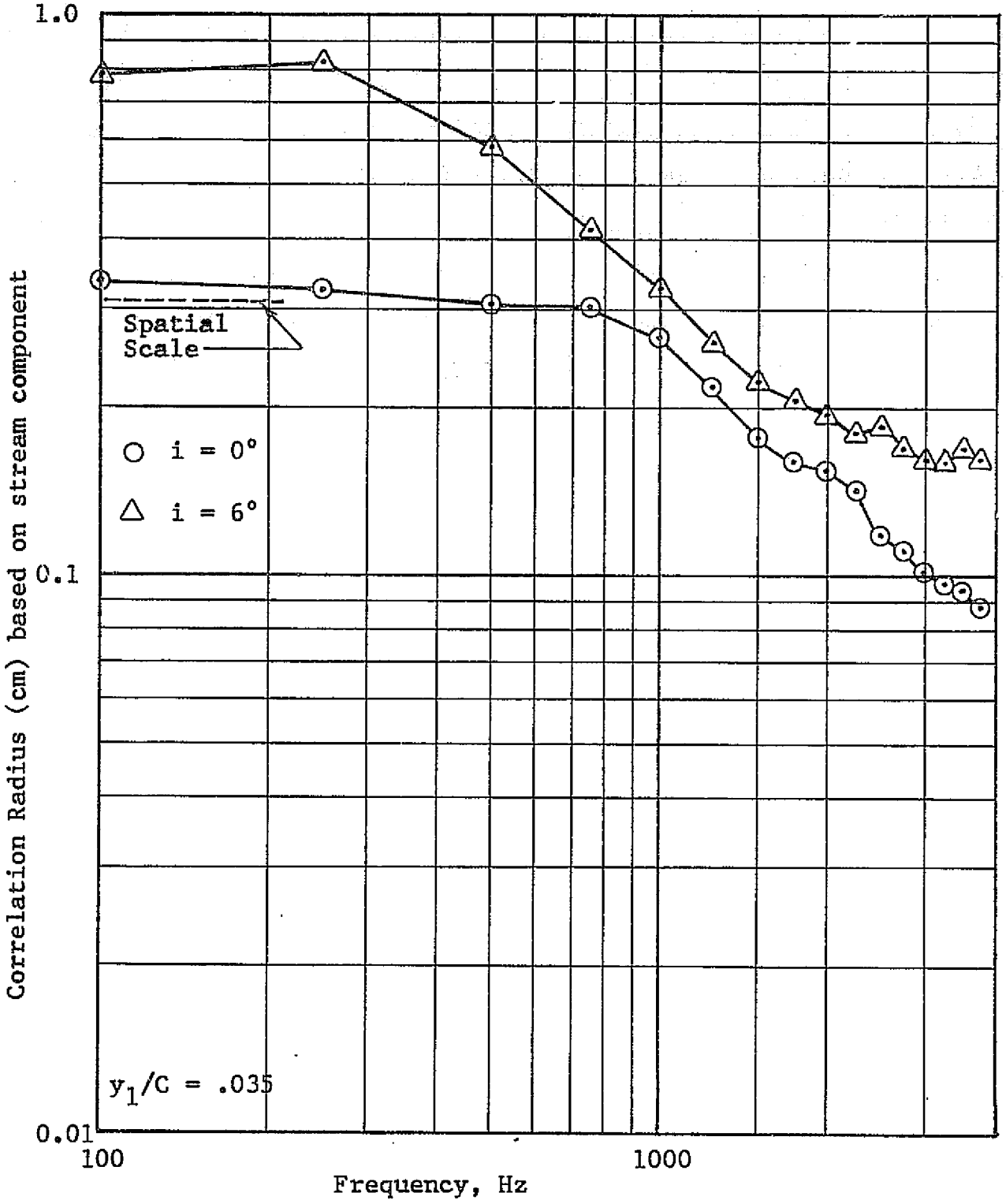

Figure 38 Frequency Dependence of the Correlation Length in the Normal Direction Stream Component

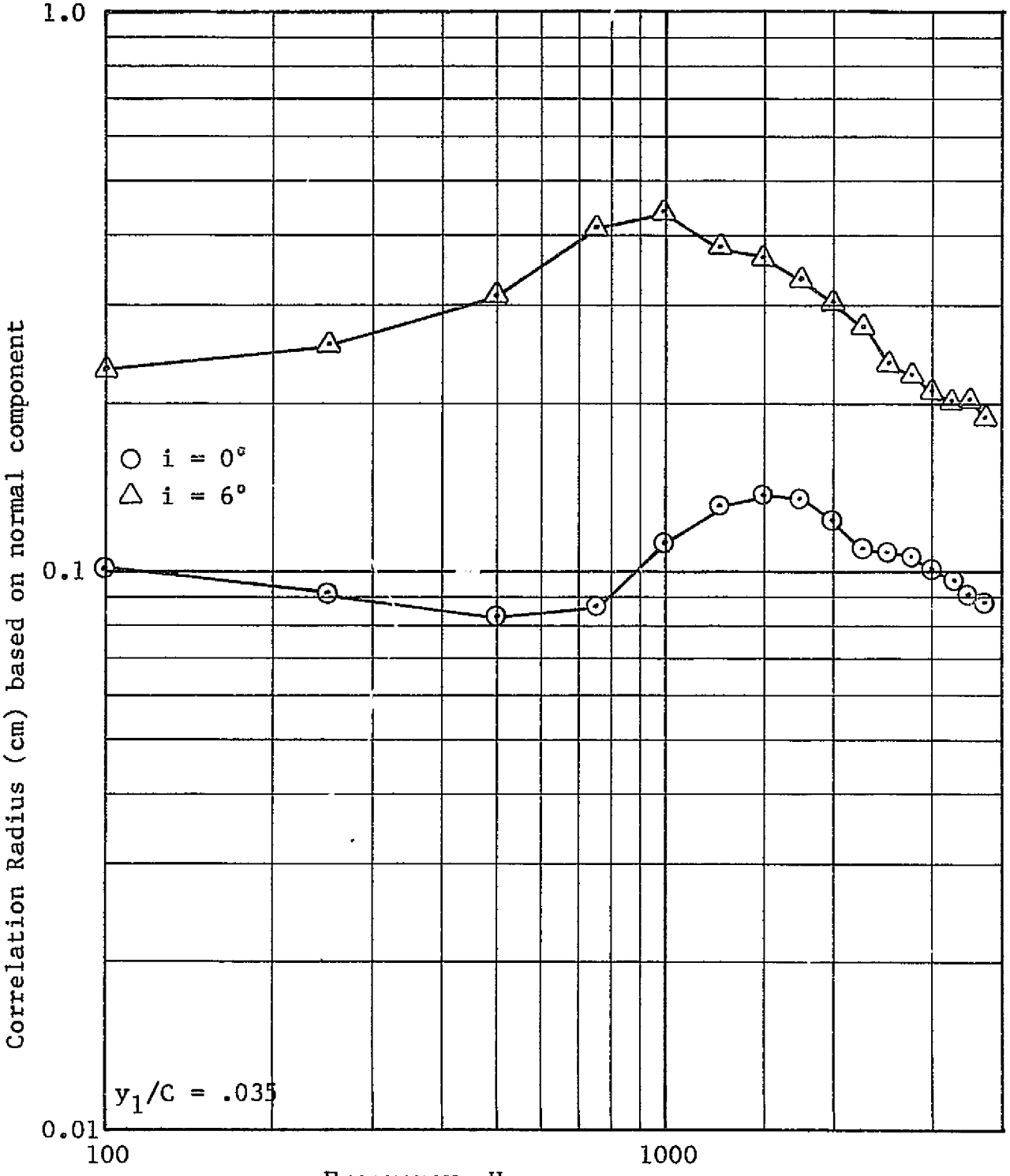

Figure 39 Frequency Dependence of the Correlation Length in the Normal Direction Normal Component

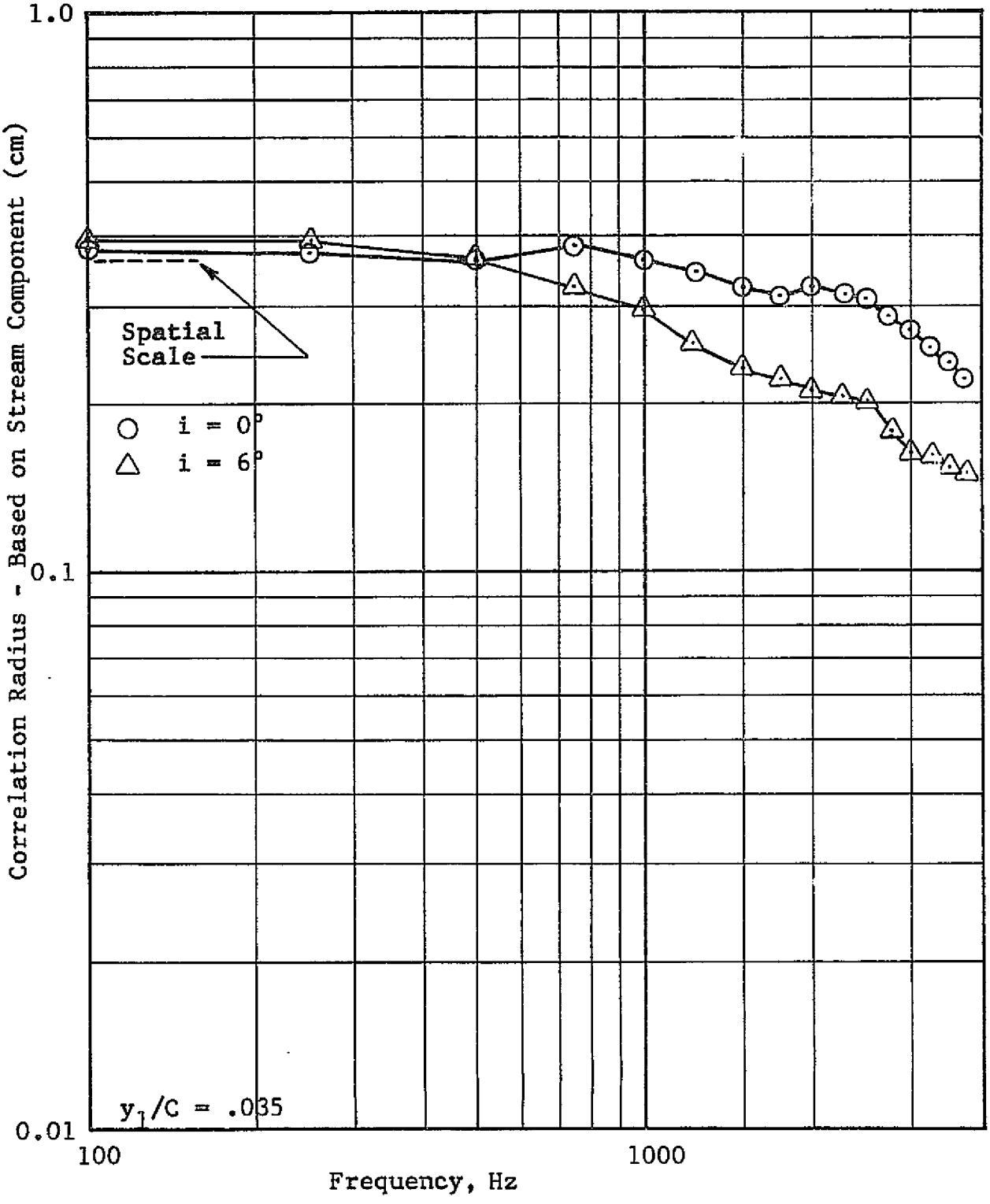

Figure 40 Frequency Dependence of the Correlation Length in the Span Direction - Stream Component

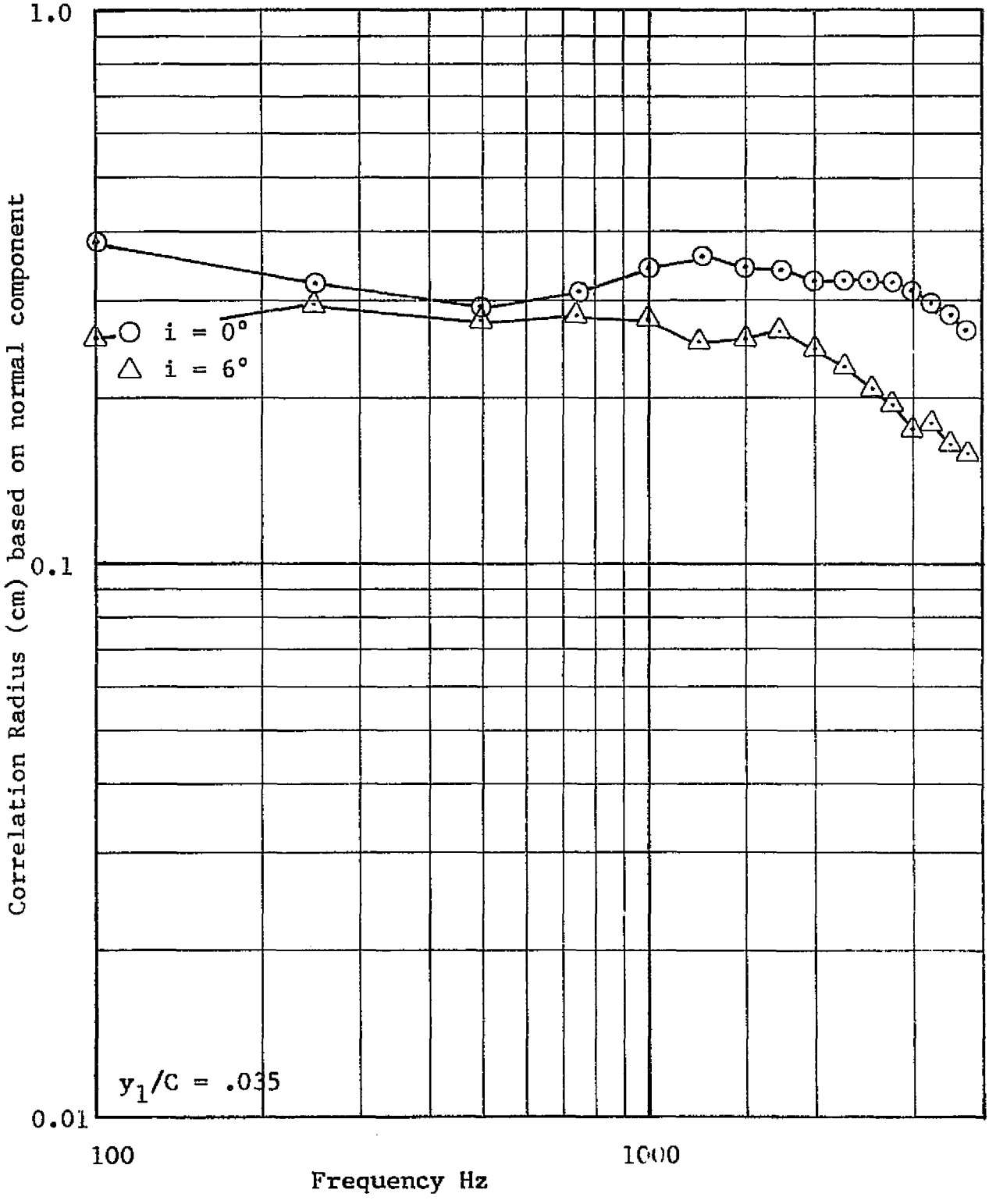

Figure 41 Frequency Dependence of the Correlation Length in the Span Direction - Normal Component

increase in the correlation length across the wake might be expected since the wake itself is thicker. The boundary layer on the suction side of the airfoil is thickened due to the increased loading. An increase of four times seems a large amount but not unreasonable since at 6° the lift coefficient is approximately 0.6 which represents a resonably high loading on this airfoil. In the current data this was observed at the rather high Reynolds number of 2×10^6 so it's doubtful it is a transition effect.

Correlation lengths measured for the longitudinal component are shown in Figure 42 for the 25.4 cm chord airfoil at 0° incidence angle. These will be used in the scaling model.

5.5 Reynolds Number Dependence of Correlation Lengths

Three different airfoils which had basically the same contours were used to provide some information on the Reynolds number dependence of the correlation lengths. The correlation length, based upon the flat part of the spectrum, to chord ratio for the three airfoils is shown as a function of Reynolds number in Figure 43. The smallest airfoil was a 5.1 cm chord series 65-010 operated at $Re = 2 \times 10^5$, the second was a 25.4 cm chord series 63-009 operated at 3×10^5, and the third was the 91.4 cm chord series 63-009 operated at 2×10^6. Distributions of the correlation lengths for the longitudinal component in the flat part of the spectrum are plotted for the three directions. Notice the normal and stream correlation length ratios decrease reasonably slowly with increased Reynolds number in a way which might be expected since the -.2 power line plotted in the figure is the same as expected for flat plate boundary layer growth

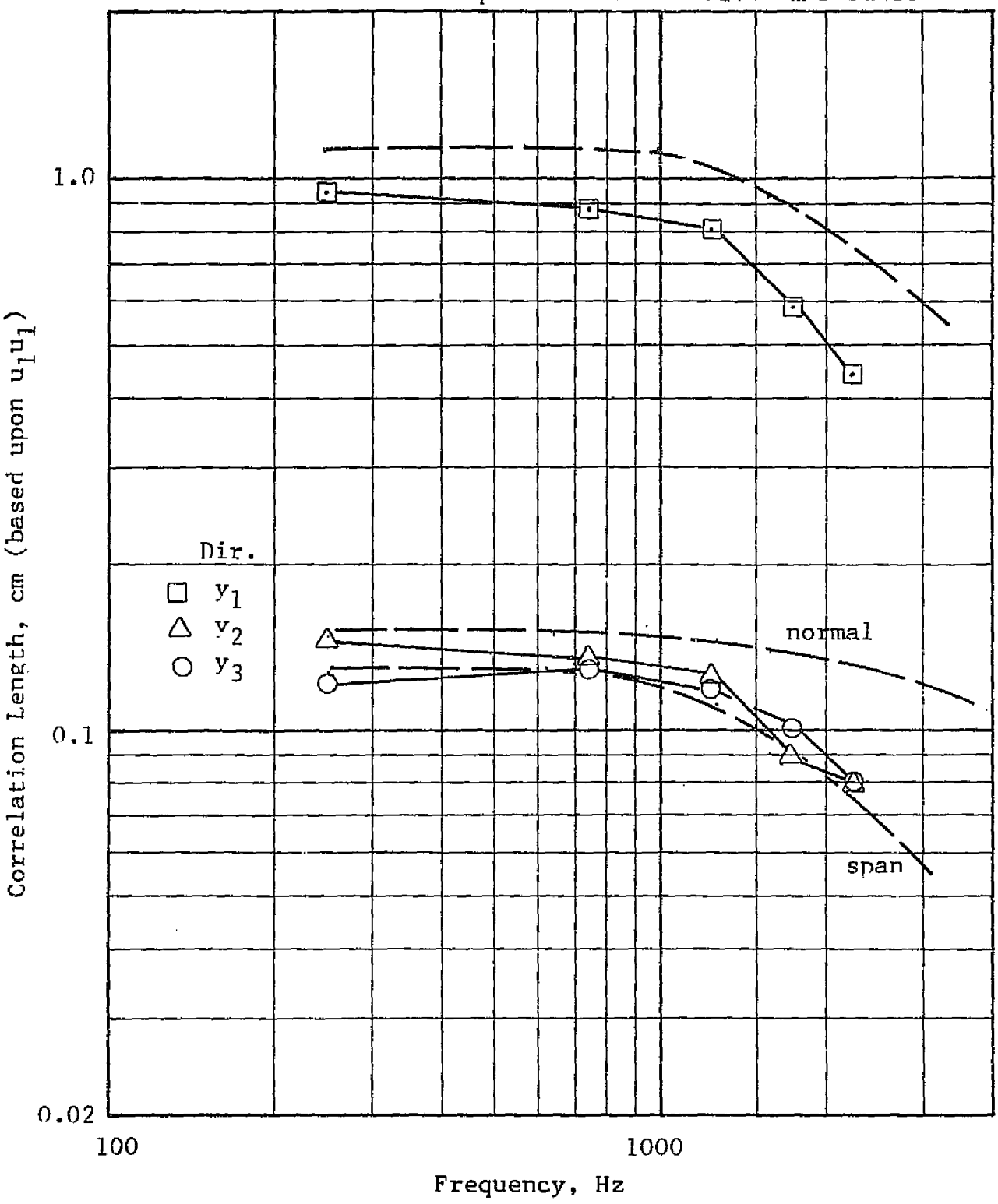

Figure 42 Measured Correlation Lengths for the 25.4 cm Chord Airfoil Shown in Comparison with Scaled 91.4 cm Chord Results

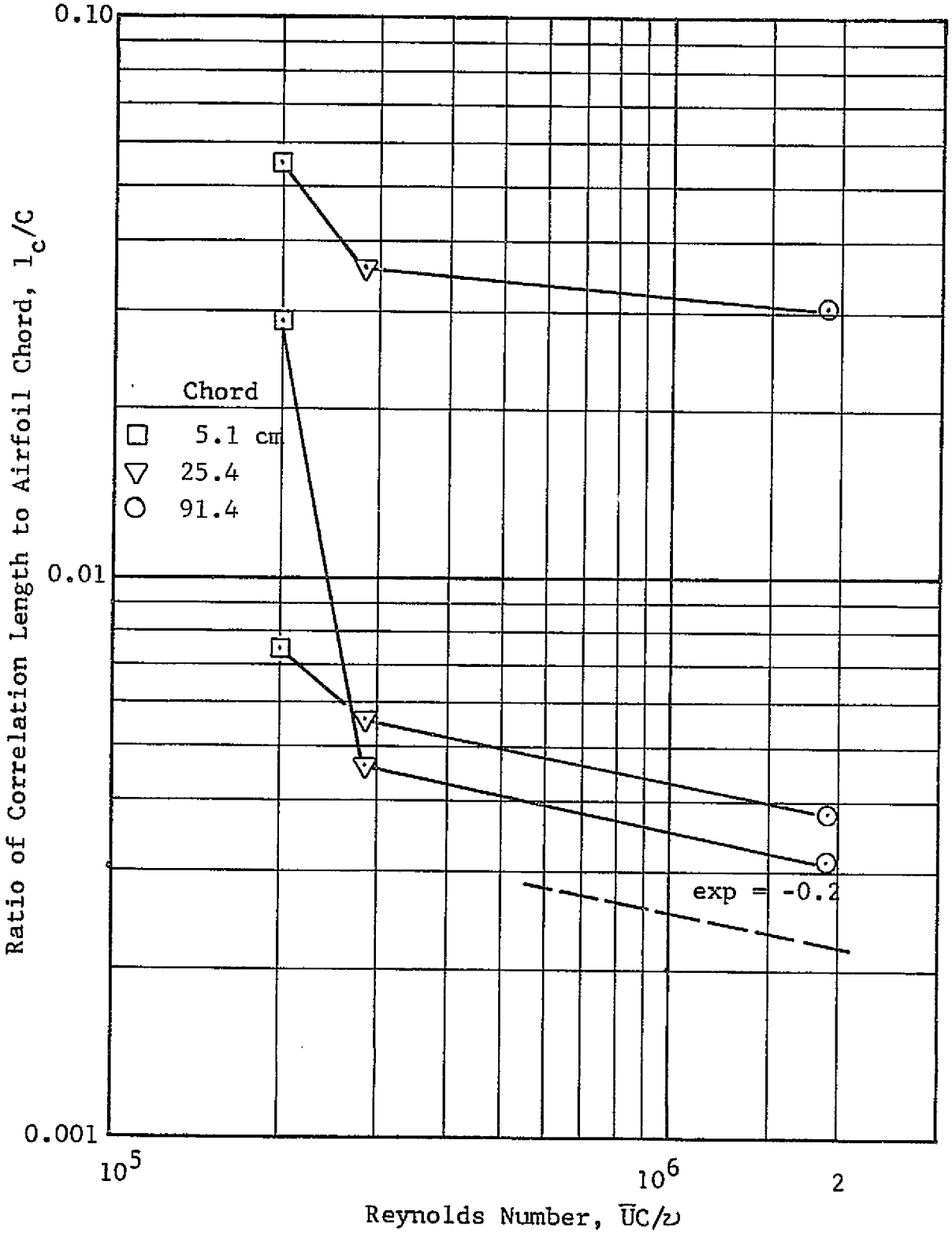

Figure 43 Correlation Lengths for the Three Coordinate Directions as Functions of Reynolds Number

dependence on Reynolds number. The major difference occurs with the span correlation length which decreases much more rapidly in the transistional region than in the fully turbulent region. There appears to be a very strong dependence of the span correlation on the Reynolds number for airfoils of this type. In fact, based on this plot, there could be a ten fold increase in the span correlation length over the range of Reynolds number from 2×10^5 to 2×10^6. Certainly much more work is needed to establish this dependence. That it is important is evidenced by the fact that if all else were equal the change in correlation length observed would result in an increase of 10 dB in the radiated sound pressure level.

5.6 Phase Measurements in the Near Wake

Phase angle measurements for different axial separations were determined as a function of frequency. This was done by computing the magnitude and phase representation of the cross power spectra. Results for the near wake are shown in Figure 44. The phase angle may be seen to plot as a straight line for each of the separations. Computations between the frequency and separation indicate the same convection velocity for all the frequency components. This suggests that the turbulence can be considered as being convected along at the same mean velocity in a kind of frozen structure.

Similar plots were not made for the transverse component but examination of the cross covariance functions suggested that the same general result would be valid. It appears that there may be some slight irregularities in that there is a small amount of distortion of the correlation function as it

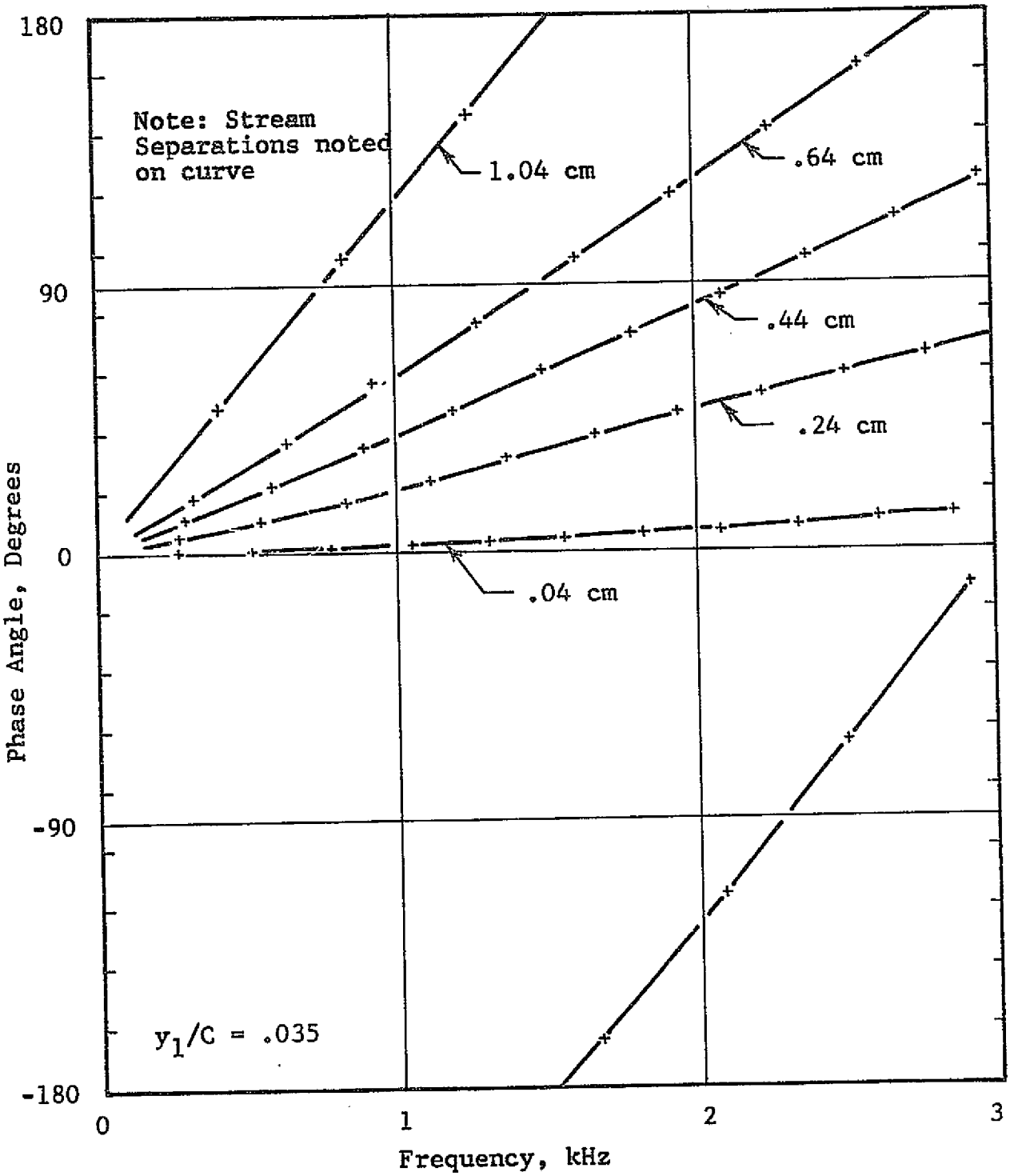

Figure 44 Frequency distribution of Phase angle Based Upon Longitudinal Turbulence Component

convects downstream. This would suggest different velocities for different frequency components. The effect is not large.

5.7 Normalized Autospectrum

In an effort to compare some of the current data with that of other investigators a normalized plot of the transverse component of turbulence is shown in Figure 45. The free stream velocity and the wake displacement thickness was used to normalize the frequency. The resulting plot seems to put the energy in the same frequency range as Mugridge found for the static pressure fluctuations.

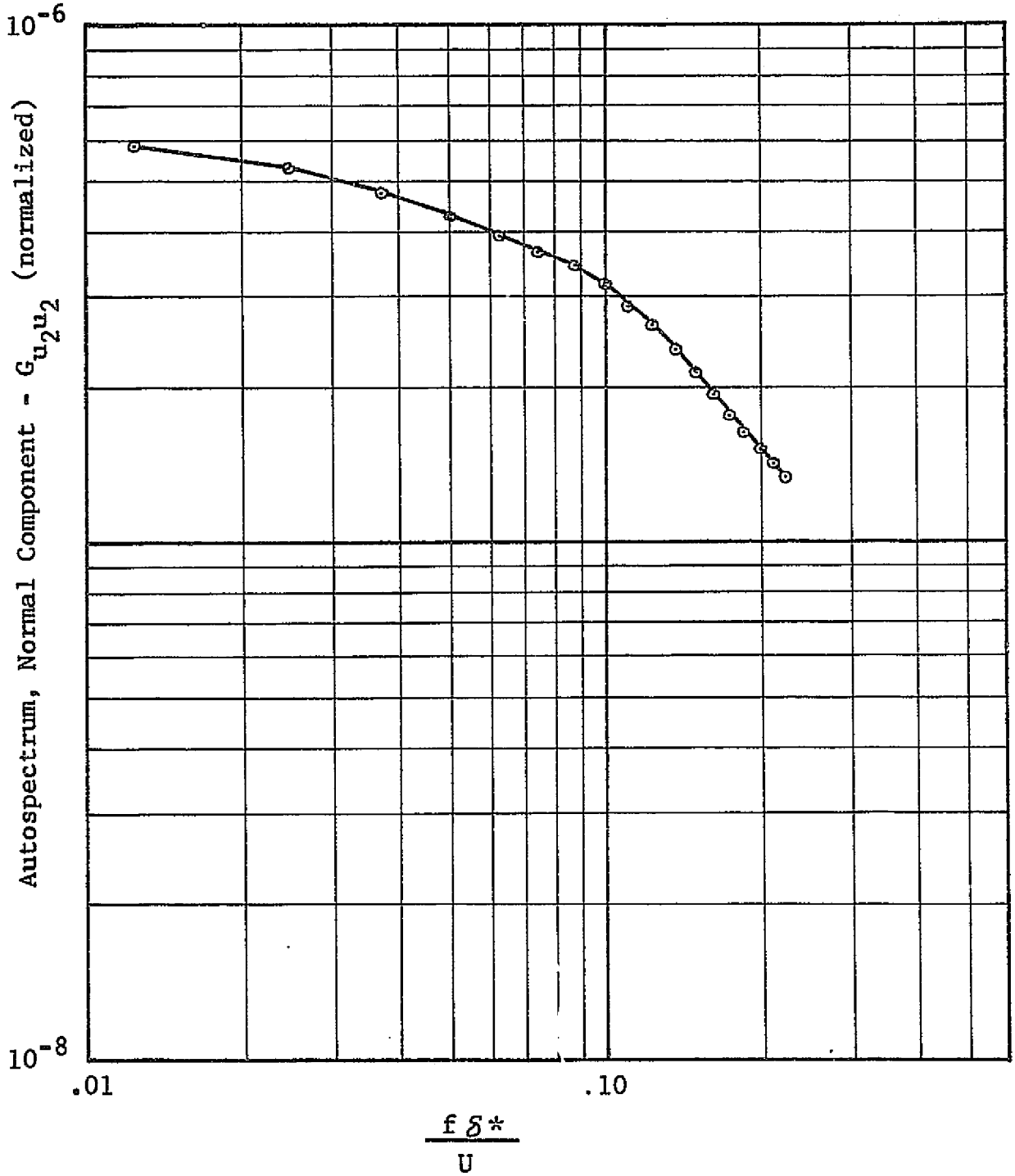

Figure 45 Nondimensionalized Spectrum of the Autospectrum of the Normal Component of Turbulence

6.0 Discussion

The results of the turbulence measurements were sufficient to complete the prediction models for the single airfoil and the rotor. In this section, the results of the predictions for the single airfoil will be compared with some experimental data in an effort to assess the effectiveness of the model. A scaling procedure is outlined and some sample computations for a large subsonic rotor design are presented.

6.1 Single Airfoil Results

The first question to be addressed is certainly how well does the model work. There are very few acoustic data available for airfoils operating in smooth flows where wake effects may be assumed to dominate the sound generation. The best that could be done was to scale the present data to the range of parameters used in the acoustic tests reported in reference 16. A summary of the pertinent variables follow:

Turbulence Measurements	Sound Measurements
series 63-009 airfoil	series 65-010 airfoil
45.7 m/sec	88.2 m/sec
91.4 cm chord	5.1 cm chord
Re = 2×10^6	Re $\times 10^5$
incidence = 0°	incidence = 0°

As may be seen the Reynolds numbers differ by an order of magnitude. The basic contours are similar; the 65 and 63 series airfoils are not substantially different. Overall RMS wake turbulence spectra were available for the 5.1 cm airfoil and these were used for this prediction. Correlations were taken from the 91.4 cm airfoil data and scaled to the 5.1 cm airfoil. The frequency was scaled by plotting the autospectra of the longitudinal component of turbulence for each case on a common

scale, then overlaying the spectra. Alignment which gave the best agreement corresponded to a frequency scaling factor of 10. Since the scaling was being done from the fully turbulent region of the large airfoil to the transitional region of the small one, this overlaying scaling method was felt to be the most valid one. The actual values of the correlation lengths were taken from Figure 46 where the Reynolds number effect was included. The scaled lengths were then used in the prediction.

Results of the predicted spectrum for sound radiation normal to the airfoil chord are shown in comparison with the measured data in Figure 46. Agreement is good considering the fact that the correlation length dependence on frequency was assumed to be scalable to the transitional flow regime to the fully turbulent regime.

It is important to observe that the roll off in the radiated SPL at higher frequency is predicted by the model. This effect is critical in predicting useful spectra since any subjective evaluation will be very sensitive to the high end of the spectrum. The importance of this can be seen in the sample rotor case to be discussed later in this section.

A radiation pattern for the airfoil is shown in Figure 47. Radiation patterns for different frequencies are plotted in the figure. A substantial difference can be seen to exist with the levels for different frequencies. The differences can be interpreted by envisioning two dipoles, one aligned parallel to the airfoil chord and the other perpendicular to it. The parallel dipole has magnitude corresponding to the longitudinal component of turbulence and the perpendicular dipole corresponds

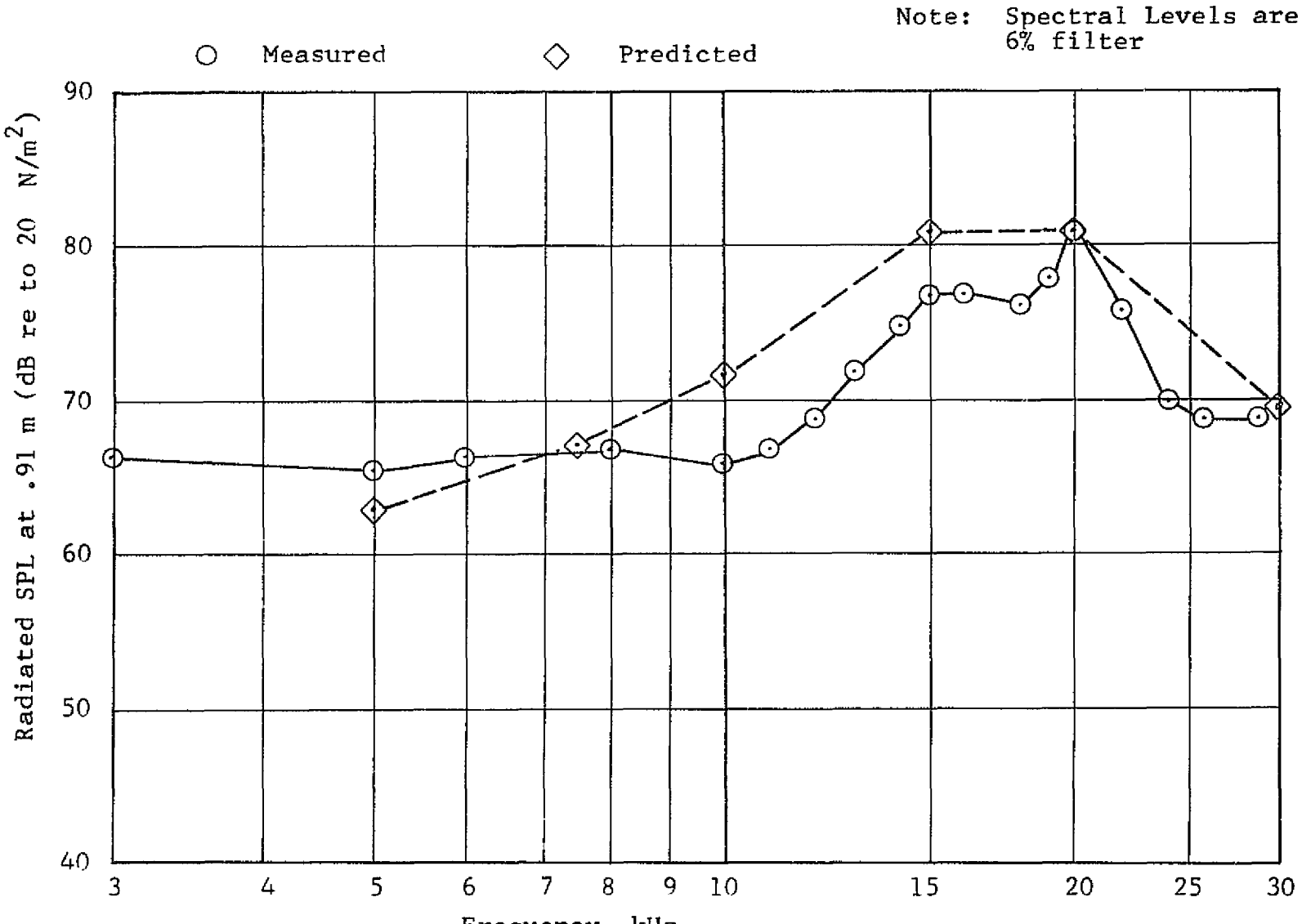

Figure 46 Comparison of Measured and Predicted Radiated SPL Spectrum for 5.10 cm Chord, Series 65-010, 0° Incidence, 88.2 m/sec

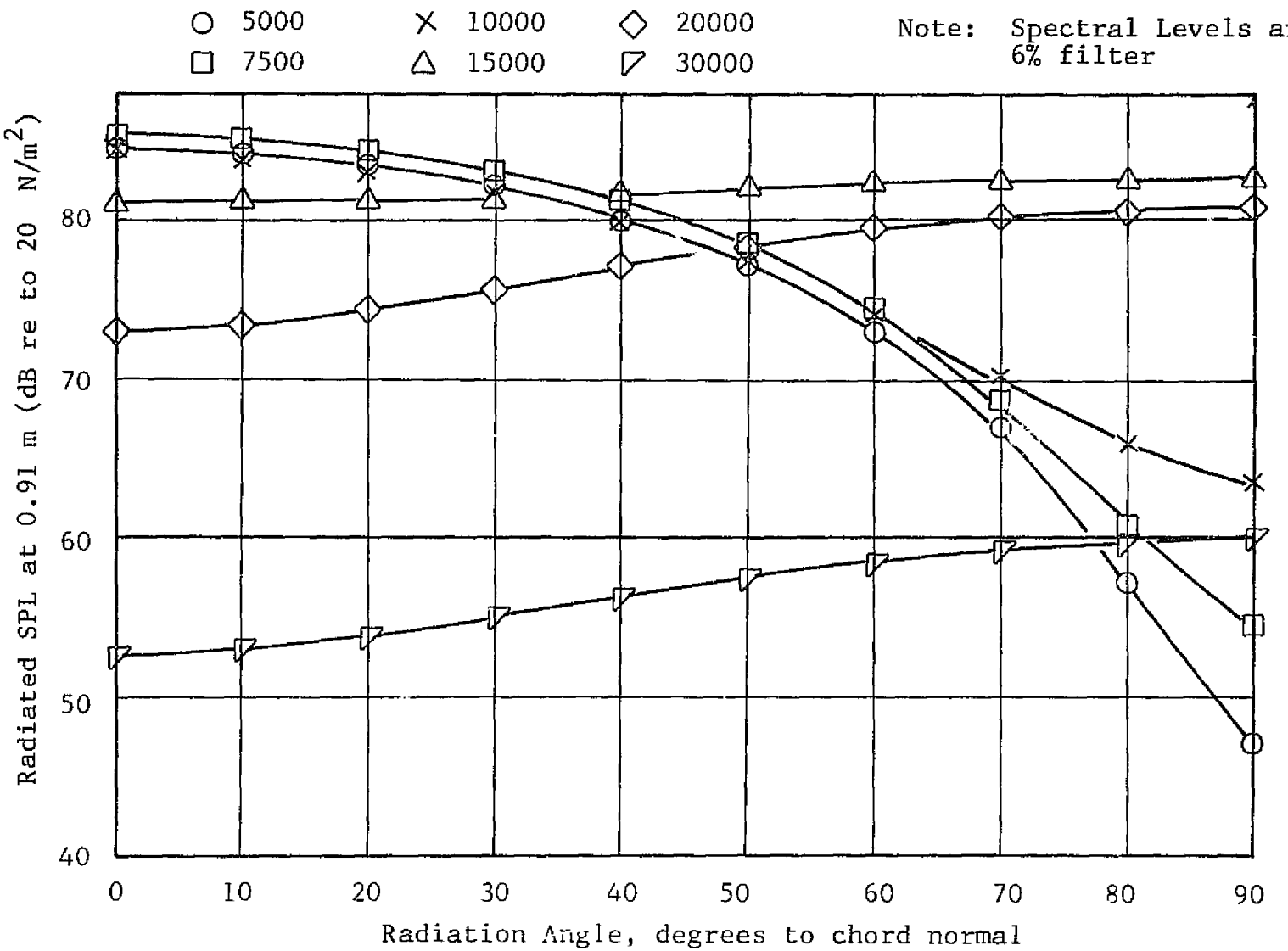

Figure 47 SPL Radiation Pattern as a Function of Frequency

to the transverse component. In those parts of the spectrum where the power spectral level of the transverse component is greater than the longitudinal component, the dipole in the perpendicular direction will dominate. The observed dominance of the transverse component of turbulence in the transitional range of Reynolds number may explain the apparent single dipole nature of the acoustic data taken there. As an example, the data shown in Figure 48 illustrate this tendency. Notice even here there is a greater fullness to the measured pattern than in the theoretical dipole. This fullness may be explainable in terms of the reduced, but still existant, contribution of the longitudinal component at this Reynolds number. Turbulence data taken at the time indicated the normal component of turbulence to be about 10 times the level of the longitudinal component (18).

When the cross terms are included the radiation pattern will no longer be symmetric but will be distorted in the forward and aft arc depending upon the net shear stress in the wake. A net shear stress will result when the wake is non-symmetric; this would occur for highly loaded airfoils.

6.2 Scaling

Before discussing any detailed scaling method it is important to be aware of the existence of the two flow regimes which may be present in any particular case. It appears that laminar separation induced vortex shedding will contribute in a major way to sound generation at transitional Reynolds numbers. This mechanism is characterized by pure tones or nearly pure tones corresponding to the frequencies in the vortex shedding.

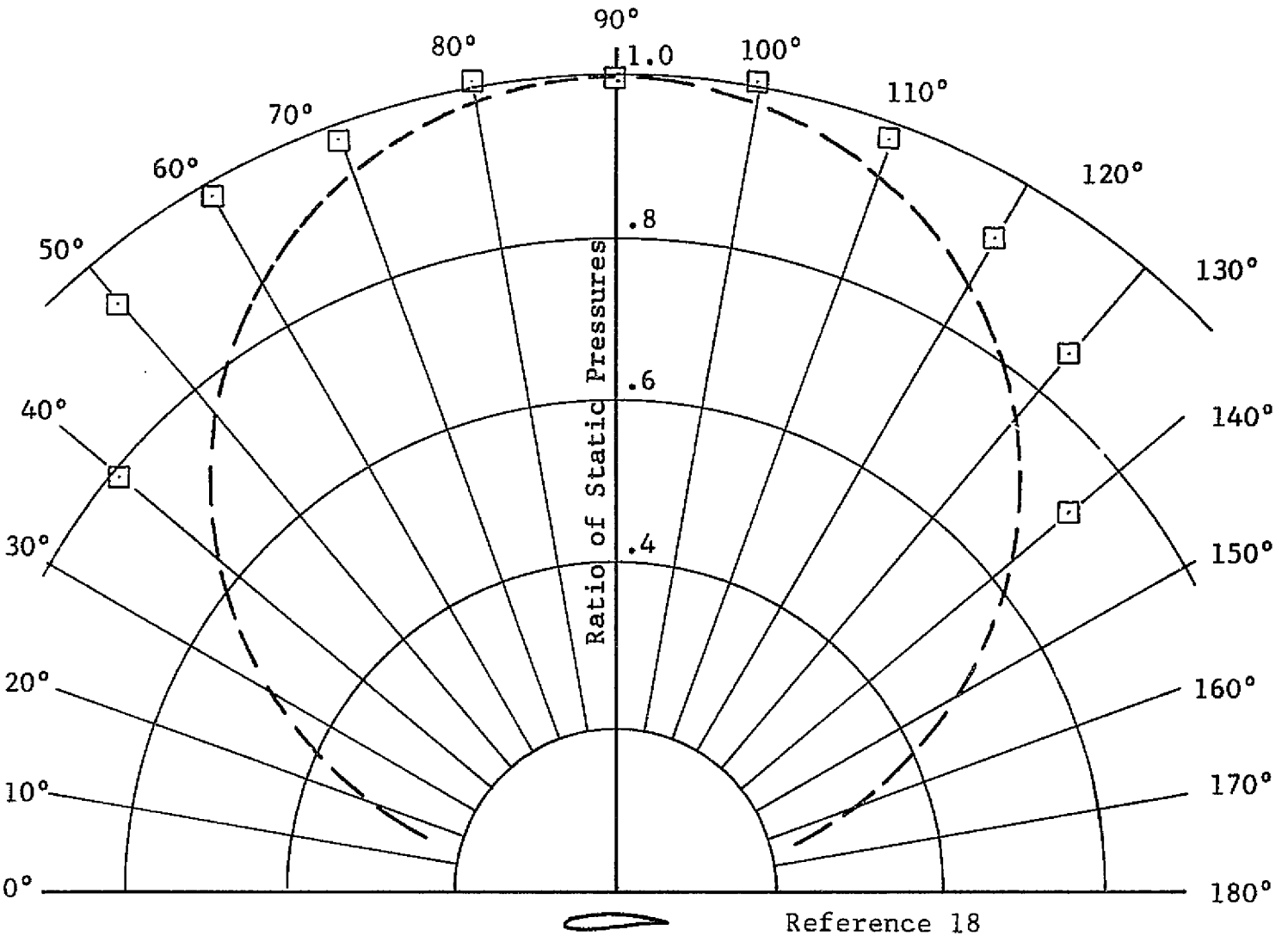

Figure 48 Comparison of Ideal Dipole Radiation Pattern with Experimental Results for Wake Effects Dominating

Patterson et al (17) have made extensive measurements of this effect and were able, through a mapping over a wide range of Reynolds number and incidence angle, to estimate the flow regimes where the tone mechanism would be present. A typical plot from their findings for an NACA 0012 airfoil is shown in Figure 49. The tone appears to be present at higher Reynolds numbers when the airfoil is operated at non-zero incidence angles. This author has observed similar effects (16); not with the pure tones observed above but rather a narrow band random type of spectrum. As the Reynolds number is increased the tone tends to change into a narrow band random shape and eventually vanish into the wide band turbulence spectrum.

A scaling procedure was suggested for frequency in reference 17 which used a relationship for the Strouhal number based upon boundary layer thickness. Recall the form

$$S_t = 2 f \delta_{lam} / \bar{U}$$

and the laminar boundary layer thickness was written

$$\delta_{lam} = K C Re^{-.5}.$$

This resulted in a frequency scaling dependence of the form

$$f \propto U^{1.5} / (C^{.5} \nu^{.5})$$

The scaling in this way was used successfully to scale the tones they observed in their experiments and also the peaks reported in the spectra in reference 16.

An approach similar to that outlined above was used in an attempt to obtain a frequency scaling rule for the fully turbulent region.

In what follows a limitation to flows where the tone does not exist is made. This generally will mean chord Reynolds

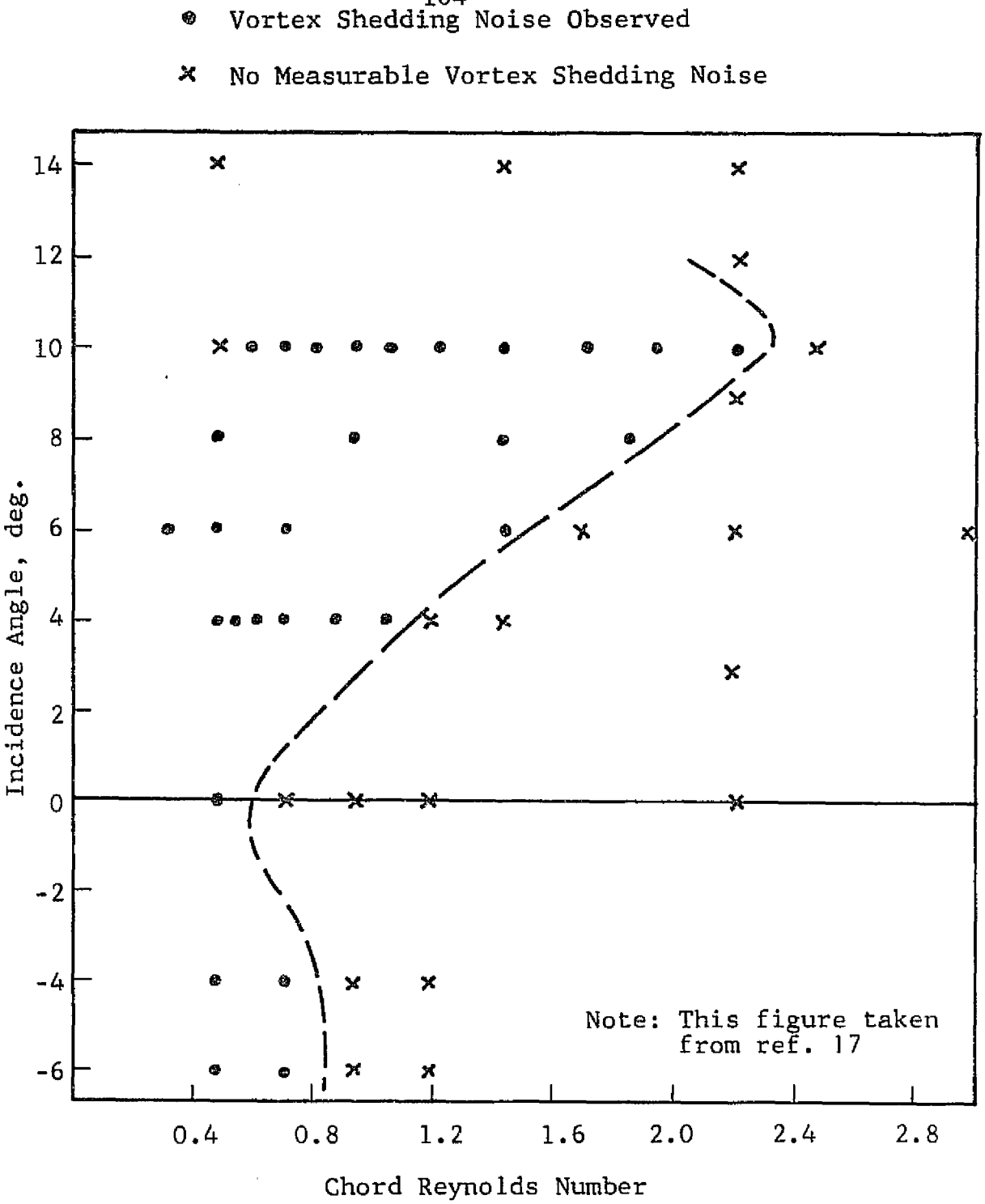

Figure 49 Observed Regions of Vortex Shedding for a NACA 0012 Airfoil as Function of Incidence Angle and Reynolds Number

greater than 3×10^5. This restriction will have little practical significance since most machines of interest operate at the higher Reynolds numbers.

The scaling procedure will be established for the correlation lengths, the frequency, and the mean flow parameters. This present method is suggested for use only with small values of incidence angle since significant amounts of non-sero incidence angle data are not yet available. The method would be expected to underestimate the actual spectral levels for the more highly loaded airfoils.

6.2.1 Correlation Lengths

Correlation lengths are assumed to be proportional to the turbulent boundary layer thickness. Dependence of the boundary layer thickness on Reynolds number for fully developed turbulent flow on a flat plate has been shown to be

$$\delta_t / C \propto Re^{-.2}$$

This approximate dependence was also observed for the correlation lengths measured for the 25.4 and 91.4 cm airfoils. Based upon this, the scaling can be written

$$(l_c/C) = (l_c/C)_{91} \, (Re/Re_{91})^{-.2}$$

where the Reynolds number for the large airfoil is $Re_{91}=2x10^6$. The above result is used as a frequency independent scaling parameter which means it is used across the entire spectrum with no further modification.

6.2.2 Frequency

An approach similar to the one described for the tone frequency scaling will be outlined here for the turbulent flow regime. Defining the Strouhal number in terms of the turbulent

boundary layer thickness

$$S_t = 2 f \delta_t / \bar{U}$$

and assuming there exists a common Strouhal number for the entire turbulent regime, this relationship can be used to scale the frequency. Dependence of the boundary layer thickness on the chord Reynolds number can be expressed in the same way as was done for the correlation lengths. Combining with the Strouhal number yields a scaling factor for frequency which is

$$f = f_{91} (U / U_{91})^{1.2} (C / C_{91})^{-.8}$$

with: U_{91} = 45.7 m/sec and C_{91} = 91.4 cm.

One opportunity exists to check the scaling rules for length and frequency by using the measured data for the 25.4 cm chord airfoil. Since only data were taken for the longitudinal component of turbulence, comparisons are limited to this component. The spectra of the correlation lengths for the 91.4 cm airfoil were scaled to the 25.4 cm case using the above rules. The scaled lengths could then be compared with those actually measured. Pertinent variables for the scaling are:

91.4 cm airfoil	25.4 cm airfoil
U = 45.7 m/sec	U = 23.7 m/sec
Re = 2 x 10^6	Re = 2 x 10^5
incidence = 0°	incidence = 0°

Results are shown in comparison with experimental lengths in Figure 42. The frequency scaling appears to be fairly good since the shapes of the scaled and measured spectra are roughly the same. The actual values of the lengths are scaling with a maximum difference of about 20 to 30%. However, it is apparent that the scaling is different in different parts of the

spectrum since the shapes of the curves are not the same. As a first approximation the procedure doesn't look too bad.

6.2.3 Mean Turbulence Levels

It is recommended that the actual results for the 91 cm airfoil as non-dimensionalized by the free stream velocity be used directly with no further correction. Measured RMS turbulence levels were very nearly the same for all three airfoils so the usage of the data from the large airfoil should introduce little error.

6.2.4 A simplified Sound Radiation Model

A simplified form of the prediction model may be established for use in trade studies where detailed aerodynamic data are not available.

Ignoring the effects of the cross terms and the spatial distribution of the wake properties, the model can be expressed in terms of mean wake parameters and a simple algebraic form written. The power spectrum for the radiated sound density:

$$G_p(\vec{x},\omega) = \frac{\rho_0^2 \bar{U}^2 \delta_\omega S}{(4\pi a_0^3 |\vec{x}|)^2} \omega^4 16 \Big[\sin^2\psi \; L_1^2(u_1,u_1,\omega) L_2(u_1,u_1,\omega) L_3(u_1,u_1,\omega) \overline{u_1 u_1}(\omega) + \cos^2\psi \; L_1^2(u_2,u_2,\omega) L_2(u_2,u_2,\omega) L_3(u_2,u_2,\omega) \overline{u_2 u_2}(\omega) \Big]$$

where it can be seen that the dependence on the velocity is to the sixth power as expected from the dipole force mechanism. This sixth power results from the second power directly on the velocity and the fourth from the frequency which is itself

approximately proportional to the velocity. The sound is proportional to the wake thickness δ_w, the airfoil span S, the stream correlation length L_1, and the correlation volume approximated by the product $L_1L_2L_3$. The velocity used probably should be a mean velocity in the wake; a value of 0.8 U would be reasonable in view of the measured velocity obtained in the experimental data.

The above method will be expected to work best for airfoils with small lift coefficients. For more highly loaded airfoils which better characterize real machines, one can expect the prediction to be low. It is expected that incidence angle correlations will be possible once more data are available, particularly on the effect of the incidence angle on the span correlation length.

6.3 Rotor Results

The scaling method established in section 6.2 was used to supply information to enable the prediction of the spectrum of sound generation by a subsonic rotor. The design chosen was to roughly approximate what might be expected for a large subsonic fan as may be used in an STOL type of aircraft. The design was approximated by a single source for each blade in the rotor. This is a crude approximation but in view of the amount of computer time required to carry out a distributed source representation and the absence of any particular design it was felt sufficient to demonstrate the effects with a simple single force per blade. The rotor program has been devised to predict the sound for the direct problem of a given aerodynamic design and must be used in this way.

The design details for the particular rotor to be studied are as follows:

Diameter: 4.56 m (15 ft)
Chord: .91 m (3 ft)
t/C: 0.09
Tip speed: 182 m/sec (600 ft/sec)
Source Radius: 0.8 R_{tip}
Stagger angle: 65°
Blade number: 12

Using these variables and the scaling procedure, the predicted sound radiation spectrum for three radiation angles measured from the inlet rotor axis are shown in Figure 50. There are some differences in the pattern at the different angles but the overall effect appears to be to radiate essentially the same amount in all directions. This essentially uniform radiation pattern has been observed experimentally by the author for several rotors ranging from 6 inch diameter compressor rigs all the way to the Pratt and Whitney JT9D engine when operated in the subsonic Mach regime.

Effects of source motion on the radiated sound can be observed in a simple way using the rotor model. If the RPM for the rotor is set to zero but the relative velocity onto the blades is left at the same value (both are independent inputs to the computer program) the rotor behaves as a stator. This stator configuration can then be used to illustrate the effects on the radiated sound spectra by Doppler changes. The two spectra for the rotor and the stator are shown in Figure 51. There is very little change in the radiated sound spectrum due to the motion of the sources. This is to be expected since the shift

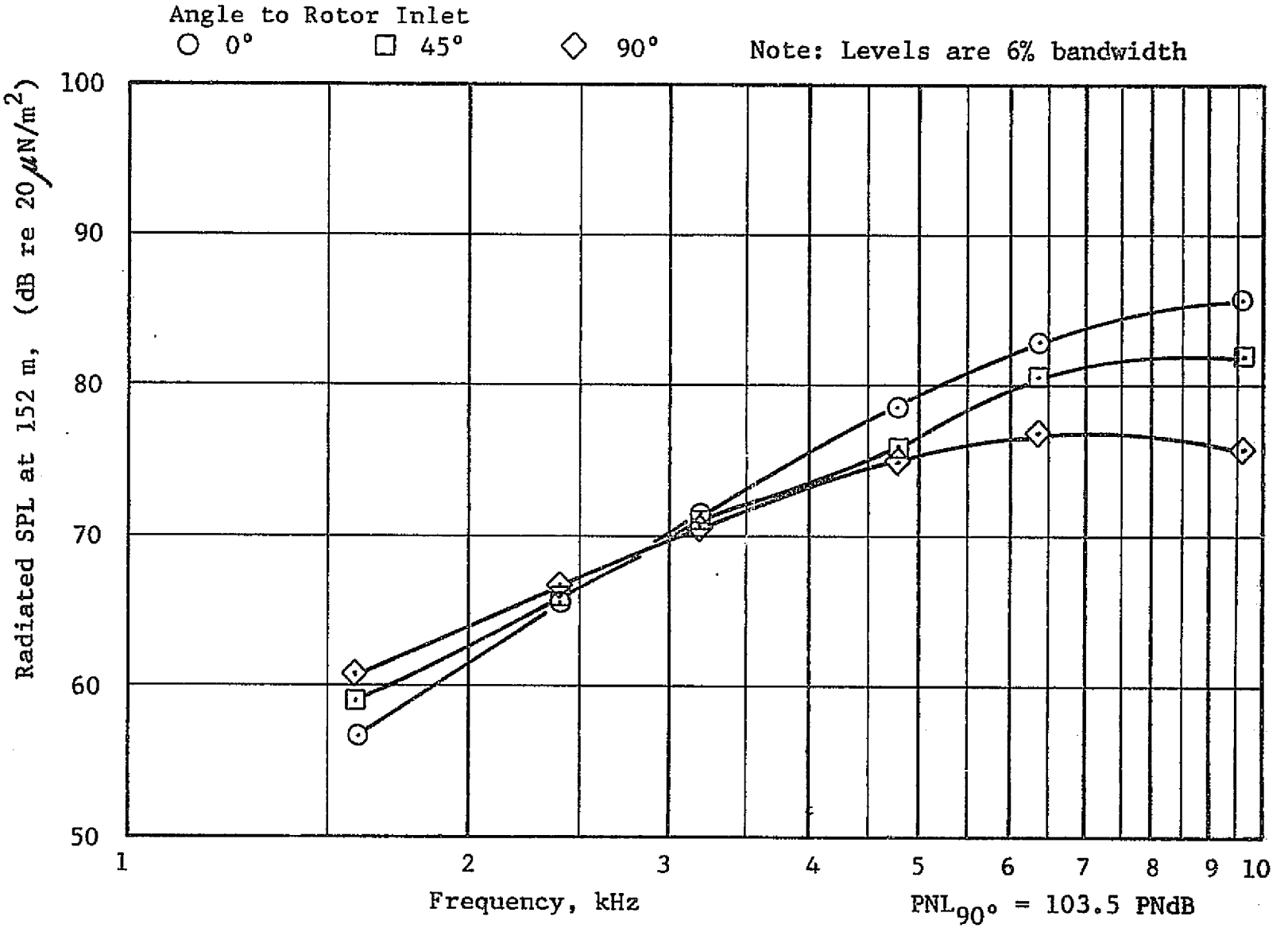

Figure 50 Radiated SPL - Spectra for Wake Related Sound by Large Subsonic Rotor - Dia. = 4.6 m, U_{tip} = 183 m/sec

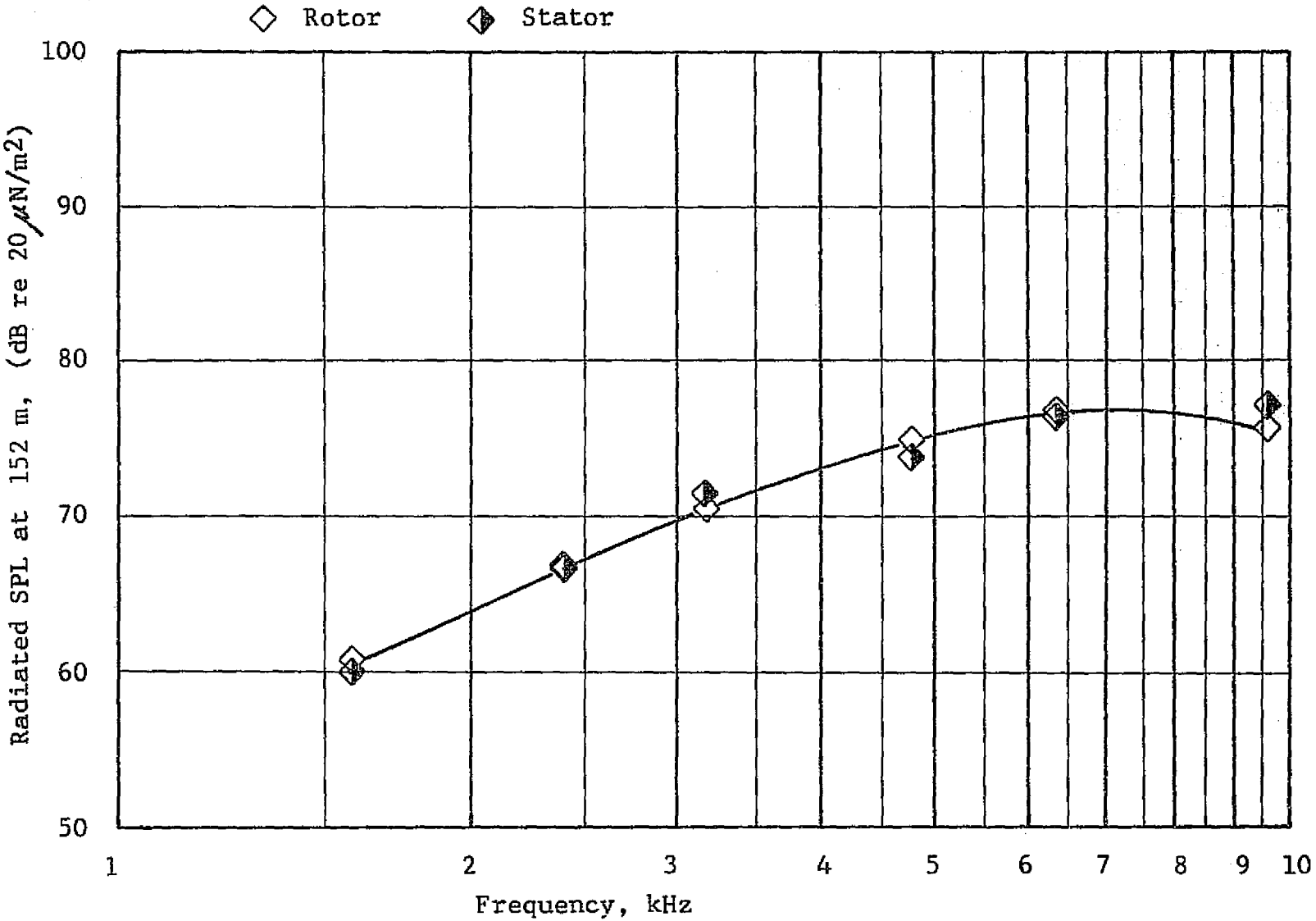

Figure 51 Illustration of the Effect of Rotation on the Radiated SPL, Design are Identical, One Source Set is Rotating

in the spectrum is to neighboring levels and since the spectra of the two point velocity correlations are essentially flat there would be little effect. However, if the source spectra were more narrow band in nature as for the case where vortex shedding might be present, then the effects of the source motion could be substantial.

The last point to be discussed is the subjective sound level of this rotor. The 500 ft (152 m) sideline noise level as indicated by the Perceived Noise Scale was computed to be 103.5 PNdB. This is the noise due to the wake related broad band effects. Any contribution by the pure tones or due to inflow turbulence would add to this figure. This is a fairly high level. It results because the frequency of the sound happens to fall at levels where the human ear is most sensitive. There are currently proposed engine designs which are similar to the one used here and they may have this noise problem. The idea of these designs is to use a relatively large number of rotor blades since cancelation effects tend to reduce pure tone noise. Based upon the present results, the trade to wake noise may be too much. The quality of the noise will be much like the jet noise from current turbojet engines but with the frequency shifted to 4 or 5 kHz from the present 1 kHz. The sound would be a scream.

These large fans may be amenable to design procedures which could reduce the wake related noise. If boundary layer control could be used on the blading, the reduction of the correlation volumes in the wake might result in reduced noise generation. A great deal of research would be needed to develop a viable

control system for a rotor of this size and complexity. One would envision a very long and costly development period.

7.0 Conclusions

1. It appears based upon the agreement obtained between measured and predicted sound spectra that a sound prediction model based on approximating the force fluctuation on an airfoil by the fluctuation of momentum in the near wake is a useful method. However, to build confidence in this approach more experimental sound radiation data from single airfoils is needed.

2. The effect of the Reynolds number can cause large variations in the extent of correlation in the span direction in the wake. Between the transitional and fully turbulent flow regimes changes in the span correlation length of an order of magnitude were observed.

3. A major effect of the incidence angle appears to be in the normal correlation length.A change of 6° resulted in a factor of nearly 4 increase in the correlation length in this direction with significantly less in the other directions.

4. Using the results for the single airfoil model a scaling procedure was developed and used to predict correlation lengths at another Reynolds number with fair success. More work is needed before an accurate scaling method can be expected.

5. When extended to a rotor configuration it was found that large scale subsonic fan rotors may be expected to generate wake related noise of significant subjective levels. The possibility exists for reducing noise by these fans through boundary layer control on the rotor blading. Development of this kind of flow control would be expected to require a substantial investment of time and money.

References

1. Lighthill, M. J.,"On Sound Generated Aerodynamically, I, General Theory", Proc. Roy. Soc., A, 221, 1952.

2. Lighthill, M. J.,"On Sound Generated Aerodynamically, II, Turbulence as a Source of Sound", Proc. Roy. Soc., A, 222, 1952.

3. Lighthill, M. J.,"The Bakerian Lecture, 1961, Sound Generated Aerodynamically", Proc. Roy. Soc., A, 267.

4. Sobelev, S. L., Partial Differential Equations of Mathematical Physics, Addison Wesley, 1964.

5. Curle, N.,"The Influence of Solid Boundaries Upon Aerodynamic Sound", Proc. Roy. Soc., A, 231, 1955.

6. Doak, P. E.,"Acoustic Radiation from a Turbulent Fluid Containing Foreign Bodies", Proc. Roy. Soc., A, 254, 1960.

7. Sharland, I. J.,"Sources of Sound in Axial Flow Fans", Jour. Sound Vib., 3, 1964.

8. Phillips, O. M.,"The Intensity of Aeolian Tones", JFM,1, 1956.

9. Kovasznay, L. S. G., Proc. Roy. Soc., A, 198, 1949.

10. Gerrard, J. H.,"An Experimental Investigation of the Oscillating Lift and Drag of a Circular Cylinder Shedding Turbulent Vortices", JFM, 18, 1961.

11. Kavrak, I., Proc. XI Yug. Cong. Rat. Appl. Mech., v 11, part 9, June 1972.

12. Kavrak, I.,"Wake Characteristics of a Two-Dimensional Asymmetric Aerofoil", AGARD CP-111, Sept. 1972.

13. Mugridge, B. D.,"Turbulent Boundary Layers and Surface Pressure Fluctuations on Two-Dimensional Aerofoils", Jour. Sound Vib., 18, 1971.

14. Schloemer, H. H.,"Effects of Pressure Gradient on Turbulent Boundary Layer Wall Pressure Fluctuations", Jour. Acoustical Soc. Amer., 42, 1967.

15. Mugridge, B. D.,"Acoustic Radiation from Aerofoils with Turbulent Boundary Layers", Jour. Sound Vib., 16, 1971.

16. Clark, L. T.,"The Radiation of Sound from an Airfoil Immersed in a Laminar Flow", ASME Jour. of Eng. for Power, 93, series A, 1971.

17. Paterson, R. W., Vogt, P. G., Fink, M. R., and Munch, C. E.,"Vortex Shedding Noise of an Isolated Airfoil", United Aircraft Research Laboratories Report K910867-6, 1971.

18. Clark, L. T.,"Results of an Experimental Investigation Relating Sound Generation by a Single Airfoil in a Turbulent Flow", Boeing Document D6-25357, 1969.

19. Noise and Acoustic Fatigue in Aeronautics, Richards, E. J. and Mead, D. J., editors, John Wiley, 1968.

20. Morse, P. M. and Ingard, K. U., Theoretical Acoustics, McGraw Hill, 1968.

21. Ffowcs Williams, J. E. and Hawkings, D. L.,"Theory Relating to the Noise of Rotating Machinery", ARC 29, 821, 1968.

22. Tanna, H. K. and Morfey, C. L.,"Sound Radiation from a Point Force in Circular Motion", Jour. Sound Vib., 15, 1971.

23. Bendat, J. S. and Piersol, A. G., Measurement and Analysis of Random Data, John Wiley, 1966.

24. Tennekes, H. and Lumley, J. L., A First Course in Turbulence, The MIT Press, 1972.

APPENDIX A

Model for the Generation of Aerodynamic Sound by a Single Airfoil

The model proposed for aerodynamic sound generation by a single airfoil is based on Curle's (5) solution of the non-homogeneous wave equation first described by Lighthill (2). Curle's solution is reduced for the case of an airfoil operating in a smooth flow. The only turbulence present in the flow is that in the wake of the airfoil. The solution is reduced to a form which relates the spectrum of sound generation to the power spectra of the two point velocity correlations in the wake. An outline of the wave equation, its solution, and reduction is presented in this appendix.

Non-homogeneous Wave Equation and General Solution

This wave equation is formed by combining the equations of continuity of mass with those for conservation of momentum. The continuity equation used is

$$\frac{\partial \rho}{\partial t} + \frac{\partial}{\partial x_i}(\rho u_i) = 0$$

and the momentum equation is used in the form

$$\frac{\partial(\rho u_i)}{\partial t} + \frac{\partial}{\partial x_j}(\rho u_i u_j) = -\frac{\partial}{\partial x_j}(p\delta_{ij}) + \frac{\partial}{\partial x_j}\tau_{ij}$$

For the energy equation, the wave propagation is assumed to be isentropic so that the density and pressure may be related by

$$\frac{\partial}{\partial x_j}(p\delta_{ij}) = a_o^2 \frac{\partial}{\partial x_j}(\rho\delta_{ij})$$

where a_o is an average wave speed in the radiative medium (air). The procedure is to take the partial derivative of the continuity equation with time and the partial space derivative of the momentum equation and subtracting the two results. A form of

the wave equation may be written

$$-\frac{\partial^2 \rho}{\partial t^2} + \frac{\partial^2}{\partial x_i \partial x_j}(\rho u_i u_j) = -a_o^2 \frac{\partial^2}{\partial x_i \partial x_j}(\rho \delta_{ij}) + \frac{\partial^2}{\partial x_i \partial x_j} \tau_{ij} .$$

If the isentropic relationship is used and the viscous stresses are neglected as small compared with the turbulent stresses, the wave equation takes the simpler form

$$\frac{\partial^2 \rho}{\partial t^2} - a_o^2 \frac{\partial^2 \rho}{\partial x_j \partial x_j} = \frac{\partial^2}{\partial x_i \partial x_j}(\rho u_i u_j) .$$

For an unbounded medium the solution is given by the Kirchhoff retarded potential solution (Sobelev, 4) but a more general form is needed for the case where bodies are immersed in the flow. A form of this type is also given by Sobelev but it is the reduction of the general solution to a form pertinent to sound generation which was the contribution of Curle (5). Curle has developed a solution which may be written for stationary surfaces as

$$4\pi a_o^2 (\rho(\vec{x},t) - \rho_o) = \frac{\partial^2}{\partial x_i \partial x_j} \int_{t'} \int_{\vec{y}} \frac{T_{ij}(\vec{y},t')}{|\vec{x}-\vec{y}|} \delta\left(t'-t+\frac{|\vec{x}-\vec{y}|}{a_o}\right) d\vec{y}\, dt'$$

$$- \frac{\partial}{\partial x_i} \int_{t'} \int_{\partial \vec{y}} \frac{P_i(\vec{y},t')}{|\vec{x}-\vec{y}|} \delta\left(t'-t+\frac{|\vec{x}-\vec{y}|}{a_o}\right) dS(\vec{y})\, dt' .$$

The delta function reflects the retarded time at which the integrands must be evaluated. The retarded time is the time it takes a disturbance to propagate from the source to the receiver. The integral must be evaluated at this retarded time unless it can be shown that negligible error results with its neglect. Fortunately for many cases in turbulence related noise generation

the retarded time effect may be safely neglected. These are typically low Mach number flows.

Before considering the retarded time some other reductions are possible. Details of these reductions have been presented by Curle however for convenience and continuity they will be outlined here.

Of the two terms in the solution the stress term is the more complicated so consider it here. Define $r \triangleq |\vec{x} - \vec{y}|$ and write

$$\frac{\partial}{\partial x_i}\int_{t'}\int_{\vec{y}} \frac{T_{ij}(\vec{y},t')}{r}\,\delta\left(t'-t+\frac{r}{a_o}\right)d\vec{y}\,dt' =$$

$$\int_{t'}\int_{\vec{y}} \frac{\partial r}{\partial x_i}\left[-\frac{1}{r^2}T_{ij}(\vec{y},t') - \frac{1}{a_o r}\,\frac{\partial T_{ij}(\vec{y},t')}{\partial t}\right]\delta\left(t'-t+\frac{r}{a_o}\right)d\vec{y}\,dt'.$$

Now repeat the same procedure with the second derivative and

$$\frac{\partial}{\partial x_j}\int_{t'}\int_{\vec{y}} \frac{\partial r}{\partial x_i}\left[-\frac{1}{r^2}T_{ij}(\vec{y},t') - \frac{1}{a_o r}\,\frac{\partial T_{ij}(\vec{y},t')}{\partial t}\right]\delta\left(t'-t+\frac{r}{a_o}\right)d\vec{y}\,dt'$$

becomes

$$\int_{t'}\int_{\vec{y}} \frac{\partial r}{\partial x_j}\frac{\partial r}{\partial x_i}\left[\frac{1}{a_o^2 r}\,\frac{\partial^2 T_{ij}(\vec{y},t')}{\partial t^2} + \frac{2}{a_o r^2}\,\frac{\partial T_{ij}(\vec{y},t')}{\partial t} + \frac{2}{r^3}T_{ij}(\vec{y},t')\right]$$

$$\delta\left(t'-t+\frac{r}{a_o}\right)d\vec{y}\,dt'.$$

Since $r = \sqrt{(x_i - y_i)^2}$ it can be shown that

$$\frac{\partial r}{\partial x_j} = \frac{x_j - y_j}{r}\,, \qquad \frac{\partial r}{\partial x_i} = \frac{x_i - y_i}{r}\,.$$

In order to get a measure of the relative magnitudes of the

three terms in the integral the method outlined in ref. 19 is used.

For data of some typical frequency f we can write an equivalent wavelength from the expression

$$f\lambda = a_o$$

With this the three terms have the relative magnitudes

$$\frac{(2\pi f)^2}{a_o^2 r} T_{ij} \quad , \quad \frac{4\pi f}{a_o r^2} T_{ij} \quad , \quad \frac{2}{r^3} T_{ij}$$

and in terms of the wavelength

$$2\pi T_{ij} \quad , \quad 2\pi \left(\frac{\lambda}{r}\right) T_{ij} \quad , \quad \left(\frac{\lambda}{r}\right)^2 T_{ij} .$$

So that for $(\lambda/r) \ll 1$ the second two terms may be neglected and the solution written

$$\int_{t'} \int_{\vec{y}} \frac{(x_i - y_i)}{r} \frac{(x_j - y_j)}{r} \frac{\partial^2 T_{ij}(\vec{y}, t')}{\partial t^2} \delta\left(t' - t + \frac{r}{a_o}\right) d\vec{y} dt' .$$

In an exactly parallel way, the surface term may be reduced to the form

$$-\int_{t'} \int_{\partial \vec{y}} \frac{(x_i - y_i)}{r} \frac{\partial P_i(\vec{y}, t')}{\partial t} \delta\left(t' - t + \frac{r}{a_o}\right) dS(\vec{y}) dt' .$$

A further reduction may now be made if the origin of the coordinate system is located within the active turbulent region (the airfoil wake). Then the source dimensions are small compared with the observer coordinates, $y_i \ll x_i$.

The far field solution may now be written

$$4\pi^2 a_o^2 (\rho(\vec{x},t)-\rho_o) = \frac{x_i x_j}{a_o^2 |\vec{x}|^3} \int_{t'}\int_{\vec{y}} \frac{\partial^2 T_{ij}(\vec{y},t')}{\partial t^2} \delta(t'-t+\frac{r}{a_o}) d\vec{y} dt'$$

$$- \frac{x_i}{a_o |\vec{x}|^2} \int_{t'}\int_{\partial\vec{y}} \frac{\partial P_i(\vec{y},t')}{\partial t} \delta(t'-t+\frac{r}{a_o}) ds(\vec{y}) dt'$$

This forms the far field solution to the wave equation with immersed bodies. Originally it was planned to include the volume stress terms in the solution and attempt to measure these as well as the force terms. This was abandoned for the reasons given in the body of the report that the dipole terms appear to dominate this mechanism of sound generation and therefore the volume terms would be of smaller importance in the sound generation problem being considered. If considerations were being made of higher Mach number flows there is evidence that the "quadrapole" terms may be of significant importance. Since the present experiment was limited to low Mach numbers, there appears to be little justification for the inclusion of those terms in this analysis. For these reasons, the rest of this development will be directed to the surface terms. It should be pointed out that a great effort has been extended in developing an understanding of free turbulent flows since these are the source of the very critical jet noise problem facing the commercial airplane industry at the present time. The problem is very complex but substantial progress has been made and it is expected that these same techniques will be applicable to the wake turbulence mechanism.

Also, it should be pointed out that sufficient data have been obtained in the present study to allow the establishment of the forcing function for the volume term. A very large data reduction effort would be required to reduce the data to a form useable for the volume source specification. These data are on magnetic tape and such a reduction effort may be undertaken in the future. For the present purposes it is felt that efforts may be more profitably directed to the study of the dominant mechanism of the fluctuating force on the airfoil. That alone has proven perplexing enough.

Conditions for Neglect of the Retarded Time

The clearest presentation, at least for this author, of the implications of the neglect of the retarded time in stochastic processes has been presented by Morse and Ingard (10). It is this general idea which is paralleled below for the present case. For simplicity in the development of the idea consider a function of form similar to the solution of the wave equation. Write

$$\eta(\vec{x},t)-\eta_o = \int_{t'}\int_{\vec{y}} P(\vec{y},t')\,\delta\left(t'-t+\frac{r}{a_o}\right)d\vec{y}\,dt'$$

Form an autocorrelation using the expectation as

$$R_\eta(\vec{x},\tau) = E\left\{\eta(\vec{x},t')-\eta_o\,,\,\eta(\vec{x},t'+\tau)-\eta_o\right\}$$

$$=E\left\{\int_{t'}\int_{\vec{y}} P(\vec{y},t')\,\delta\left(t'-t+\frac{r}{a_o}\right)\int_{\vec{z}} P(\vec{z},t'+\tau)\,\delta\left(t'+\tau-t+\frac{r'}{a_o}\right)d\vec{z}\,d\vec{y}\,dt'\right\}$$

$$=\int_{t'}\int_{\vec{y}}\int_{\vec{z}} E\left\{P(\vec{y},t')P(\vec{z},t'+\tau)\right\}\delta\left(t'-t+\frac{r}{a_o}\right)\delta\left(t'+\tau-t+\frac{r'}{a_o}\right)d\vec{z}\,d\vec{y}\,dt'$$

The process is assumed statistically stationary so that the only significance is the time difference between the two signals and not the absolute time. This difference between the times of the two signals may be written

$$(t'+\tau)-t' = t+\tau-\frac{|\vec{x}-\vec{z}|}{a_o}-t+\frac{|\vec{x}-\vec{y}|}{a_o}$$

$$= \tau+\frac{|\vec{x}-\vec{y}|}{a_o}-\frac{|\vec{x}-\vec{z}|}{a_o}$$

Expand these functions to

$$|\vec{x}-\vec{y}| = \sqrt{(x_i-y_i)^2} = \left(|\vec{x}|^2+|\vec{y}|^2-2x_1y_1-2x_2y_2-2x_3y_3\right)^{1/2}$$

$$= |\vec{x}|\left(1-\frac{2x_1y_1}{|\vec{x}|^2}-\frac{2x_2y_2}{|\vec{x}|^2}-\frac{2x_3y_3}{|\vec{x}|^2}+\left(\frac{|\vec{y}|}{|\vec{x}|}\right)^2\right)^{1/2}$$

To the first order in $\vec{y}/\vec{x}$ the expansion may be written

$$|\vec{x}-\vec{y}| = |\vec{x}|-\frac{x_1y_1}{|\vec{x}|^2}-\frac{x_2y_2}{|\vec{x}|^2}-\frac{x_3y_3}{|\vec{x}|^2}$$

$$= |\vec{x}|-\frac{\vec{x}\cdot\vec{y}}{|\vec{x}|}$$

and similarly for the other source position vector, z:

$$|\vec{x}-\vec{z}| = |\vec{x}|-\frac{\vec{x}\cdot\vec{z}}{|\vec{x}|}$$

Using these results the time difference becomes

$$\tau+\frac{|\vec{x}-\vec{y}|}{a_o}-\frac{|\vec{x}-\vec{z}|}{a_o} = \tau+\frac{\vec{x}\cdot(\vec{z}-\vec{y})}{a_o|\vec{x}|} \triangleq \tau+\delta\tau$$

Notice that $\vec{x}/|\vec{x}|$ is the unit vector in the direction of the observer. The second group is the time for a sound signal to travel from $\vec{y}$ to $\vec{z}$ in the direction of the observer.

Write the correlation in these terms as

$$R_\eta(\vec{x},\tau) = \int_{\vec{y}} \int_{\vec{z}} E\left\{P(\vec{y})\, P(\vec{z},\tau+\delta\tau)\right\} d\vec{z}\, d\vec{y}$$

It can be seen that if the additional time caused by $\delta\tau$ results in no significant difference in the correlation between the two functions P then we may neglect the retarded time difference $\delta\tau$. Consider this further. Notice:

$$\vec{x}/|\vec{x}| \cdot (\vec{x} - \vec{y}) = l_c = \text{a projected length of correlation in the observer direction}$$

Therefore, write:

$$\tau + \delta\tau = \tau + l_c/a_o$$

and consider it in terms of the Fourier transform. The argument for the transform will be

$$\omega(\tau+\delta\tau) = \omega\tau + \frac{\omega l_c}{a_o} = \omega\tau + \frac{2\pi l_c}{\lambda}$$

It can be seen from this that there will occur phase changes which are dependent on the ratio of the correlation length to the wavelength of the sound. Some interference will occur while the sound traverses the correlation length if the wavelength is not much larger than the correlation length. A condition for the neglect of retarded times can be written as

$$\frac{2\pi l_c}{\lambda} \ll 1$$

For the single airfoil data this requirement appears to be satisfied. However for the higher Mach numbers it may not be sufficient over the entire frequency range of interest; this must be remembered when extending these results to higher Mach number flows. If the retarded time is neglected the solution may be written in the form

$$\rho(\vec{x},t)-\rho_0 = \frac{1}{4\pi a_0^3}\frac{x_i}{|\vec{x}|^2}\frac{\partial}{\partial t}\int_{\partial\vec{y}} P_i(\vec{y},t)\,dS(\vec{y})$$

This is the form which will be reduced using the momentum equation so that the surface integral can be replaced by a volume integral over the wake near the airfoil trailing edge.

Change of Surface Pressure Term to Volume Momentum Term

Because of the difficulties in making static pressure correlation measurements on the surface of airfoils, the present approach of relating the force fluctuations on the surface of an airfoil to the momentum fluctuations in the wake was taken. A more detailed discussion of how this approach was decided upon and its limitations are presented in the body of the report. Details of the development of the actual model are presented in this section.

What will be done is to relate the surface static pressure on the airfoil to the gradient of the static pressure in the wake volume using the Gauss divergence theorem. The resulting (grad p) term will be expressed in terms of velocities in the wake through the linear momentum balance equation. Covariances of the resulting terms will provide the relationship between sound generation and the spectra of the two point velocity correlations in the airfoil wake.

First, consider the surface integral over the boundary of the control volume shown in figure 55. The control volume is such that the only non-steady velocities (other than lower order acoustic velocities) are confined to the turbulence of

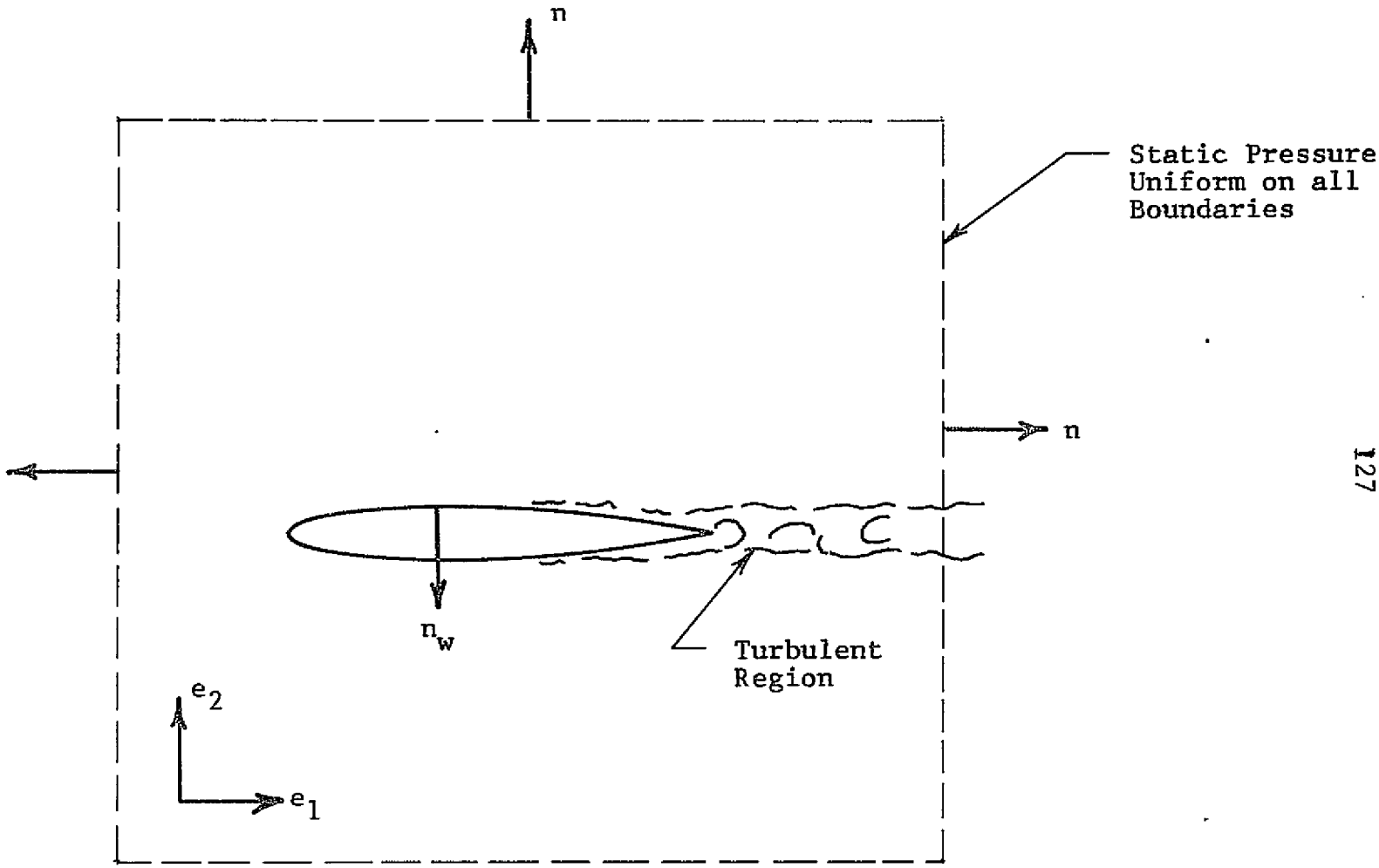

Figure 52 Control Volume Used in Application of Momentum Equation

the airfoil wake. For the simply connected region shown the divergence theorem can be used to write

$$\int_{\partial\vec{y}} p\vec{n}\, dS(\vec{y}) = \int_{\vec{y}} grad\, p\, d\vec{y}.$$

Taking the derivative of the expression allows the regions having steady properties to be eliminated from the integrations and simplifies the algebra. The result is

$$\frac{\partial}{\partial t}\int_{\partial\vec{y}} p\vec{n}\, dS(\vec{y}) = \frac{\partial}{\partial t}\int_{airfoil} p\vec{n}\, dS(\vec{y}) + \frac{\partial}{\partial t}\int_{WAKE\ EXIT\ PLANE} p\vec{n}\, dS(\vec{y}).$$

Through the divergence theorem these are then equal to the unsteady volume integral of the (grad p) in the wake. Therefore write

$$\frac{\partial}{\partial t}\int_{airfoil} p\vec{n}\, dS(\vec{y}) + \frac{\partial}{\partial t}\int_{exit} p\vec{n}\, dS(\vec{y}) = \frac{\partial}{\partial t}\int_{\vec{y}} grad\, p\, d\vec{y}.$$

The (grad p) integral may now be related to the velocity fluctuations by means of the linear momentum equation. For our case of incompressible flow $\rho = \rho_0$

$$-grad\, p = \rho_0 \frac{\partial \vec{u}}{\partial t} + \rho_0\, div(\vec{u}\vec{u})$$

so that

$$\frac{\partial}{\partial t}\int_{\vec{y}} grad\, p\, d\vec{y} = -\frac{\partial}{\partial t}\int_{\vec{y}} \rho_0\left(\frac{\partial \vec{u}}{\partial t} + div(\vec{u}\vec{u})\right) d\vec{y}.$$

The second term may be expressed as a surface integral by again using the divergence theorem. The total expression becomes

$$\frac{\partial}{\partial t}\int p\vec{n}\, dS(\vec{y}) = \frac{\partial}{\partial t}\int_{\vec{y}} \rho_0 \frac{\partial \vec{u}}{\partial t} d\vec{y} + \frac{\partial}{\partial t}\int_{exit} (p\vec{n} + \rho_0 \vec{u}\vec{u}\cdot\vec{n})\, dS(\vec{y}).$$

The force on the body is to be approximated by the momentum fluctuation in the wake immediately downstream of the airfoil trailing edge. The assumption is that the force on the blade can be approximated by a kind of correlation volume of momentum nearest the trailing edge. This assumption then eliminates the dependence upon the terms in the exit plane integral since these will be uncorrelated and may be ignored.

Using these conditions the relationship between surface pressure fluctuations and those of wake momentum become

$$\frac{\partial}{\partial t}\int_{airfoil} -p\vec{n}\, dS(\vec{y}) = \frac{\partial}{\partial t}\int_{\vec{y}} \rho_0 \frac{\partial \vec{u}}{\partial t}\, d\vec{y}.$$

With this equality the radiated sound can be written. It is necessary to first introduce a negative sign since the sound is generated by the force on the fluid where in the above the force of the fluid on the body has been determined. Write for the radiated density

$$\rho(\vec{x},t) - \rho_0 = \frac{-\rho_0}{4\pi a_0^3} \frac{\vec{x}\cdot}{|\vec{x}|^2} \frac{\partial}{\partial t}\int_{\vec{y}} \frac{\partial \vec{u}}{\partial t}\, d\vec{y}$$

Notice that the density has been taken outside the integral under the assumption of incompressible flow. At this point an examination of the consequences of this assumption and the expected error due to density fluctuations will be made.

Estimate of Error Due to Neglect of Density Fluctuations

As a means of getting a measure of the error due to the neglect of the density fluctuations the energy equation for one dimensional compressible flow will be used.

Write the energy equation

$$c_p \theta_t = c_p \theta + \frac{1}{2} u^2$$

and introduce the normal turbulence assumptions

$$u = \bar{U} + u' \qquad \rho = \bar{\rho} + \rho'$$

Factor the energy equation into the form

$$u^2 = 2 c_p \theta_t \left(1 - \frac{\theta}{\theta_t}\right) = 2 c_p \theta_t \left(1 - \frac{\rho_t}{\rho}\right)$$

Where the fluctuations in static pressure have been assumed small compared with those of velocity and density. This can be taken as generally true for free flows such as the wake. Rewrite the energy equation as

$$\rho u^2 = 2 c_p \theta_t (\rho - \rho_t)$$

and insert the turbulent velocities and densities to yield

$$(\bar{\rho} + \rho')(\bar{U}^2 + 2\bar{U}u' + u'u') = 2 c_p \theta_t (\bar{\rho} + \rho' - \rho_t)$$

Solve this for the density fluctuation:

$$2\bar{U}\bar{\rho}\, u' = (2 c_p \theta_t - \bar{U}^2)\rho' = 2 c_p \theta \rho'$$

For air ($\gamma = 1.4$) and the fluctuations in density are related to those for the longitudinal component of turbulence by

$$\frac{\rho'}{\bar{\rho}} = (\gamma - 1) M^2 \frac{u'}{\bar{U}}$$

This suggests that for $M < 1$ the density fluctuations may be safely neglected. This is therefore within the context of the other assumptions made in the current model.

Sound Radiation in Terms of Two Point Velocity Correlations

With the assumption of constant density the covariance of the radiated sound density may be simply related to the covariances of the two point velocity correlations.

Separate the velocity into a steady part and a fluctuating part in the typical turbulent assumption:

$$u_i(\vec{y},t) = \bar{U}_i(\vec{y}) + u_i'(\vec{y},t)$$

and use the direction cosines

$$\hat{r}_k = \vec{x}_k / |\vec{x}|$$

Refer to figure 4 and write the direction cosines to agree with the nomenclature of the figure. They become

$$\frac{\vec{x}\cdot\vec{e}_1}{|\vec{x}|} = \sin\psi \qquad \frac{\vec{x}\cdot\vec{e}_2}{|\vec{x}|} = \cos\psi$$

Further, assume the velocities are represented by the following components:

$$\bar{U}_k = \bar{U}_1 \;,\; \bar{U}_2 = 0 = \bar{U}_3 \;,\; u_3' = 0 \;,\; \hat{r}_3 = 0$$

Using index notation, write the solution as

$$\rho(\vec{x},t) - \rho_0 = \frac{\rho_0}{4\pi a_0^3 |\vec{x}|}\, \hat{r}_i \int_{\vec{y}} \frac{\partial^2}{\partial t^2}\left(u_i(\vec{y},t)\right) d\vec{y}$$

then expand and normalize with the free stream velocity to get

$$\rho(\vec{x},t) - \rho_0 = \frac{\rho_0 \bar{U}_1}{4\pi a_0^3 |\vec{x}|} \int_{\vec{y}} \left[\sin\psi \frac{\partial^2}{\partial t^2}\left(\frac{u_1'}{\bar{U}_1}(\vec{y},t)\right) + \cos\psi \frac{\partial^2}{\partial t^2}\left(\frac{u_2'}{\bar{U}_1}(\vec{y},t)\right)\right] d\vec{y}$$

Define the following coefficients to help simplify the formulation of the covariances:

$$A_1 \triangleq \frac{\rho_o \bar{U}_1}{4\pi a_o^3 |\vec{x}|} \sin\psi$$

$$A_2 \triangleq \frac{\rho_o \bar{U}_1}{4\pi a_o^3 |\vec{x}|} \cos\psi$$

Write the expected value of the radiated sound density as

$$R_\rho(\vec{x},\tau) = E\left\{\rho(\vec{x},t), \rho(\vec{x},t+\tau)\right\}$$

$$= A_1^2 \int_{\vec{y}} \int_{\vec{z}} E\left\{\frac{\partial^2}{\partial t^2}\left[\frac{u_1'}{\bar{U}_1}(\vec{y},t)\right], \frac{\partial^2}{\partial t^2}\left[\frac{u_1'}{\bar{U}_1}(\vec{z},t+\tau)\right]\right\} d\vec{z}\, d\vec{y}$$

$$+ A_1 A_2 \int_{\vec{y}} \int_{\vec{z}} E\left\{\frac{\partial^2}{\partial t^2}\left[\frac{u_1'}{\bar{U}_1}(\vec{y},t)\right], \frac{\partial^2}{\partial t^2}\left[\frac{u_2'}{\bar{U}_1}(\vec{z},t+\tau)\right]\right\} d\vec{z}\, d\vec{y}$$

$$+ A_2 A_1 \int_{\vec{y}} \int_{\vec{z}} E\left\{\frac{\partial^2}{\partial t^2}\left[\frac{u_2'}{\bar{U}_1}(\vec{y},t)\right], \frac{\partial^2}{\partial t^2}\left[\frac{u_1'}{\bar{U}_1}(\vec{z},t+\tau)\right]\right\} d\vec{z}\, d\vec{y}$$

$$+ A_2^2 \int_{\vec{y}} \int_{\vec{z}} E\left\{\frac{\partial^2}{\partial t^2}\left[\frac{u_2'}{\bar{U}_1}(\vec{y},t)\right], \frac{\partial^2}{\partial t^2}\left[\frac{u_2'}{\bar{U}_1}(\vec{z},t+\tau)\right]\right\} d\vec{z}\, d\vec{y}$$

Replace the expectations with the cross covariance functions to obtain the form

$$R_\rho(\vec{x},\tau) = \int_{\vec{y}} \int_{\vec{z}} \left[A_1^2 R_{\ddot{u}_1\ddot{u}_1}(\vec{y},\vec{z},\tau) + A_1 A_2 R_{\ddot{u}_1\ddot{u}_2}(\vec{y},\vec{z},\tau)\right.$$

$$\left. + A_2 A_1 R_{\ddot{u}_2\ddot{u}_1}(\vec{y},\vec{z},\tau) + A_2^2 R_{\ddot{u}_2\ddot{u}_2}(\vec{y},\vec{z},\tau)\right] d\vec{z}\, d\vec{y}$$

In order to cast the solution into a form usable with the experimental data the Fourier transform of the covariances must be taken. The one-sided power spectral form of the transfrom will be used. This may be written

$$G_{xy}(\vec{x},\omega) = 2\int_{-\infty}^{+\infty} R_{xy}(\vec{x},\tau)\, e^{-i\omega\tau}\, d\tau$$

Using this and the identity

$$G_{\ddot{u}\ddot{u}}(\vec{x},\omega) = \omega^4 G_{uu}(\vec{x},\omega)$$

write the solution in terms of the cross power spectral densities of the two point velocity correlations. The result is

$$G_p(\vec{x},\omega) = \omega^4 \int_{\vec{y}}\int_{\vec{z}} \left[A_1^2 G_{u_1u_1}(\vec{z},\vec{y},\omega) + A_1 A_2 G_{u_1u_2}(\vec{z},\vec{y},\omega)\right.$$

$$\left. + A_2 A_1 G_{u_2u_1}(\vec{z},\vec{y},\omega) + A_2^2 G_{u_2u_2}(\vec{z},\vec{y},\omega)\right] d\vec{z}\, d\vec{y}$$

This is the general form of the present solution for sound radiation from a single airfoil in a smooth flow. It is the basis for the model and these are the quantities which were measured in the experimental program.

Determination of the Momentum Fluctuation

For the rest of this appendix the summation convention is suspended. The spectrum of the radiated sound can be written in the index form as

$$G_p(\vec{x},\omega) = \sum_{i=1}^{2}\sum_{j=1}^{2} G_p(u_i u_j, \vec{x}, \omega)$$

where

$$G_p(u_i u_j, \vec{x}, \omega) = \omega^4 \int_{\vec{y}} \int_{\vec{z}} A_i A_j G_{u_i u_j}(\vec{z}, \vec{y}, \omega)\, d\vec{z}\, d\vec{y}$$

Now change variables and let one of the position vectors of the sources be defined relative to the other as

$$\vec{z} \triangleq \vec{y} + \vec{\eta}$$

and write

$$G_p(u_i u_j, \vec{x}, \omega) = \int_{y_1} \int_{y_2} \int_{y_3} A_i A_j\, \overline{u_i u_j}(y_1, y_2, y_3, \omega)$$

$$\omega^4 \int_{\eta_1} \int_{\eta_2} \int_{\eta_3} \hat{G}_{u_i u_j}(y_1, \eta_1, \eta_2, \eta_3, \omega)\, d\eta_3\, d\eta_2\, d\eta_1\, dy_3\, dy_2\, dy_1$$

where: $u_i u_j(y_1, y_2, y_3, \omega)$ = the distribution of the autospectrum in the wake

$G_{u_i u_j}(y_1, \eta_1, \eta_2, \eta_3, \omega)$ = a coherency spectrum

The term labeled a coherency spectrum in the above is similar to the normal coherency as used in texts on time series analysis with the difference that the normalization is done with only one autospectrum, that of the signal on the stationary probe, and not with both signals as is the normal procedure. With this type of a definition it is possible to have values of the coherency greater than one. The Schwartz inequality does not apply.

Notice that the coherency spectrum has been assumed independent of y_2 and y_3 but the dependency upon y_1 has been retained. The argument to support this is that the magnitude in

the y_2 direction decreases so rapidly (as one nears the edge of the wake) that differences in the spatial distribution of velocity will be of small effect in the overall integrated result. In the y_3 (span) direction the assumption is valid since spatial homogeneity may be correctly assumed in this direction. The fact that the stream dependence cannot be neglected is due to the fact that significant differences may exist in this direction.

Usage of Correlation Length Concept

It will prove convenient in terms of handling the experimental results to carry out the integration of the coherency function in each of the coordinate directions at each frequency. The lengths that result will be termed correlation lengths as a method of labeling. Notice that implicit in this method is the assumption that the integration can be done in each direction independently of the others and the integral can be expressed as a product of the three lengths.

Each length becomes a function of y_1 and ω. The integral may be written

$$\int_{\eta_1}\int_{\eta_2}\int_{\eta_3} \hat{G}_{u_i u_j}(y_1, \eta_1, \eta_2, \eta_3, \omega)\, d\eta_3\, d\eta_2\, d\eta_1 =$$

$$8 L_1(u_i u_j, y_1, \omega)\, L_2(u_i u_j, y_1, \omega)\, L_3(u_i u_j, y_1, \omega)$$

where the correlation lengths may be different for the various two point velocity correlations; hence the dependence on $u_i u_j$ is retained in the lengths.

The sound radiation due to one particular $u_i u_j$ may be written as

$$G_p(u_i u_j, \vec{x}, \omega) = 8 \int_{y_1} L_1(u_i u_j, y_1, \omega)\, L_2(u_i u_j, y_1, \omega)\, L_3(u_i u_j, y_1, \omega)$$

$$\omega^4 \int_{y_2} \int_{y_3} A_i A_j \; \overline{u_i u_j}(y_1, y_2, y_3, \omega)\, dy_3\, dy_2\, dy_1$$

In line with the assumptions of the model, assume the relevant volume of integration to be that correlation volume immediately downstream of the airfoil. y_1 is then taken over the range $-L_1$ to L_1 and the expression for the sound radiation is

$$G_p(\vec{x}, \omega) = \sum_{i=1}^{2} \sum_{j=1}^{2} 16\, L_1^2(u_i u_j, \omega)\, L_2(u_i u_j, \omega)\, L_3(u_i u_j, \omega)$$

$$\omega^4 \int_{y_2} \int_{y_3} A_i A_j \; \overline{u_i u_j}(y_2, y_3, \omega)\, dy_3\, dy_2$$

This is the final result for the model which will be used to relate sound generation to wake turbulence. The first integral (that of the longitudinal component of turbulence) will correspond to a dipole oriented along the chord direction. The last integral, the transverse component, will be a dipole oriented along a line perpendicular to the chord of the airfoil. This is the dipole normally used in models for the prediction of vortex shedding noise. The cross terms will act to modify the radiation pattern from the symmetric form. If, however, the wake is symmetric these terms will integrate to zero.

APPENDIX B

Wake Related Sound Generation by a Rotor

The mathematical model used to predict sound generation by a rotor using the general results of the single airfoil was that of Ffowcs Williams and Hawkings(21). There is available another analysis based on the Lowson theory for moving sources which was recently presented by Morfey and Tanna(22). The quantity of algebraic detail required to extend this latter analysis to include both forces and stresses is considerable and the application to specific designs was felt to be substantially more laborious than the method of ref. 21. Actually there are many rotor analyses springing up like mushrooms but these do not appear to offer any particular advantages over those already mentioned for practical designs.

An outline of the original analysis by Ffowcs Williams and Hawkings will be given in this appendix with the bulk of the space used to develop their results into a form usable for the particular problem of wake related sound generation. For a general discussion of multipole analysis, of which this is an example, the reader is referred to Doak(6) and to Morse and Ingard(20).

The sound generation is taken as governed by a non-homogeneous wave equation of the form

$$\frac{\partial^2 \rho}{\partial t^2} - a_o^2 \nabla^2 \rho = Q(\vec{x}, t)$$

which has the solution

$$\rho(\vec{x}, t) = \frac{1}{4\pi a_o^2 r} \int_{\vec{y}} Q(\vec{y}, t') \delta(t' - t + r/a_o) d\vec{y}$$

and in terms of its generalized Fourier transform,

$$\rho(\vec{x},\omega) = \frac{e^{-i\omega r/a_o}}{4\pi a_o^2 r} Q\left(-\frac{\omega}{a_o}\frac{\vec{x}}{|\vec{x}|},\omega\right)$$

As may be seen from Curle's solution to the Lighthill equation, the forcing function may contain simple sources, dipoles and quadrapole elements. In general the form is

$$Q(\vec{y},t) = S(\vec{y},t) + \frac{\partial D_i(\vec{y},t)}{\partial y_i} + \frac{\partial^2 T_{ij}(\vec{y},t)}{\partial y_i\, \partial y_j}$$

So that S, D_i, and T_{ij} are the source strength densities of the three most common source types. For present purposes, only the force and stress densities will be considered.

The source expression may be Fourier transformed to express it in the form

$$Q(\vec{k},\omega) = \int_{\vec{y}}\int_{t} Q(\vec{y},t)\, e^{-i\vec{k}\cdot\vec{y}}\, e^{-i\omega t}\, dt\, d\vec{y}$$

from which,

$$Q(\vec{k},\omega) = S(\vec{k},\omega) + i\, k_i D_i(\vec{k},\omega) - k_i k_j T_{ij}(\vec{k},\omega)$$

The components radiating in the direction of the observer can be taken as the spectral level with, $\vec{k} = -\frac{\omega}{a_o}\frac{\vec{x}}{|\vec{x}|}$

thus,

$$Q\left(-\frac{\omega}{a_o}\frac{\vec{x}}{|\vec{x}|},\omega\right) = S\left(-\frac{\omega}{a_o}\frac{\vec{x}}{|\vec{x}|},\omega\right) - i\frac{\omega}{a_o}\hat{r}_i D_i\left(-\frac{\omega}{a_o}\frac{\vec{x}}{|\vec{x}|},\omega\right) - \frac{\omega^2}{a_o^2}\hat{r}_i\hat{r}_j T_{ij}\left(-\frac{\omega}{a_o}\frac{\vec{x}}{|\vec{x}|},\omega\right)$$

The general solution was then developed by substitution and reduction of the above equation inserted into the general solution as it was originally put down. What resulted were the following forms for sources moving in a plane circular

motion (a rotor). Details of this reduction are lengthy and best left to the original paper. The results for the two source types of interest here, i.e. dipoles and quadrapoles, are presented below.

ROTATING FORCES (DIPOLES)

$$\rho_{d,k}(\vec{x},\omega) = -\frac{e^{-i\omega r/a_o}}{4\pi a_o^2 r}\left(\frac{i\omega}{a_o}\right)\hat{r}_\ell \sum_{n=-\infty}^{+\infty} d_\ell(\theta_k, f-n\Omega)\, e^{-in(\pi/2-\theta_k)} J_n\left(-\frac{\omega R_s \sin\phi}{a_o}\right)$$

ROTATING STRESSES (QUADRAPOLES)

$$\rho_{q,k}(\vec{x},\omega) = -\frac{e^{-i\omega r/a_o}}{4\pi a_o^2 r}\left(\frac{\omega}{a_o}\right)^2 \hat{r}_\ell \hat{r}_m \sum_{n=-\infty}^{\infty} t_{\ell m}(\theta_k, f-n\Omega)\, e^{-in(\pi/2-\theta_k)} J_n\left(-\omega R_s \sin\phi/a_o\right)$$

These solutions are written for a point dipole having a generalized spectrum $d_i(\theta_k,\alpha)$ and a point quadrapole with a generalized spectrum $t_{ij}(\theta_k,\alpha)$. The spectrum is the Fourier transform of the time dependent source strength. The position is the angular location (θ_k) of the kth source at time, t = 0. Ω is the angular frequency of the source and ϕ is the radiation angle measured from the inlet fan axis.

In order to put these solutions in a form usable for the prediction of wake related sound, an auto power spectrum of the radiated sound density must be formed. This will result in cross power spectra of the various terms in the solution. The details of this procedure for combined forces and stresses are developed in the following paragraphs.

Reduction of the Solution for Multibladed Rotors

The total radiated sound is taken as the sum of the two components written above.

For one blade of a rotor, write

$$\rho_k(\vec{x},\omega) = \rho_{d,k}(\vec{x},\omega) + \rho_{q,k}(\vec{x},\omega)$$

The total for the entire rotor is the sum over the number of rotor blades.

$$\rho(\vec{x},\omega) = \sum_{k=1}^{B} \rho_{d,k}(\vec{x},\omega) + \sum_{k=1}^{B} \rho_{q,k}(\vec{x},\omega)$$

To obtain the radiated sound power spectrum multiply the above equation by its complex conjugate to form the modulus squared.

$$|\rho(\vec{x},\omega)|^2 = \left[\sum_{k=1}^{B} \rho_{d,k}(\vec{x},\omega) + \sum_{k=1}^{B} \rho_{q,k}(\vec{x},\omega)\right] \times \left[\sum_{\ell=1}^{B} \rho_{d,k}(\vec{x},\omega) + \sum_{\ell=1}^{B} \rho_{q,k}(\vec{x},\omega)\right]^*$$

expand the form to

$$|\rho(\vec{x},\omega)|^2 = \sum_{k=1}^{B}\sum_{\ell=1}^{B}\left[\rho_{d,k}(\vec{x},\omega)\rho_{d,\ell}^*(\vec{x},\omega) + \rho_{d,k}(\vec{x},\omega)\rho_{q,\ell}^*(\vec{x},\omega) + \rho_{q,k}(\vec{x},\omega)\rho_{d,\ell}^*(\vec{x},\omega) + \rho_{q,k}(\vec{x},\omega)\rho_{q,\ell}^*(\vec{x},\omega)\right]$$

For algebraic convenience consider the first term in the following development as representative of the others.

$$\sum_{k=1}^{B}\sum_{\ell=1}^{B} \rho_{d,k}(\vec{x},\omega)\rho_{d,\ell}^*(\vec{x},\omega) = \frac{1}{16\pi^2 a_o^4 r^2}\left(\frac{\omega}{a_o}\right)^2 \sum_{n=-\infty}^{+\infty}\sum_{m=-\infty}^{+\infty} \sum_{k=1}^{B}\sum_{\ell=1}^{B} d_r(\theta_k, f-n\Omega) d_r^*(\theta_\ell, f-m\Omega)$$

$$e^{-in(\pi/2-\theta_k)} e^{-im(\pi/2-\theta_\ell)} J_n\left(-\frac{\omega R_s \sin\phi}{a_o}\right) J_m\left(-\frac{\omega R_s \sin\phi}{a_o}\right)$$

where d_r is the component in the direction of the observer.

Consequences of the Assumption of Stationarity

If the force fluctuations are assumed to be statistically stationary, then a reduction in the complexities will result. For stationary random processes the expected value of a form similar to the solution may be expressed.

$$E\left[X_k(f)\, Y_k(g)\right] = S_{xy}(f)\, \delta(f-g)$$

where $S_{xy}(f)$ is the cross power spectrum. This states that for stationary processes the Fourier coefficients are uncorrelated.

Using the above result the only terms which will remain in the summation are those for which m = n. The solution reduces for this case to

$$\frac{1}{16\pi^2 a_0^4 r^2}\left(\frac{\omega}{a_0}\right)^2 \sum_{n=-\infty}^{+\infty} \sum_{k=1}^{B} \sum_{l=1}^{B} d_r(\theta_k, f-n\Omega)\, d_r^*(\theta_l, f-n\Omega)$$

$$e^{-in(\theta_l-\theta_k)}\, J_n^2\left(-\frac{\omega R_s \sin\phi}{a_0}\right)$$

The Assumption of Uncorrelated Blades

If the process at each blade is assumed uncorrelated with those at each of the other blades, then the double sum on the blade number may be reduced to a single sum.

If the processes are mutually uncorrelated from blade to blade

$$d_r(\theta_k, f)\, d_r^*(\theta_l, f) = 0 \quad \text{if} \quad k \neq l$$

Notice if a model is being developed for inflow turbulence related noise generation the reduction made here would not be correct since the scale of the turbulence would be expected to encompass more than one blade in the interaction and response.

For the present case of uncorrelated blades it is sufficient to write the dipole solution.

$$\frac{1}{16\pi^2 a_o^4 r^2}\left(\frac{\omega}{a_o}\right)^2 \sum_{n=-\infty}^{+\infty}\sum_{k=1}^{B} d_r(\theta_k, f-n\Omega)\, d_r(\theta_k, n\Omega-f)\, J_n^2\left(-\frac{\omega R_s \sin\phi}{a_o}\right)$$

where the identity $d_r^*(\theta_k, f-n\Omega) = d_r(\theta_k, n\Omega-f)$ has been used.

Consideration of the other three terms in the solution will exactly parallel the above arguements so it is sufficient just to write the result. The solution becomes

$$|p(\vec{x},\omega)|^2 = \frac{1}{16\pi^2 a_o^4 r^2}\sum_{n=-\infty}^{+\infty}\sum_{k=1}^{B}\left\{\left(\frac{\omega}{a_o}\right)^2 d_r(\theta_k, f-n\Omega)\, d_r(\theta_k, n\Omega-f)\right.$$

$$+\left(\frac{\omega}{a_o}\right)^4 t_{rr}(\theta_k, f-n\Omega)\, t_{rr}(\theta_k, n\Omega-f)$$

$$\left.+i\left(\frac{\omega}{a_o}\right)^3\left[d_r(\theta_k, f-n\Omega)\, t_{rr}(\theta_k, n\Omega-f) - t_{rr}(\theta_k, f-n\Omega)\, d_r(\theta_k, n\Omega-f)\right]\right\}$$

$$J_n^2\left(-\frac{\omega R_s \sin\phi}{a_o}\right)$$

Notice that there appears to be an imaginary part to the modulus. This of course is not possible. Actually the apparent complex nature of the expression is not really there since the non-vanishing part of the term in square brackets is the imaginary part which is multiplied by $\sqrt{-1}$ and produces a real number. This may be shown by expressing the result in terms of co- and quad-spectral components; the co-spectral components will cancel leaving only the quad components (see Bendat and Piersol, page 83).

Representation in Terms of Wake Parameters

Since the rotor model is developed here for point sources, the distributed results to be taken from the single airfoil results must be expressed as an equivalent point dipole. The method used for the force will be developed. The stress term was not developed farther for the wake case since for the range of variables studied here the sound generation was dominated by the dipole mechanism. Originally it was expected that the quadrapole terms in the wake would be included so the rotor analysis was set up to handle both. It is still expected that for higher Mach numbers wake stress terms will assume importance. The rest of this rotor development will consider only the force fluctuations on the blading.

The total force on the blade is taken as the integral of the static pressure over the surface of the blade.

$$d(\theta_k, t) = \int_S p(\vec{y}, t)\, dS(\vec{y})$$

As was seen for the case of the single airfoil, this static pressure distribution could be written in terms of the momentum fluctuations in the near wake of the airfoil.

$$\int_S p(\vec{y}, t)\, dS(\vec{y}) = \int_{\vec{y}} \frac{\partial}{\partial t}(\rho u_i)\, d\vec{y}$$

In terms of frequency the force may be expressed

$$d(\theta_k, \omega) = \sqrt{-1}\, \omega \rho \int_{\vec{y}} u_i(\vec{y}, \omega)\, d\vec{y}$$

This is the form used in the rotor model.

Substitution of the force into the general solution for the sound radiation gives the force modulus for the component in the direction of the observer.

write the force modulus

$$d_r(\theta_k, f-n\Omega)\, d_r^*(\theta_k, f-n\Omega) =$$

$$(\omega - 2\pi n\Omega)^2 \rho_o^2\, \hat{r}_\ell\, \hat{r}_m \int_{\vec{z}} \int_{\vec{y}} u_\ell(\vec{y}, f-n\Omega)\, u_m^*(\vec{z}, f-n\Omega)\, d\vec{y}\, d\vec{z}$$

The computer program which was developed to predict the rotor sound included both the stress terms and the force terms as well as the cross terms for the correlation between the stress and force. As the program is used for this current work only the force, or dipole, part will be employed. It is expected that as more understanding of the relationship of the contribution of the wake stress is developed these results can be included in the rotor computations.

Nomenclature

a_o	speed of sound in air (m/sec)
c_p	specific heat at constant pressure (Kcal/Kg °K)
$D_i(\vec{y},t)$	dipole rotor source term (N/m^2)
$d_r(\theta_k,f)$	spectral level of blade force component in the direction of the observer (N)
$\vec{e}_k$	base vector, rotor model
E	expectation operation (expected value)
f	frequency (Hz)
$G_\rho(\vec{x},f)$	density power spectrum at the observer (Kg^2/m^6Hz)
$\vec{g}_k$	base vector, rotor model
$G_{u_iu_j}$	one sided power spectral density (m^2/sec^2 Hz)
$\vec{i}_k$	base vector, rotor model
l_c	typical correlation length (m)
L_k	correlation length for the k coordinate direction (cm)
M	Mach number
$\vec{n}$	unit normal to control volume
p	static pressure (N/m^2)
p_k	force per unit area (N/m^2)
$Q(\vec{x},t)$	total rotor source term (N/m^2)
r	$\lvert\vec{x} - \vec{y}\rvert$ distance from source to observer (m)
$R_{u_iu_j}$	cross covariance function (m^2/sec^2)
$\hat{r}_k$	direction cosine, $x_k/\lvert\vec{x}\rvert$
$S(\vec{y},t)$	simple source term, rotor model (Kg/m^4)
S	airfoil span (m)
T_{ij}	Lighthill stress tensor (N/m^2) (used in single airfoil model)
$T_{ij}(\vec{y},t)$	quadrapole rotor source term (N/m^2)

$t_{rr}(\theta_k, f)$	spectral level of the stress component in the direction of the observer (N/m^2)
t	time (sec)
$\overline{U}_1$	free stream velocity (m/sec)
$\overline{U}_i$	mean velocity (m/sec)
u_i'	fluctuating component of velocity (m/sec)
$u_i u_j$	two point velocity correlation (m^2/sec^2)
$\vec{x}$	position vector for sound observer (m)
$\vec{y}$	position vector for source (m)
$\vec{z}$	position vector for source (m)
ρ_o	density of fluid (Kg/m^3)
ω	radian frequency (rad/sec)
δ_w	wake thickness (cm)
ψ	angle from perpendicular to airfoil chord to the sound observer (deg)
τ_{ij}	shear stress tensor (N/m^2)
λ	wavelength (1/m)
$\eta(\vec{x}, t)$	arbitrary function, used in Appendix A
γ	ratio of specific heats ($\gamma = 1.4$)
θ_t	total temperature (°K)
θ	static temperature (°K)
ρ'	fluctuating density (Kg/m^3)
$\vec{\eta}$	displacement vector, $\vec{z} - \vec{y}$
Ω	rotor frequency (1/sec)
ϕ	radiation angle from inlet rotor axis to sound observer (deg)
θ_k	angular location of rotor source at t = 0 (deg)